NASA-CR-175665

NASA-CR-175665
19850015958

N85 24269

COMET

NOTICE

THIS REPRODUCTION WAS MADE FROM THE BEST AVAILABLE COPY OF WHICH A NUMBER OF PAGES WERE OF POOR REPRODUCTION QUALITY.

JPL PUBLICATION 85-2

(NASA-CR-175665) GEOMETRIC ERROR ANALYSIS FOR SHUTTLE IMAGING SPECTROMETER EXPERIMENT (Jet Propulsion Lab.) 172 p HC A08/MF A01 CSCL 14B

N85-24269

Unclas

G3/35 14802

Geometric Error Analysis for Shuttle Imaging Spectrometer Experiment

Shyh Jong Wang
Che-Hang Charles Ih

December 15, 1984

NASA
National Aeronautics and Space Administration

Jet Propulsion Laboratory
California Institute of Technology
Pasadena, California

JPL PUBLICATION 85-2

Geometric Error Analysis for Shuttle Imaging Spectrometer Experiment

Shyh Jong Wang
Che-Hang Charles Ih

December 15, 1984

National Aeronautics and
Space Administration

Jet Propulsion Laboratory
California Institute of Technology
Pasadena, California

The research described in this publication was carried out by the Jet Propulsion Laboratory, California Institute of Technology, under a contract with the National Aeronautics and Space Administration

Reference herein to any specific commercial product, process, or service by trade name, trademark, manufacturer, or otherwise, does not constitute or imply its endorsement by the United States Government or the Jet Propulsion Laboratory, California Institute of Technology

Acknowledgements

The authors wish to express their gratitude to Y. H. Lin and J. M. Cameron for their contributions at the early stage of this work, and to M. Herring, P. N. Kupferman, and J. B. Wellman for their support.

ABSTRACT

The demand of more powerful tools for remote sensing and management of earth resources has been steadily increasing over the last decade. With the recent advancement of area array detectors, high resolution multichannel imaging spectrometers can be realistically constructed.

This report documents the error analysis study for the Shuttle Imaging Spectrometer Experiment system for the purpose of providing information for design, tradeoff, and performance prediction.

Error sources including the Shuttle attitude determination and control system, instrument pointing and misalignment, disturbances, ephemeris, earth rotation, etc., have been investigated. Geometric error mapping functions were developed, characterized, and illustrated extensively with tables and charts. Selected ground patterns and the corresponding image distortions have been generated for direct visual inspection of how the various error sources affect the appearance of the ground object images.

TABLE OF CONTENTS

Page

List of Illustrations

Page

List of Tables

I. INTRODUCTION

A. BACKGROUND

Earth resource management and utilization have experienced great success over the last decade through the Landsat programs. In more recent years, both NASA and user communities have envisioned the need for development of better and more powerful instruments for surveying and managing earth resources. The Landsat D's new sensor, Thematic Mapper (TM), the proposed utilization of Tracking and Data Relay Satellite System (TDRSS), and a more advanced ground system represent an advancement in the earth resource satellite development [1].

The Thematic Mapper of the Landsat D (launched in 1982) has seven spectral bands, two more than those of the Multispectral Scanner associated with the earlier Landsats. However, study shows that the reflectance spectrum of earth surface materials contains a significant amount of information which can only be identified with spectral resolution much finer than those of the Thematic Mapper [2]. With the advancement of area array detectors, a push broom imaging spectrometer can be realistically constructed for simultaneous imaging and registration of hundreds of spectral bands. For the case of Shuttle Imaging Spectrometer Experiment, 128 spectral channels have been proposed to cover the spectral range of 0.4 to 1.0 μm for VNIR (visible and near infrared) and 1.0 to 2.5 μm for SWIR (short-wavelength infrared) with instantaneous field of view of 30m. Table 1 shows the required sensor performance [2].

The purpose of this report is to document the error analysis study for the imaging spectrometer experiment. Error analysis is an important aspect of the overall remote sensing system, since errors from many sources, including the spectrometer itself, the spacecraft that carries the instrument, knowledge limitations on the true spacecraft attitude and locations, earth rotation, curvature, and terrain variations, etc., will all contribute to image distortion, shift, rotation, and misregistration. Error correction or compensation are necessary and are an integral part of the image processing. This work covers the analysis of fundamental and geometric errors and error sensitivities, the development of geometric mapping functions, and the computation of ground

Table 1. Sensor Performance Requirements

Parameter	Value	Comments
Spectral Coverage	0.4 to 2.5 μm	Although the entire spectrum is probably not required for any one discipline, in the aggregate of all remote sensing disciplines, the entire region is required
Spectral Sampling Interval		
VNIR (0.4 to 1.0 μm)	0.01 μm or better	
SWIR (1.0 to 2.5 μm)	0.02 μm or better	
Instantaneous Field of View	30 m	Adequate for most research topics
Swath Width	at least 10-12 km	This is adequate for research if pointing capability is provided to assure target access
Pointing Mirror Range		
Along track	at least ± 45 deg	Essential for atmospheric and BRDF (Bidirectional Reflectance Distribution Function) Studies
Cross track	not more than ± 25 deg	
Radiometric Performance (NEdR)		
VNIR	≤ 0.5%	
SWIR	≤ 1.0%	

pattern distortions. The results are translated into many tables, plots, and patterns for visual apprehension. It is believed that the results reported here are important for design, trade-off, and performance prediction.

B. APPROACH

This study has been performed in four progressive stages as shown in block diagram form in Fig. 1. In Stage I, the error sources were identified, dynamic disturbances and the Space Shuttle error dynamics were modeled, and the error power spectral densities for two in-orbit configurations were developed. Stage II of this study concentrated on the development of geometric error mapping functions and error sensitivity analysis. Geometric errors due to ephemeris uncertainties, attitude deviations, earth rotation, etc., were studied. In Stage III, ground pattern image distortions caused by various error effects and forward and side looking angular offsets, altitude change, and effect of earth rotation were generated. Stage IV consists of the analysis of the imaging spectrometer instrument errors. These errors include optical jitter, nonlinearities, processing errors, and repeatability. The study of Stages I, II, and III has been completed and the results are included in this report. The study called for by Stage IV has not been planned. It is emphasized here that the imaging spectrometer error model development is an important step for the overall performance prediction and design of the imaging spectrometer system.

Major findings of this work are summarized in the following subsection. In Section II, the orbital and imaging spectrometer configurations are described. The attitude dynamics and error power spectral densities are documented in Section III; and parametric analysis of geometric errors are treated in Section IV. Section V deals with the ground pattern image distortions. Conclusions are summarized in Section VI.

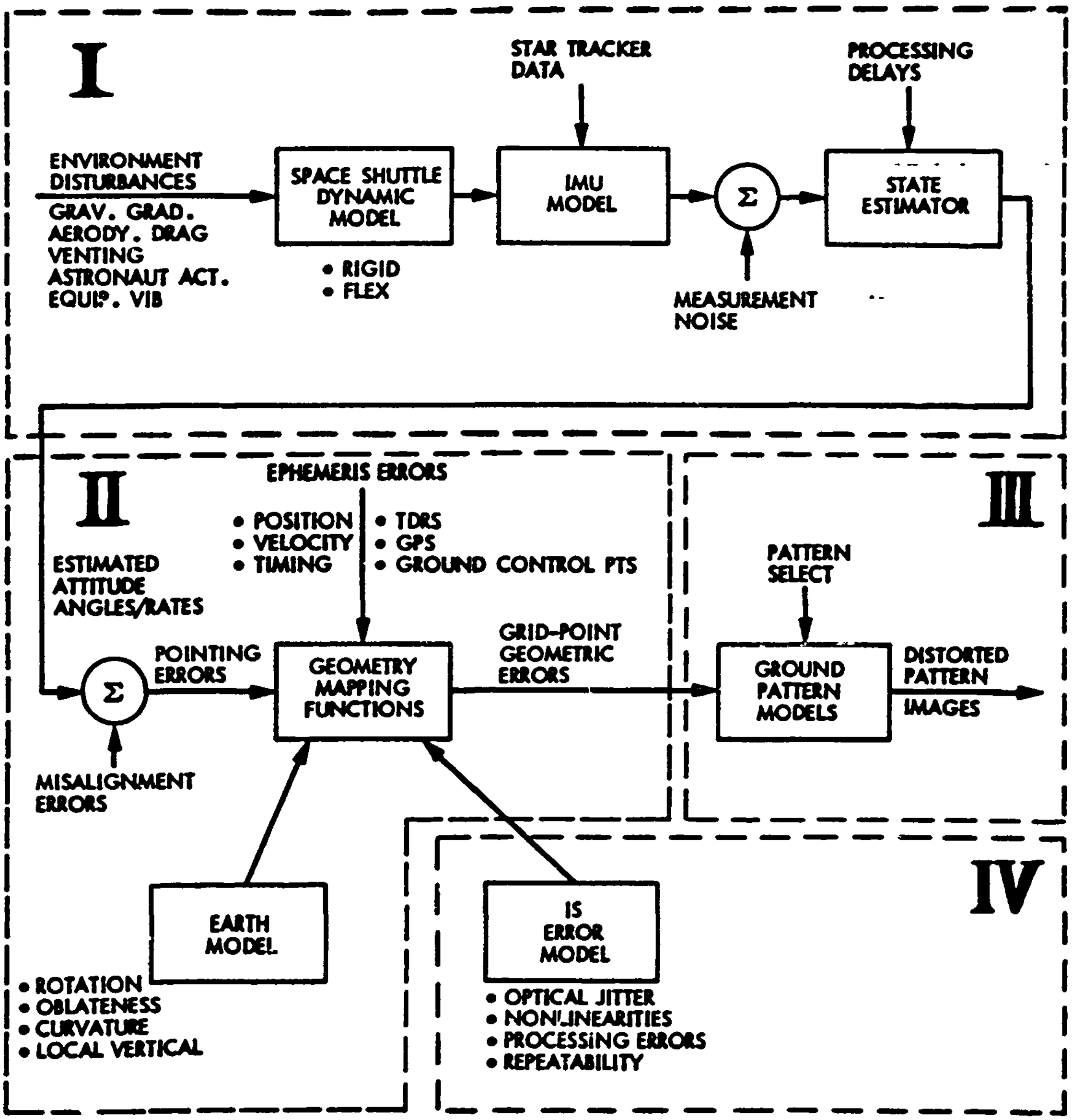

Figure 1. IS Error Analysis System Block Diagram

C. SUMMARY OF MAJOR FINDINGS

The following is a summary of major findings. The details of these are treated in the sections to follow.

1. The results show that the IS Experiment with image pickup period of 20 seconds at a time is feasible with the shuttle properly phased inside the control deadband. The error PSD (power spectral density) characteristic reveals that the system resonates at very low frequencies (in the 10^{-5} to 10^{-2} Hz region). Excitations at these frequencies must be avoided through design precautions. The analysis also showed that errors below 0.01 Hz are dominated by the shuttle dynamics reacting to disturbances, whereas those above 0.01 Hz are dominated by the shuttle inertial measurement system uncertainties and its inherent noise. These high frequency errors limit pointing performance and result in a one-sigma ground track error of 54.8 meters per axis. One-sigma rate errors are shown to be less than 4 meters per second per axis in the frequency range of 10^{-5} to 4×10^{-2} Hz. The image smear is not significant because of the short millisecond-level line time.
2. The effects of earth curvature are very small for the application here (see Fig. 42).
3. Altitude uncertainties cause only moderate geometric errors. The worst 1σ geometric errors are 11.71 m in position and 0.133 m/sec in rate with STDN and large unmodeled perturbations at 200 km orbit. The performance improves with TDRSS. For the 300 km orbit and with small unmodeled perturbations, the 1σ geometric errors will reduce to 0.22m and 0.0032 m/sec (see Table 11).

4. The effects of other navigation errors are significantly greater. The 1σ downtrack errors range from 203m (300 km orbit) to 8128m (200 km orbit); and those for the crosstrack are 152m to 508m (see Table 12).
5. The effects of roll and pitch attitude errors are relatively large compared with, for instance, those caused by yaw errors and altitude uncertainties. The error sensitivity is 1.94 m/arc sec or approximately 7000 m/degree. The yaw sensitivity is 0 for 0° view angle and 0.028 m/arc sec for the maximum view angle of $\pm 0.825^{\circ}$ (see Table 13).
6. The error sensitivities of attitude errors increase significantly for large attitude offsets. For 20° side looking, the sensitivity increases to 2.28 m/arc sec for roll errors and to 0.75 m/arc sec for yaw errors and the pitch error sensitivity is almost unaffected. For the 45° forward looking case, the sensitivities for the pitch, roll, and yaw errors increase to 2.83, 4.36, and 1.97 m/arc sec, respectively (see Table 13).
7. The performance of the Shuttle Imaging Spectrometer is limited by the Shuttle IMU (Inertial Measuring Unit) accuracy, instrument misalignment, etc., Shuttle RCS (Reaction Control Subsystem) deadband, etc. unless some means of error reduction are employed. For instance, ground control points may be used to reduce navigation prediction errors; and precision point mounts, such as AGS (ASPS* Gimbal System) and IPS (Instrument Pointing System), may be used to reduce the

*Annular Suspension Pointing System

attitude errors.

The single axis geometric errors due to the combined Shuttle/IS misalignment, for instance, for normal nadir pointing, 20° side looking, and 45° forward looking are 169m, 198m, and 379m, respectively (refer to Table 10 for detailed breakdowns).

8. Earth rotation causes shifts of images toward the direction of rotation. The magnitude of this shift depends on the latitude of the object. For instance, at the equator the object moves approximately 462m in one second (for 400 km orbit), and at 60° latitude it moves only 231m in one second.

II. ORBITAL AND IMAGING SPECTROMETER CONFIGURATIONS

A. SHUTTLE NOMINAL FLIGHT CONFIGURATIONS

Two shuttle in-orbit configurations have been considered, the Payload-Bay Nadir and the Nose-Down Nadir, as illustrated in Figures 2 and 3, respectively. It will be shown later that the Nose-Down Configuration is gravity gradient stabilized and the Payload-Bay Nadir Configuration is not. However, the Payload-Bay Nadir Configuration offers simpler instrument mounting and less aerodynamic drag. Besides, for certain experiments that require large forward looking angles, the Nose-Down Configuration will be unsuitable.

A circular orbit of 400 km altitude has been selected for this analysis. This selection is consistent with the SIS-B parameters.*

There are a number of possible instrument mounting options that will affect the pointing and the geometric errors of the instrument. These options include:

a) Direct mount

b) AGS (ASPS Gimbal System) mount

c) IPS (Instrument Pointing System) mount

Since both the AGS and IPS systems are capable of providing precision payload pointing and measurements, the system performance will be improved at the expense of significant extra cost. The direct mount approach is the least complex and most cost effective, provided that the errors are within the tolerance. In this report the direct mount approach is considered. Furthermore, the shuttle IMU

---

*During the period when this part of the work was performed, SIS-B (Shuttle Imaging Spectrometer-Configuration B) was considered. However, the methods used here are mostly generic, and hence, can be applied to systems of similar configurations.

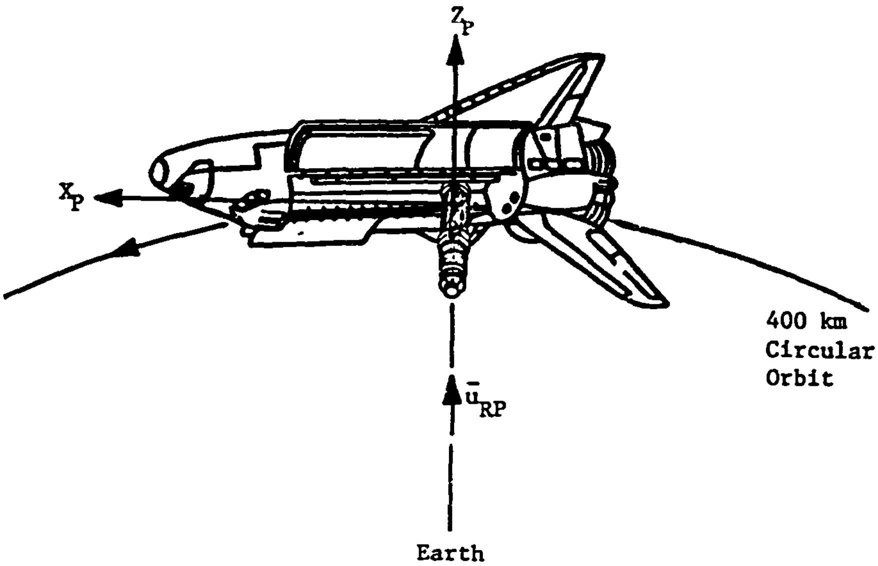

Figure 2. Payload-Bay Nadir Pointing Configuration (A)

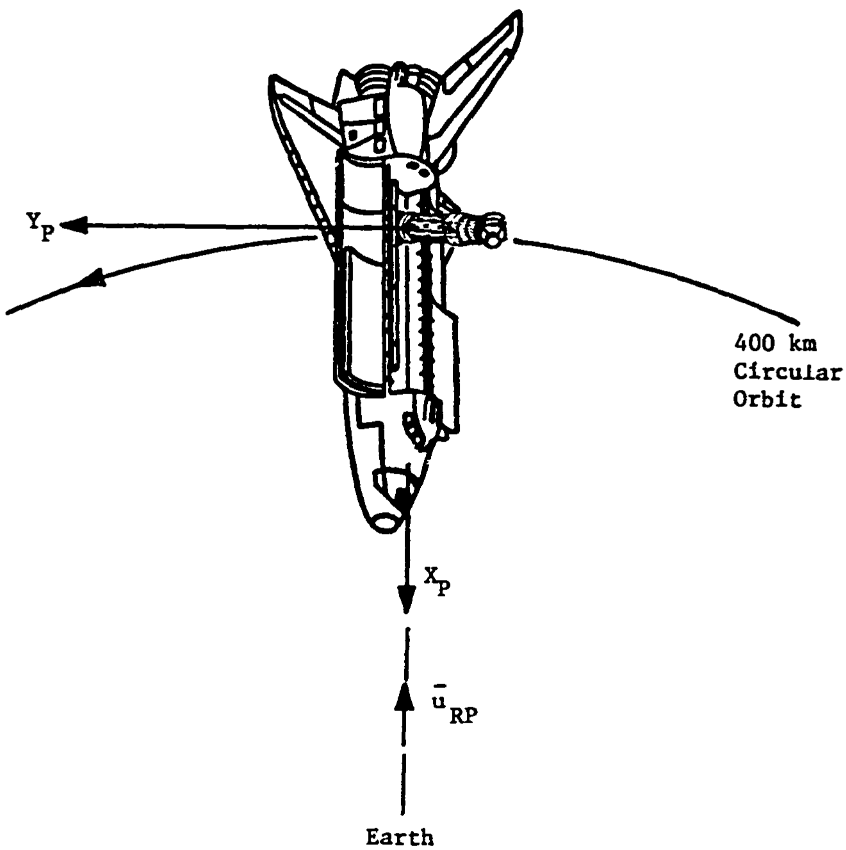

Figure 3. Nose-Down Nadir Pointing Configuration (B)

(Inertial Measurement Unit) and the shuttle state estimator unit are used for obtaining attitude and rate information, without additional instrumentation. Other options may be studied in the future if necessary.

B. IMAGING SPECTROMETER SYSTEM DESCRIPTION

In order to correlate the analysis reported here to the IS applications, it is desirable to understand the basic operating principle of the IS instrument. Figure 4 shows a sketch of the basic elements of the IS, except the memory banks, registers, and the processors. Some of the IS parameters that are relevant to the geometric error analysis, along with definitions of the IS terminologies, are also listed in Fig. 4. It is understood that the sketch and the parameter values used are for illustrative purposes only since the parameters may change as the development of the IS system is finalized.

Referring to Fig. 4, as the reflection from the ground objects passes through a narrow slit, it strikes the incident surface of the prism. The prism separates the incident light into spectral images projected onto an area array of light detectors. The area array consists of 384 linear arrays, corresponding to 384 spectral channels. Each linear array consists of 384 detector elements. Each detector element corresponds to an image area of 30m x 30m on the ground. Hence, each linear array corresponds to an image of a specific spectral channel of the same ground area of 30m (along-track) x 11520m (cross-track). This 11.52 km cross-track measure, referred to as the swath width, defines the IS coverage for each orbit pass. The 30m x 30m area is referred to as the pixel (picture element) which defines the resolution of the image, i.e., within this element no features can be resolved. The IS is operated based on a push broom principle. That is, a specific detector element on the instrument (moving with the spacecraft) collects photons from the 30m x 30m moving window for a specific period

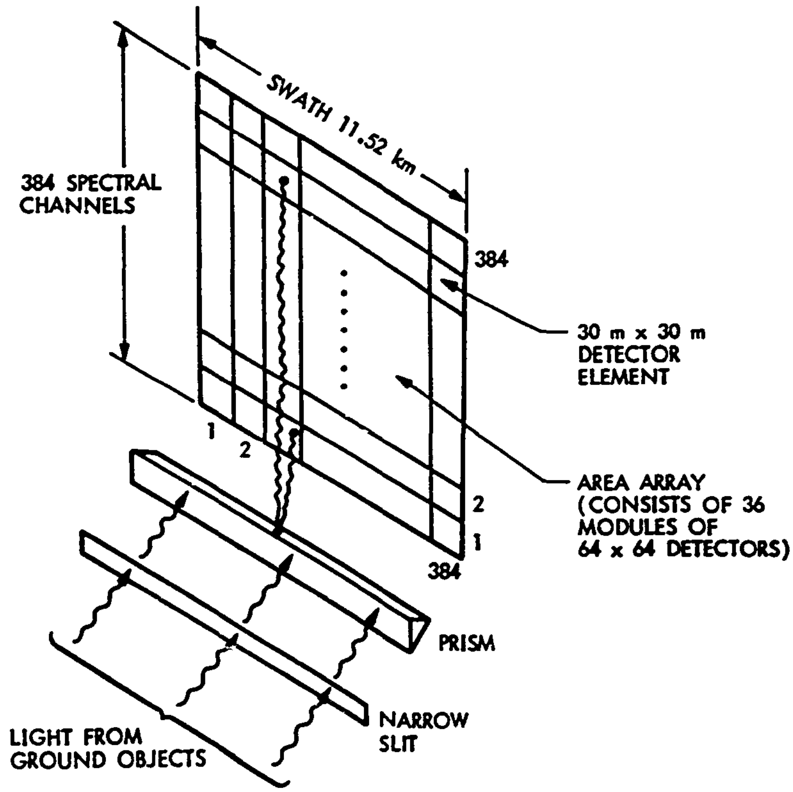

KEY PARAMETERS

- LINE TIME = 4 ms
- SPECTRUM:
  VISIBLE REGION 0.4 - 1.0 μm
  SHORT WAVELENGTH IR 1.0 - 2.5 μm
- FIELD OF VIEW: ± 0.825°
- SWATH WIDTH: 11.52 km
- POINTING ANGLES (RANGE):
  ± 45° (PITCH)
  ± 20° (ROLL)
- ORBIT: 400 km CIRCULAR

DEFINITIONS

GIFOV (GROUND INSTANTANEOUS FIELD OF VIEW): PROJECTION ON THE GROUND OF EACH SQUARE DETECTOR

LINE TIME: TIME TO MOVE ALONG THE GROUND A DISTANCE OF 1 GIFOV

DN: DATA NUMBER, THE "BRIGHTNESS" OF OF THE ASSOCIATED PIXEL

PIXEL: PICTURE ELEMENT (30 m x 30 m HERE, IT DEFINES THE RESOLUTION OF THE IMAGE)

SWIR: SHORT WAVE LENGTH IR

VIS: VISIBLE WAVE LENGTH

Figure 4. Imaging Spectrometer Basic Operating Principles

of time called the line time. The line time in this case is the time required to move 30m along-track, which is determined by the orbit. For a 400 km circular orbit, it is about 4 ms. At the end of each line time, the total number of photons collected by each detector is recorded and processed and the detector/register is reset and a new 4 ms cycle is repeated. For digital processing, the amount of light collected by a collector is assigned a number called DN (data number), which is proportional to the number of photons accumulated. Therefore, the processor has to record and process 384 x 384, or approximately 1.475×10^5 DN's every 4 ms.

As the shuttle flies over an area, banks after banks of DN's are collected. By spacing the banks of DN's 30m apart, the features of the ground image emerge. The ratios of the DN's of various channels for the same area are of special interest, as these ratios are closely correlated to geological and ecological states of the earth including mineral deposits, forestry, crops,

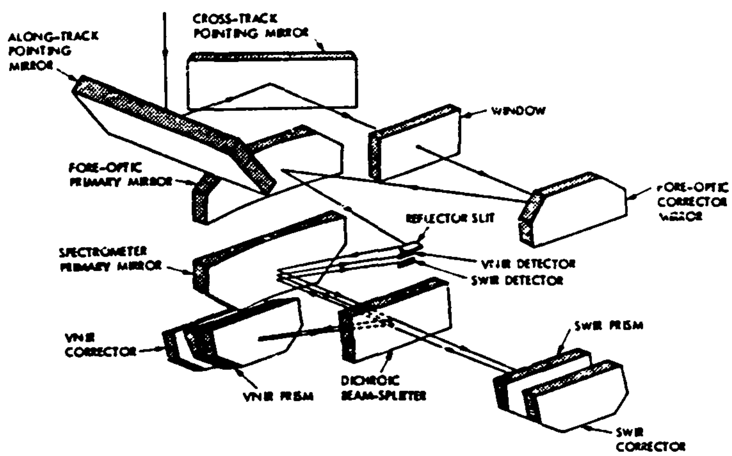

Figure 5. Shuttle Imaging Spectrometer Optical System Configuration

disease and insect infestations, land and soil erosion, precipitation in the form of snow and ice, air and water quality, etc.

The Imaging Spectrometer optical system configuration and the arrangement of lenses, mirrors, slit, prisms, focal plane detector, etc. are shown in Fig.5 [2]. Additional information on the instrument design and requirements can be found in Refs. 2 and 3.

III. ERROR SOURCES AND SHUTTLE ATTITUDE DYNAMICS

A. ERROR SOURCES

There are two types of errors that are important to the imaging spectrometer experiment — the direct errors and the derived errors. The direct errors are those pertaining to the spacecraft and instrument pointing, ephemeris, and instrument errors as shown in Fig. 6. The derived errors are the geometric errors and pattern distortions of ground objects which result from the direct errors and the effects of earth rotation, curvature, oblateness, and local vertical uncertainties. Fig. 1 shows relationships of the error sources and the system dynamics.

- ATTITUDE DEVIATIONS, RATE ERRORS AND STRUCTURAL VIBRATION
- MEASUREMENT NOISE AND DRIFT
- MISALIGNMENT OF SHUTTLE IMU AND ATTITUDE REFERENCE FRAME
- MISALIGNMENT BETWEEN SHUTTLE AND IS INSTRUMENT REFERENCES
- EPHEMERIS PREDICTION ERRORS
- EARTH ROTATION, CURVATURE, AND OBLATENESS
- IS INSTRUMENT ERRORS INCLUDING
  - OPTICAL JITTER
  - NONLINEARITIES
  - PROCESSING
  - REPEATABILITY

Figure 6. Error Sources

In this section, the steady state analysis is performed in the frequency domain. The PSD (power spectral density) for the pointing errors and the rate errors were obtained by considering the dynamics of the Space Shuttle Orbiter, the IMU (Inertial Measurement Unit), the attitude control state estimator, the measurement noise, the misalignment of reference frames, and the disturbances including gravity gradient, gyroscopic torques, and aerodynamic drag torques.

B. SHUTTLE MASS PROPERTY

The shuttle mass properties employed here were obtained from the Shuttle Operational Data Book [4] for OV-102/STS-3. The mass and the c.m. are, respectively:

Shuttle mass: 102,153.73 kg (224,738.21 lbs)

Shuttle c.m.: X_o = 1105.5", Y_o = 0 , Z_o = 374.3"

where the coordinates X_o, Y_o, and Z_o are the Orbiter Coordinates [5] defined in Figure 7. The moment of inertia matrix (kg-m^2) is, in the shuttle body frame (refer to Fig. 8),

$$I_B = \begin{bmatrix} 1.36 \times 10^6 & -4.69 \times 10^3 & -3.49 \times 10^5 \\ -4.69 \times 10^3 & 1.00 \times 10^7 & -3.32 \times 10^3 \\ -3.49 \times 10^5 & -3.32 \times 10^3 & 1.05 \times 10^7 \end{bmatrix}$$

$$\doteq \begin{bmatrix} 1.36 \times 10^6 & 0 & -3.49 \times 10^5 \\ 0 & 1.00 \times 10^7 & 0 \\ -3.49 \times 10^5 & 0 & 1.05 \times 10^7 \end{bmatrix} \quad (1)$$

The magnitude of the off-diagonal terms of the inertia matrix I_B suggests strong couplings exist especially between the X_B- and the Z_B-axis. To simplify the dynamic equations, it is convenient to consider principal-axis

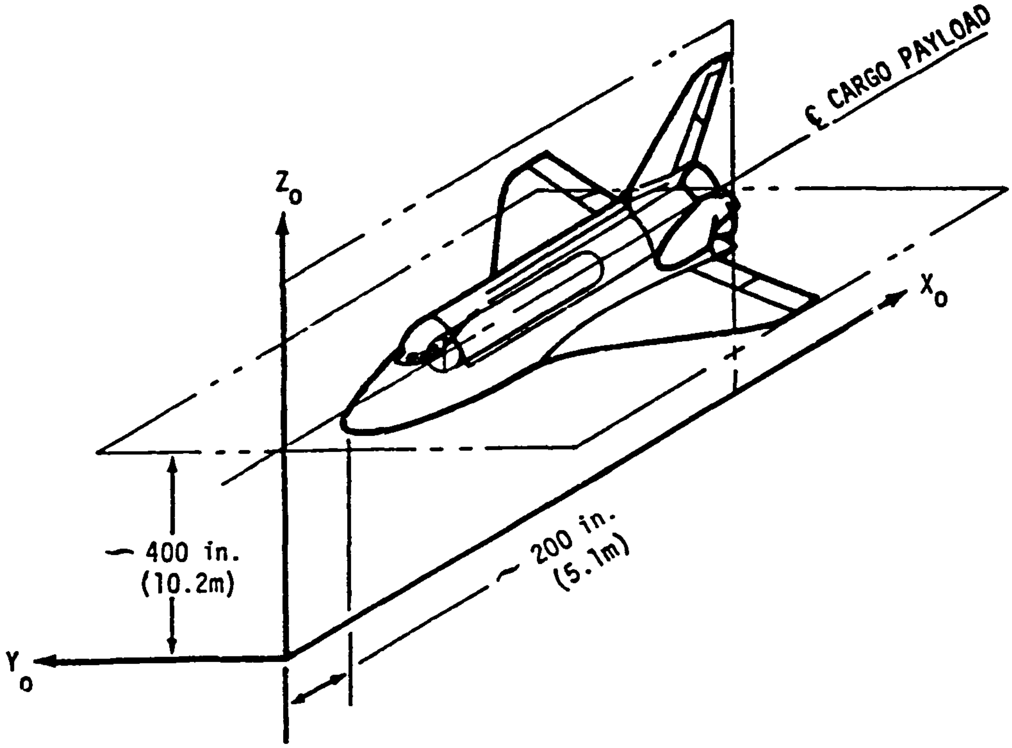

ORBITER COORDINATES

TYPE: Rotating, Orbiter referenced

ORIGIN: Approximately 200 inches (5.1m) ahead of the nose and approximately 400 inches (10.2m) below the centerline of the cargo bay

ORIENTATION AND LABELING:

The X-axis is parallel to the centerline of the cargo bay, negative in the direction of launch

The Z-axis is positive upward in landing attitude

The Y-axis completes the right-handed system

The standard subscript is 0

Figure 7. Orbiter Coordinate System

pointing instead of body-axis pointing, e.g., pointing $-Z_p$ rather than $-Z_B$ as illustrated in Figure 8.

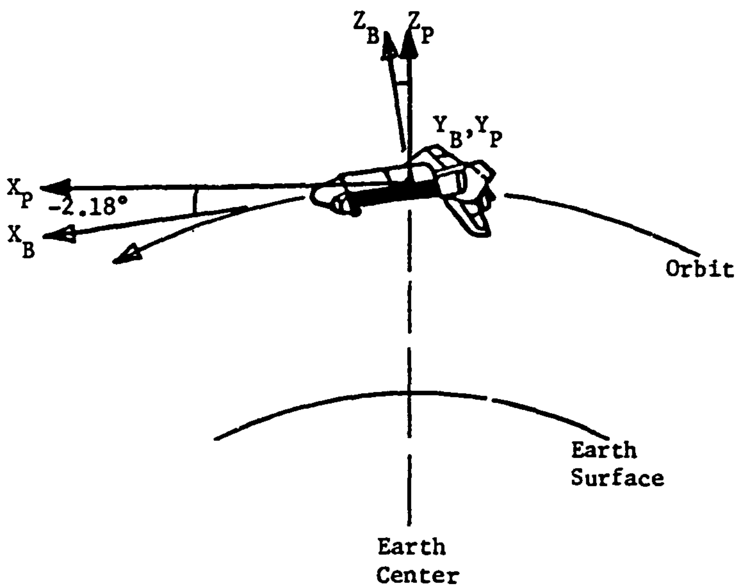

(X_B, Y_B, Z_B) -- Shuttle Body Coordinates

(X_P, Y_P, Z_P) -- Shuttle Principal Axes

Figure 8. Shuttle Body and Principal Coordinates (Payload-Bay Nadir Pointing Shown)

The orientations of the principal axes can be determined by rotating the body frame an angle α about the Y_B-axis, i.e., let $B: X_B \rightarrow X_p$, then

$$B = \begin{bmatrix} \cos\alpha & 0 & -\sin\alpha \\ 0 & 1 & 0 \\ \sin\alpha & 0 & \cos\alpha \end{bmatrix} \tag{2}$$

and

$$I_P = B\, I_B\, B^T \tag{3}$$

It can be shown that

$$\alpha = \frac{1}{2} \tan^{-1} \left(\frac{-2\, I_{BXZ}}{I_{BZZ} - I_{BXX}} \right) \tag{4}$$

provided that $I_{BXY} = I_{BYZ} = 0$.

For $I_{BXX} = 1.36 \times 10^6$ kg-m^2, $I_{BZZ} = 1.05 \times 10^7$ kg-m^2, and $I_{BXZ} = 3.49 \times 10^5$ kg-m^2, the angle $\alpha = -2.18^\circ$. Therefore, in order to do principal-axis nadir pointing, the shuttle has to rotate 2.18° about the orbit normal (see Figure 8). The moments of inertia about the principal axes are

$$I_P \cong \text{diag}\ (1.38 \times 10^6,\ 1.00 \times 10^7,\ 1.05 \times 10^7),\ \text{kg-m}^2.$$

C. ASSESSMENT OF DISTURBANCES

The shuttle motion is characterized in part by the environmental disturbances, the major sources of which are the aerodynamic drag, gravity gradient, gyroscopic effect, solar radiation, and on-board causes such as astronaut activities, equipment vibrations, and venting. On-board activities may be partially eliminated or reduced through mission planning and their effects will be assessed in the future. In this subsection, the gyroscopic torques, the gravity gradient torques, and the aerodynamic drag torques are estimated. The solar pressure is at least one order of magnitude less than the aerodynamic drag forces and, hence, it is not included in this analysis.

C.1 The Aerodynamic Drag Torques

To estimate the aerodynamic drag torques, an approach referred to as the three-plate model [6] has been used. Referring to Figure 9, let $\bar{n}_1$, $\bar{n}_2$, and $\bar{n}_3$ be the unit normal vectors for the equivalent plates 1, 2, and 3. Where $\bar{n}_1$, $\bar{n}_2$, and $\bar{n}_3$ are in the direction of X_B-, Y_B-, and Z_B-axis, respectively. To express $\bar{n}_1$ in body frame,

$$\bar{n}_1 = \begin{bmatrix} 1 \\ 0 \\ 0 \end{bmatrix}, \bar{n}_2 = \begin{bmatrix} 0 \\ 1 \\ 0 \end{bmatrix}, \bar{n}_3 = \begin{bmatrix} 0 \\ 0 \\ 1 \end{bmatrix} \quad (5)$$

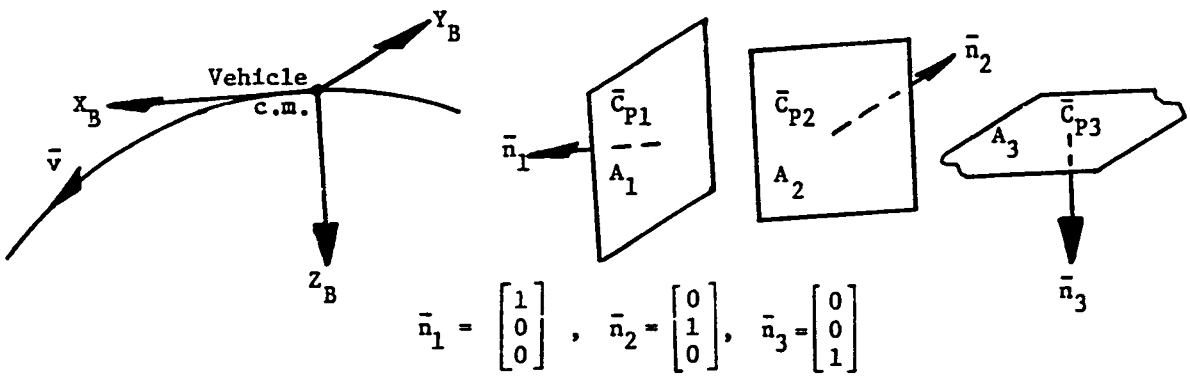

Figure 9. The Three-Plate Aerodynamic Model in Body Frame

Let A_1, A_2, and A_3 be the corresponding areas on which the aerodynamic pressure applies, and $\bar{C}_{P1}$, $\bar{C}_{P2}$, and $\bar{C}_{P3}$ the three corresponding centers of pressure, respectively. The model assumes that the aerodynamic force applies to each area in the direction opposite to the vehicle velocity vector and assumes no shading among the plates. It is further assumed that the drag coefficient C_D is constant and the lift coefficient C_L is zero.

Let $\bar{v}_B = (v_{B1}, v_{B2}, v_{B3})^T$ be the inertial velocity vector in the body frame, with magnitude v. The force and torque applied on A_i are

$$\bar{F}_{Bi} = -(\frac{1}{2} C_D \rho\, v^2 A_i) |(\bar{n}_i, \bar{u}_B)| \bar{u}_B \quad (6)$$

$$\bar{T}_{Bi} = \bar{r}_{Bi} \times \bar{F}_{Bi} = -(\frac{1}{2} C_D \rho\, v^2 A_i) |(\bar{n}_i, \bar{u}_B)| \bar{r}_{Bi} \times \bar{u}_B \quad (7)$$

where ρ is the atmospheric density at the orbital altitude, $\bar{u}_B = \bar{v}_B/v$ the unit velocity vector, and r_{Bi} the vectors of the center of pressure of A_i relative to the vehicle center of mass.

The total aerodynamic forces and torques on the vehicle are

$$\overline{F}_B = \sum_{i=1}^{3} - (\frac{1}{2} C_D \rho \, v^2 \, A_i) \, | \, (\overline{n}_i, \overline{u}_B) \, | \, \overline{u}_B \tag{8}$$

$$\overline{T}_B = \sum_{i=1}^{3} - (\frac{1}{2} C_D \rho \, v^2 \, A_i) \, | \, (\overline{n}_i, \overline{u}_B) \, | \, \overline{r}_{Bi} \times \overline{u}_B \tag{9}$$

The value of C_D depends on the shape of the vehicle. In Ref. 7, the values of 2.5 to 3.0 were suggested. The value of $C_D = 2.0$ is used here as it was used in Ref. 6 for Space Shuttle Simulation.

The atmospheric mass density ρ can be found in a JPL internal memorandum. For 1985 mission time, the peak density is expected to occur in April for the 400 km orbit; the densities are

2.64×10^{-12} kg/m^3 (predicted)

and

3.77×10^{-12} kg/m^3 (97.7 percentile)

The orbital velocity v for a 400 km circular orbit is computed as $v = 7669.60$ m/sec or $v^2 = 5.882 \times 10^7$ (m/sec)^2.

The plate areas, according to the attachment (SSFS On-Orbit Aero Data, 7/24/80) to Ref. 6, with Cargo Bay doors open, are

$$\begin{aligned} A_1 &= 119.45 \text{ m}^2 \\ A_2 &= 229.92 \text{ m}^2 \\ A_3 &= 454.46 \text{ m}^2 \end{aligned} \tag{10}$$

However, a different set of values are given in Ref. 8.

$$\begin{aligned} A_1 &= 64.1 \text{ m}^2 \\ A_2 &= 212.7 \text{ m}^2 \\ A_3 &= 367.0 \text{ m}^2 \end{aligned} \tag{11}$$

The values in (10) were used in this work.

The position vectors $\bar{r}_{Bi}$ may be obtained using data given in Ref. 4 and Ref. 6. The values are,

$$\bar{r}_{B1} = \begin{bmatrix} 3.797 \\ 0 \\ -.231 \end{bmatrix} \text{m}$$

$$\bar{r}_{B2} = \begin{bmatrix} .927 \\ 0 \\ -.742 \end{bmatrix} \text{m} \qquad (12)$$

$$\bar{r}_{B3} = \begin{bmatrix} 1.166 \\ 0 \\ -1.074 \end{bmatrix} \text{m}$$

The torques $\bar{T}_{Bi}$ for the predicted density, are

$$\bar{T}_{B1} = -1.855 \times 10^{-2}|u_{B1}| \begin{bmatrix} -r_{B13}u_{B2} + r_{B12}u_{B3} \\ r_{B13}u_{B1} + r_{B11}u_{B3} \\ -r_{B12}u_{B1} + r_{B11}u_{B2} \end{bmatrix}$$

$$\bar{T}_{B2} = -3.570 \times 10^{-2}|u_{B2}| \begin{bmatrix} -r_{B23}u_{B2} + r_{B22}u_{B3} \\ r_{B23}u_{B1} - r_{B21}u_{B3} \\ -r_{B22}u_{B1} + r_{B21}u_{B2} \end{bmatrix} \qquad (13)$$

$$\bar{T}_{B3} = -7.057 \times 10^{-2}|u_{B3}| \begin{bmatrix} -r_{B33}u_{B2} + r_{B32}u_{B3} \\ r_{B33}u_{31} - r_{B31}u_{B3} \\ -r_{B32}u_{Bi} + r_{B31}u_{B2} \end{bmatrix}$$

In Eq. (13), the torques are known once the unit velocity vector $\bar{u}_B$ is specified; $\bar{u}_B$ varies with the pointing configuration and spacecraft attitude.

C.1.1. Drag Torques for Configuration A

Referring to Fig. 2, since this is "$-Z_P$" pointing, for nominal attitude, the vehicle moves in the X_P direction. Let $\bar{u}_P$ be the unit velocity vector in the P-frame and let A_α be the rotation matrix due to α, then

$$\bar{u}_B = A_\alpha^T \bar{u}_P = \begin{bmatrix} \cos\alpha & 0 & \sin\alpha \\ 0 & 1 & 0 \\ -\sin\alpha & 0 & \cos\alpha \end{bmatrix} \begin{bmatrix} 1 \\ 0 \\ 0 \end{bmatrix}$$

$$= \begin{bmatrix} \cos\alpha \\ 0 \\ -\sin\alpha \end{bmatrix} \tag{14}$$

Since $\alpha (= -2.18^\circ = -.038 \text{ rad})$ is small,

$$\bar{u}_B \doteq \begin{bmatrix} 1 \\ 0 \\ -\alpha \end{bmatrix} \tag{15}$$

Using Eqs. (12), (13), and (15), and

$$\bar{T}_P = \sum_{i=1}^{3} A_\alpha \bar{T}_{Bi} \tag{16}$$

the torques in the P-Frame, for nominal attitude, are

$$\bar{T}_P = \begin{bmatrix} 0 \\ 9.84 \times 10^{-3} \\ 0 \end{bmatrix} \quad \text{N-m} \tag{17}$$

For small attitude errors, φ, θ, and ψ, from the rotating orbital frame,

$$\bar{u}_P = A \begin{bmatrix} 1 \\ 0 \\ 0 \end{bmatrix} \tag{18}$$

where,

$$\tilde{A} = \begin{bmatrix} 1 & \psi & -\theta \\ -\psi & 1 & \phi \\ \theta & -\phi & 1 \end{bmatrix}$$

and

$$\bar{u}_B = A_\alpha^T \tilde{A} \begin{bmatrix} 1 \\ 0 \\ 0 \end{bmatrix} \qquad (20)$$

Using Eqs. (12), (13), and (20), the predicted aerodynamic torques become, by retaining only the first order terms, in N-m,

$$\bar{T}_P = \sum_{i=1}^{3} A_\alpha \bar{T}_{Bi} \qquad (21)$$

$$= \begin{bmatrix} 4.29 \times 10^{-3} \psi \\ 4.29 \times 10^{-3} + 7.04 \times 10^{-2} (\theta-\alpha) + 7.58 \times 10^{-2} |\theta-\alpha| + 2.65 \times 10^{-2} |\psi| \\ 7.04 \times 10^{-2} \phi \end{bmatrix}$$

C.1.2. Drag Torques for Configuration B

Referring to Figure 3, under this configuration, X_P is in the Nadir direction and Y_P is in the direction of motion for nominal attitude. In this case,

$$\bar{u}_P = \begin{bmatrix} 0 \\ 1 \\ 0 \end{bmatrix} \qquad (22)$$

$$\bar{u}_B = A_\alpha^T \bar{u}_P = \begin{bmatrix} 0 \\ 1 \\ 0 \end{bmatrix} \qquad (23)$$

and from Eqs. (12), (13), and (23),

$$\bar{T}_P = \sum_{i=1}^{3} A_\alpha \bar{T}_{Bi}$$

$$= \begin{bmatrix} -3.96 \times 10^{-2} \\ 0 \\ -4.53 \times 10^{-2} \end{bmatrix} \text{ N-m} \qquad (24)$$

In the presence of small attitude errors, ϕ, θ, and ψ, the aerodynamic drag torques are

$$\bar{T}_P = \begin{bmatrix} -2.45 \times 10^{-2} - 7.58 \times 10^{-2}|\phi| - 4.29 \times 10^{-3}|\phi| + 3.31 \times 10^{-2}\alpha \\ -3.31 \times 10^{-2}\phi + 2.65 \times 10^{-2}\psi \qquad (25) \\ -(3.31 \times 10^{-2} + 8.23 \times 10^{-2}|\phi| + 7.04 \times 10^{-2}|\psi| + 2.65 \times 10^{-2}\alpha) \end{bmatrix} \qquad (25)$$

C.1.3. Estimation of Disturbance PSD

Before the PSD's are estimated, the uncertainty part of the disturbance torques has to be determined. The torques of Eqs. (21) and (25) consist of static parts and the dynamic parts. The dynamic parts are functions of the attitude errors ϕ, θ, and ψ. The attitude errors are assumed to be random and time-varying with standard deviation of 1° (.01745 rad.) per axis. Therefore, the estimated values of the random disturbance torques are, for Configuration A

$$\bar{\sigma}_{T_{PA}} = \begin{bmatrix} 7.48 \times 10^{-5} \\ 1.86 \times 10^{-3} \\ 1.23 \times 10^{-3} \end{bmatrix} \text{ N-m} \qquad (26)$$

and that for Configuration B are,

$$\bar{\sigma}_{T_{PB}} = \begin{bmatrix} 1.33 \times 10^{-3} \\ 7.40 \times 10^{-4} \\ 1.89 \times 10^{-3} \end{bmatrix} \text{ N-m} \qquad (27)$$

and the corresponding PSD's are obtained by the following approximation with the correlation time of T = 180 seconds,

$$Q_{T_{PA}} = 2T\ (\bar{\sigma}^2_{T_{PA}})$$

$$= \begin{bmatrix} 2.01 \times 10^{-6} \\ 1.25 \times 10^{-3} \\ 5.44 \times 10^{-4} \end{bmatrix} \quad (N\text{-}m)^2 - sec \qquad (28)$$

$$\bar{Q}_{T_{PB}} = 2T\,(\bar{\sigma}^2_{T_{PB}})$$

$$= \begin{bmatrix} 6.32 \times 10^{-4} \\ 1.97 \times 10^{-4} \\ 1.29 \times 10^{-3} \end{bmatrix} \quad (N\text{-}m)^2 - sec \qquad (29)$$

C.2 The Gravity Gradient Torques and Gyroscopic Torques

The gravity gradient torques and the gyroscopic torques can be estimated using the following equations, respectively:

$$\bar{T}_{gP} = 3\omega_o^2\, \tilde{u}_{RP}\, I_P\, \bar{u}_{RP} \qquad (30)$$

and

$$\bar{T}_{GRP} = \bar{\omega}_{oP} \times \bar{H}_P = \tilde{\omega}_{oP}\, I_P\, \bar{\omega}_{oP} \qquad (31)$$

Where $\bar{u}_{RP}$ and $\bar{\omega}_{oP}$ are the unit earth vector and the spin velocity vector, respectively, in principal frame, and $\tilde{u}_{RP}$ is the skew symmetric matrix of the vector $\bar{u}_{RP}$. For Configuration A,

$$\bar{u}_{RP} = A \begin{bmatrix} 0 \\ 0 \\ 1 \end{bmatrix} \qquad (32a)$$

$$\bar{\omega}_{oP} = \begin{bmatrix} 0 \\ 1 \\ 0 \end{bmatrix} \omega_o \qquad (32b)$$

and for Configuration B,

$$\bar{u}_{RP} = A \begin{bmatrix} -1 \\ 0 \\ 0 \end{bmatrix} \quad (33a)$$

$$\bar{\omega}_{oP} = A \begin{bmatrix} 0 \\ 0 \\ -1 \end{bmatrix} \omega_o \quad (33b)$$

the corresponding torques, to include only the first order effect, are, for Configuration A

$$\bar{T}_{gP} = 3\,\omega_o^2 \begin{bmatrix} (I_{PZZ} - I_{PYY})\phi \\ (I_{PZZ} - I_{PXX})\theta \\ 0 \end{bmatrix} = \begin{bmatrix} 1.92\ \phi \\ 33.11\ \theta \\ 0 \end{bmatrix} \text{N-m} \quad (34a)$$

$$\bar{T}_{GRP} = \omega_o^2 \begin{bmatrix} -(I_{PZZ} - I_{PYY})\phi \\ 0 \\ (I_{PYY} - I_{PXX})\psi \end{bmatrix} = \begin{bmatrix} -.64\ \theta \\ 0 \\ 11.04\ \psi \end{bmatrix} \quad (34b)$$

and for Configuration B

$$\bar{T}_{gP} = -\,3\,\omega_o^2 \begin{bmatrix} 0 \\ (I_{PZZ} - I_{PXX})\theta \\ (I_{PXX} - I_{PYY})\psi \end{bmatrix} = \begin{bmatrix} 0 \\ -\ 35.03\ \theta \\ 43.71\ \psi \end{bmatrix} \quad (35a)$$

$$\bar{T}_{GRP} = \omega_o^2 \begin{bmatrix} -(I_{PZZ} - I_{PYY})\phi \\ (I_{PZZ} - I_{PXX})\theta \\ 0 \end{bmatrix} = \begin{bmatrix} -.64\ \phi \\ 11.68\ \theta \\ 0 \end{bmatrix} \quad (35b)$$

Since the gravity gradient torques and gyroscopic torques are proportional to the attitude errors, they may be included in the equations of motion as part of the vehicle dynamics rather than disturbances to the plant.

D. THE MISALIGNMENT AND MEASUREMENT NOISE

In this subsection, the errors that will contribute to pointing uncertainties are estimated. These error sources include the misalignment errors of the IMU and the IS instrument, and the sensor noise.

D.1 The Misalignment Errors

Let b_{MS} be the misalignment between the IMU and the shuttle reference frame; let b_{SI} be the misalignment between the shuttle and the imaging spectrometer reference frame.

Based on the space shuttle performance requirement [5], the IMU 3σ misalignment uncertainty is $\pm .133^{o}$/axis, hence,

$$\sigma_{bMS} = .044^{o}/\text{axis} = 159.6 \ \text{arc-sec/axis} \qquad (36a)$$

However, based on a JPL internal memorandum, the shuttle flight test performance is much better,

$$\sigma_{bMS} = 82 \ \text{arc-sec/axis} \qquad (36b)$$

The performance data Eq. (36b) was used in this report.

The misalignment data for the IS instrument is not directly available. Based on Ref. 9, the estimated LANDSAT D initial alignment bias between the sensor optical axis and the vehicle pointing vector was ± 200 arc-sec. The alignment bias can be measured before launch and can be removed from the image data. The variation part that cannot be removed without ground control points was estimated as ± 30 arc-sec. This latter number was used in this work,

$$\sigma_{b_{SI}} = 30 \ \text{arc-sec/axis} \qquad (37)$$

Therefore, the total misalignment error becomes

$$\sigma_{b_o} = (\sigma_{b_{MS}}^2 + \sigma_{b_{SI}}^2)^{1/2}$$

$$= 87.32 \ \text{arc-sec.} \qquad (38)$$

D.2 The IMU Model

The sensor dynamics for the shuttle IMU was modeled approximately by the first order low pass filter as shown in Figure 10.

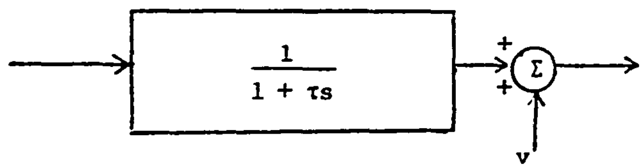

Figure 10. Simplified IMU Model

Where τ is the time constant and v the white gaussian noise. The time constant was estimated from a DRIRU II Model,

$$\tau = \frac{1}{\omega_s} = \frac{1}{14\pi} = .023 \text{ sec} \qquad (39)$$

That is, this measurement is assumed to have a 7 Hz bandwidth.

To determine v, from Ref. 5, the 3σ IMU readout error is $\pm .073^{\circ}$/axis. Assume that the measurement noise is the readout error, then

$$\sigma_v = .0243^{\circ}/\text{axis} = 87.6 \text{ arc-sec/axis} \qquad (40)$$

However, the actual performance of the shuttle IMU was much better; it has a 1σ gyro resolution error (σ_{RESO}) of 20 arc-sec/axis. If we assume the random noise has the same amplitude as that of the resolution noise, then

$$\sigma_v = \sqrt{2}\,\sigma_{RESO} \qquad (41)$$

The corresponding measurement noise PSD, R, is estimated as,

$$R \simeq 2\left(\frac{1}{14\pi}\right)\sigma_v^2$$

$$= 8.55 \times 10^{-10} \text{ (rad)}^2\text{-sec} \qquad (42)$$

E. SHUTTLE DYNAMICS AND INSTRUMENT POINTING ERRORS

E.1 The Equations of Motion

Consider Configuration A. For simplicity, the subscript P for principal axes is dropped from all equations. Again, let ϕ, θ, and ψ be the small roll, pitch, and yaw angles, respectively. Let $\bar{\omega} = (\omega_X, \omega_Y, \omega_Z)^T$ be the angular velocity vector of the shuttle, then for small attitude errors,

$$\begin{aligned} \omega_X &= \dot{\phi} + \psi\, \omega_o \\ \omega_Y &= \dot{\theta} + \omega_o \\ \omega_Z &= \dot{\psi} - \phi\, \omega_o \end{aligned} \tag{43}$$

and

$$\begin{aligned} \dot{\omega}_X &= \ddot{\phi} + \dot{\psi}\, \omega_o \\ \dot{\omega}_Y &= \ddot{\theta} \\ \dot{\omega}_Z &= \ddot{\psi} - \dot{\phi}\, \omega_o \end{aligned} \tag{44}$$

With this simplified relation between the inertial rates and the attitude error rates, one can show that the equations of motion may be summarized as follows, accounting only for first order effects:

$$\begin{bmatrix} I_X\ddot{\phi} + (I_X - I_Y + I_Z)\, \omega_o\dot{\psi} + 4\,(I_Y - I_Z)\, \omega_o^2\phi \\ I_Y\ddot{\theta} + 3\,(I_X - I_Z)\, \omega_o^2\theta \\ I_Z\ddot{\psi} - (I_X - I_Y + I_Z)\, \omega_o\dot{\phi} - (I_X - I_Y)\, \omega_o^2\psi \end{bmatrix} = \bar{T}_d + \bar{T}_c \tag{45}$$

The left-hand side of Eq. (45) accounts for the body dynamics and the gravity gradient and the gyroscopic torques; and on the right-hand side of Eq. (45) $\bar{T}_d$ and $\bar{T}_c$ are the disturbance torques and the control torques, respectively.

E.2 The Space Shuttle State Estimator

The Shuttle State Estimator consists of two parallel Kalman-type filters, one for acceleration estimation and one for rate estimation [10]. The attitude estimate is the extrapolation of the measured attitude and the rate estimate may be approximated by using a second order filter with parameters determined by the filter gains. With the current baseline filter data, the equivalent damping coefficient and the corner frequency for the rate filter are .8 and .04 Hz (for vernier rate filter), respectively [11].

E.3 The System Pointing Errors

E.3.1. The Pitch Loop (Configuration A)

From Eq. (45) and ignoring the initial conditions, one has the following output function,

$$\theta(S) = \frac{1}{I_Y S^2 + 3\omega_o^2 (I_X - I_Z)} (T_{dY} + T_{cY}) \tag{46}$$

Figure 11 shows the open-loop block diagram for the dynamics of the instrument pointing error excited by the random disturbances. Included in the diagram are the dynamics of the vehicle, the IMU, and the rate filter. Measurement error and the misalignment error are also included.

E.3.2. The Roll and Yaw Loops (Configuration A)

The output equations for the coupled roll and yaw dynamics are, from Eq. (45)

$$\begin{bmatrix} \phi(S) \\ \psi(S) \end{bmatrix} = \frac{1}{D(S)} \begin{bmatrix} I_Z S^2 + \omega_o^2 (I_Y - I_X) & -\omega_o (I_X - I_Y + I_Z) S \\ \omega_o (I_X - I_Y + I_Z) S & I_X S^2 + 4\omega_o^2 (I_Y - I_Z) \end{bmatrix} \begin{bmatrix} T_X \\ T_Z \end{bmatrix} \tag{47}$$

where

$$D(S) = I_X I_Z S^4 + \omega_o^2 (I_X I_Z + I_Y^2 + 3 I_Y I_Z - 3 I_Z^2) S^2 + 4\omega_o^4 (I_Y - I_X)(I_Y - I_Z) \tag{48}$$

and

$$T_X = T_{cX} + T_{dX} \tag{49a}$$

$$T_Z = T_{cZ} + T_{dZ} \tag{49b}$$

Figure 12 shows the block diagram for the roll and yaw instrument error dynamics. The block diagrams for the pitch and the roll-yaw loops are similar except for the coupling terms for the roll and yaw axes.

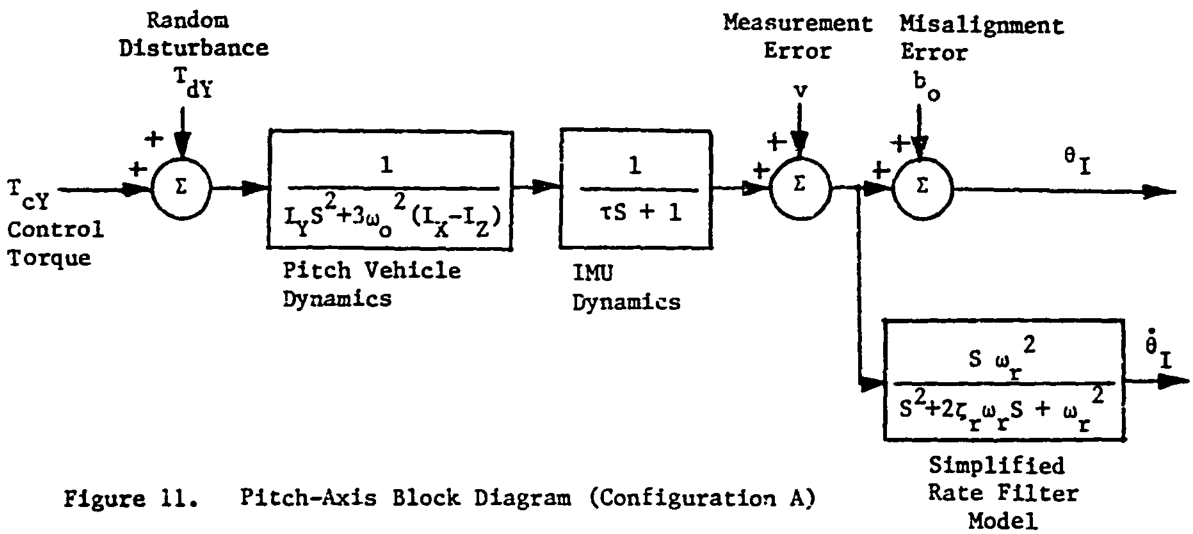

Figure 11. Pitch-Axis Block Diagram (Configuration A)

E.4 The Instrument Pointing Error PSD

E.4.1 The Pitch Error PSD (Configuration A)

The PSD's for the pitch-axis instrument pointing error and the rate error are,

$$P_\theta(\omega) = F_\theta^*(\omega)\ F_\theta(\omega)Q_Y + R + \sigma_{bo}^2\ \delta(\omega) \tag{50}$$

$$P_{\dot{\theta}}(\omega) = (F_\theta^*(\omega)\ F_\theta(\omega)Q_Y + R)\ H_r^*(\omega)\ H_r(\omega) \tag{51}$$

where $Q_Y = Q_{T_{PA}Y}$ and $Q_{T_{PA}Y}$ is the second component of Eq. (28), and where R, and σ_{bo} are defined in preceding sections, and $\delta(\omega)$ is the Dirac delta function; and where,

$$F_\theta(\omega) = G_\theta(\omega)\ H(\omega) \tag{52a}$$

$$G_\theta(\omega) = \left[\frac{1}{I_Y S^2 + 3\ \omega_o^2(I_X-I_Z)}\right]_{S=j\omega} \tag{52b}$$

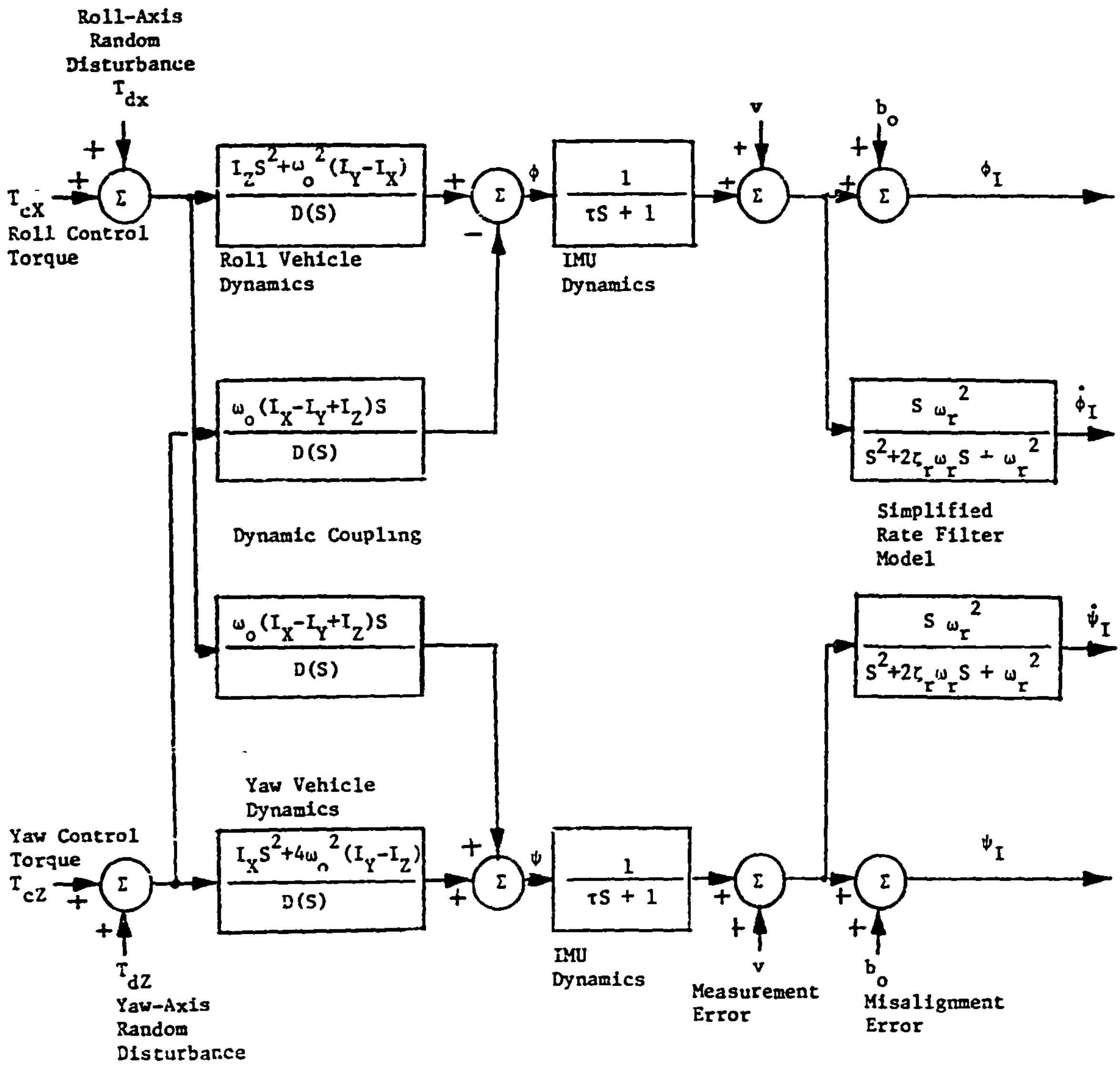

Figure 12. Roll and Yaw Axes Block Diagram. (Configuration A)

$$H(\omega) = \left[\frac{1}{\tau S + 1}\right]_{S=j\omega} \tag{52c}$$

$$F_\theta^*(\omega) = F_\theta\ (-\omega) \tag{52d}$$

$$H_r(\omega) = \left[\frac{S\ \omega_r^{\ 2}}{S^2 + 2\zeta_r\omega_r S + \omega_r^{\ 2}}\right]_{S=j\omega} \tag{52e}$$

The output power spectral density for the system is closely related to the frequency response of the system, which characterizes the steady state dynamics of the system, and, hence, it is meaningful only if the system is stable. Unfortunately, in Eq. (52b), $I_x < I_z$ which implies that the system is unstable. The destabilizing term comes from the gravity gradient because the nadir pointing axis is not the axis of minimum inertia. To proceed, one has to consider the gravity gradient as external disturbance rather than a part of the dynamics. Figure 13 shows the instrument pointing error PSD in $(\text{rad})^2$-sec as a function of frequency in Hz. Figure 14 shows the rate error PSD in $(\text{rad/sec})^2$-sec as a function of frequency.

E.4.2. The Roll and Yaw Error PSD (Configuration A)

The instrument pointing error PSD's for the roll and yaw axes are,

$$P_\phi(\omega) = F_\phi^*(\omega)\ F_\phi(\omega)\ Q_x + F_{\phi\psi}^*\ (\omega)\ F_{\phi\psi}\ (\omega)\ Q_z + R + \sigma_{bo}^2\ \delta(\omega) \tag{53a}$$

$$P_\psi(\omega) = F_\psi^*(\omega)\ F_\psi(\omega)\ Q_z + F_{\phi\psi}^*\ (\omega)\ F_{\phi\psi}\ (\omega)\ Q_x + R + \sigma_{bo}\ \delta(\omega) \tag{53b}$$

and the instrument pointing rate error PSD's for the roll and yaw axes are,

$$P_{\dot\phi}(\omega) = [F_\phi^*(\omega)\ F_\phi(\omega)\ Q_x + F_{\phi\psi}^*\ (\omega)\ F_{\phi\psi}(\omega)\ Q_z + R]\ H_r^*(\omega)\ H_r(\omega) \tag{54a}$$

$$P_{\dot\psi}(\omega) = [F^*_\psi(\omega)\; F_\psi(\omega)\; Q_z + F^*_{\phi\psi}\; (\omega)\; F_{\phi\psi}\; (\omega)\; Q_x + R]\; H^*_r(\omega)\; H_r(\omega) \qquad (54b)$$

where

$$F_\phi(\omega) = G_\phi(\omega)\; H(\omega) \qquad (55a)$$

$$G_\phi(\omega) = \left[\frac{I_z\; S^2 + \omega_o{}^2(I_y - I_x)}{D(S)}\right]_{S=j\omega} \qquad (55b)$$

$$F_{\phi\psi}(\omega) = G_{\phi\psi}(\omega)\; H(\omega) \qquad (56a)$$

$$G_{\phi\psi}(\omega) = \left[\frac{\omega_o(I_x - I_y + I_z)}{D(S)}\right]_{S=j\omega} \qquad (56b)$$

$$F_\psi(\omega) = G_\psi(\omega)\; H(\omega) \qquad (57a)$$

$$G_\psi(\omega) = \left[\frac{I_x S^2 + 4\omega_o{}^2(I_y - I_z)}{D(S)}\right]_{S=j\omega} \qquad (57b)$$

and Q_x and Q_z are the first and the third components of $\overline{Q}_{T_{PA}}$ in Eq. (28).

For the same reason discussed earlier, the roll and yaw dynamics are also unstable (referring to Eq. (48), D(s) has roots in the right-half complex plane). The PSD's for this case are obtained again by treating gravity gradient and gyroscopic torques as disturbances. Figures 13 and 14 show the roll and yaw power spectral densities.

E.4.3. The Error PSD's for Configuration B

The stability problem may be resolved by reorienting the shuttle from payload-bay nadir (Configuration A) to nose-down nadir (Configuration B). The advantage of this new configuration is that it is a gravity gradient stabilized system. However, there are drawbacks for this configuration. First, it will require a larger support-tower for the IS instrument, and the second drawback is that the aerodynamic forces and torques have increased significantly over the payload-bay nadir case.

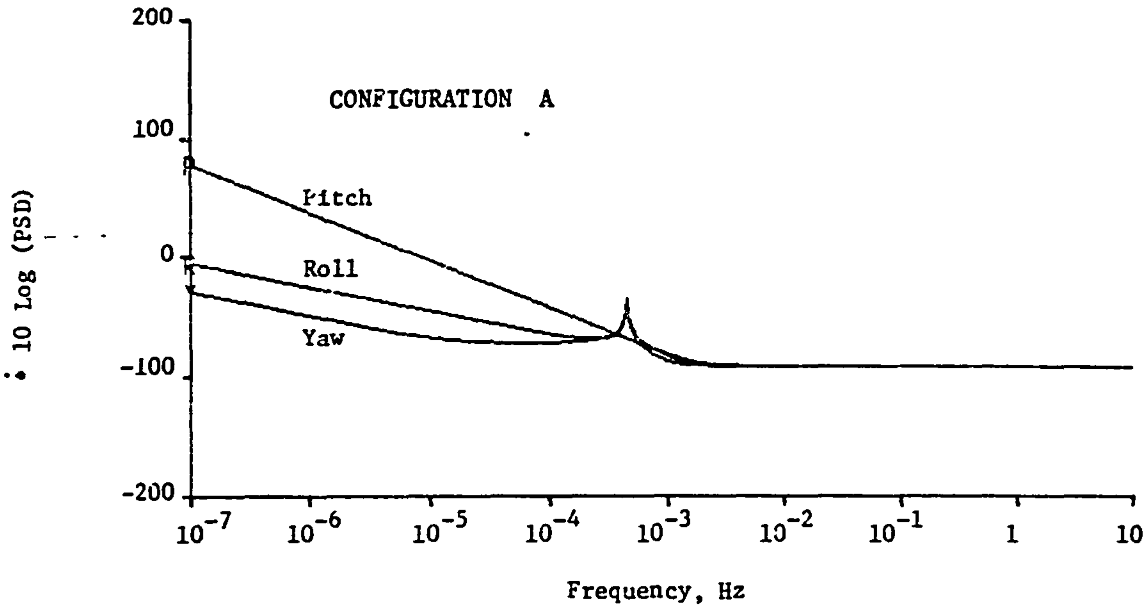

Figure 13. Instrument Pointing Error PSD, $(rad)^2$-sec

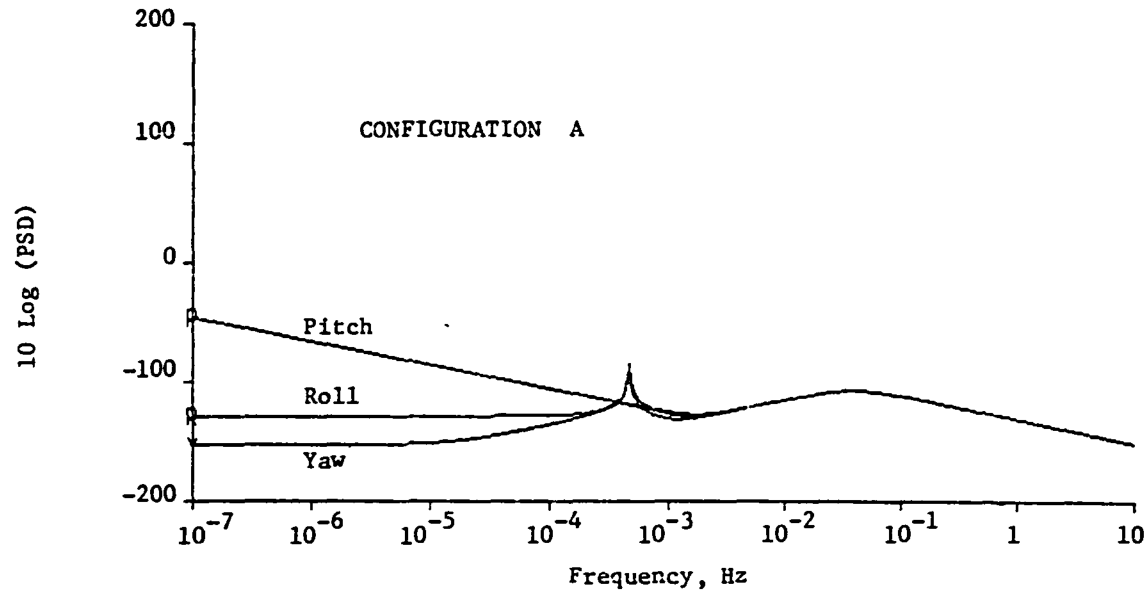

Figure 14. Instrument Pointing Rate Error, $(rad/sec)^2$-sec

To obtain the error power spectral density for Configuration B, it is only necessary to replace $\begin{bmatrix} X \\ Y \\ Z \end{bmatrix}_A$ and the corresponding notations of the equations in this section by $\begin{bmatrix} Y \\ -Z \\ -X \end{bmatrix}_B$. That is, for instance, Eq. (52b) becomes,

$$G_\theta(\omega) = \left[\frac{1}{I_Z S^2 + 3\, \omega_o^{\,2} (I_Y - I_X)} \right]_{S=j\omega} \tag{58}$$

where $G_\theta(\cdot)$ here still represents the pitch dynamics. Since $I_Y > I_X$, Eq. (58) is stable.

The instrument pointing error PSD's are shown in Figure 15 and the rate error PSD's are illustrated in Figure 16.

The computer programs that are used for generating these results are included in Appendices C and D.

F. SUMMARY OF MAJOR FINDINGS

F.1 The Major Environmental Disturbances

The major disturbance sources that are modeled are the aerodynamic drag torques, the gravity gradient torques, and the gyroscopic torques. The unmodeled disturbances are the solar pressure torques, the on-board equipment vibrations, crew motions, and venting. Table 2 shows the static disturbance torques in N-m and the stochastic torque PSD's in $(N\text{-}m)^2$-sec for both Configurations A and B with a circular orbit of 400 km altitude.

F.2 The Measurement Uncertainties

The modeled measurement uncertainties are summarized in Table 3.

F.3 Ground Track Errors and Navigation Uncertainties

The power spectral densities for the ground track errors and the rate errors due to instrument pointing uncertainties for Configurations A and B are shown in Figure 17. It is important to note that strong resonances occur within the frequency band of 10^{-5} Hz to 10^{-3} Hz. The ground track errors at higher frequencies, .01 Hz and above, are dominated by the measurement noise. Recall that the 1σ measurement noise is 28.28 arc-sec/axis. The corresponding ground track error is 54.84 m/axis or 77.56 m/lateral motion.

The 3σ ground track errors due to navigational uncertainties are about one order of magnitude greater than the attitude errors with the aid of TDRSS; and the error is greater with STDN as indicated in Table 4 [12]. Note that the values tabulated in Table 3 are the 3σ rms values.

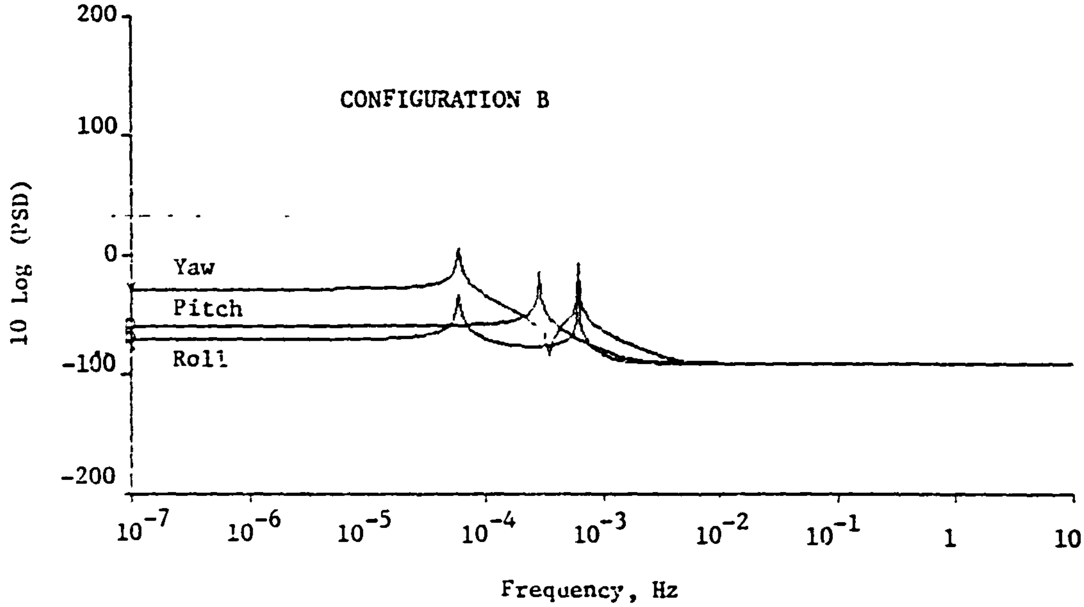

Figure 15. Instrument Pointing Error PSD, $(rad)^2$-sec

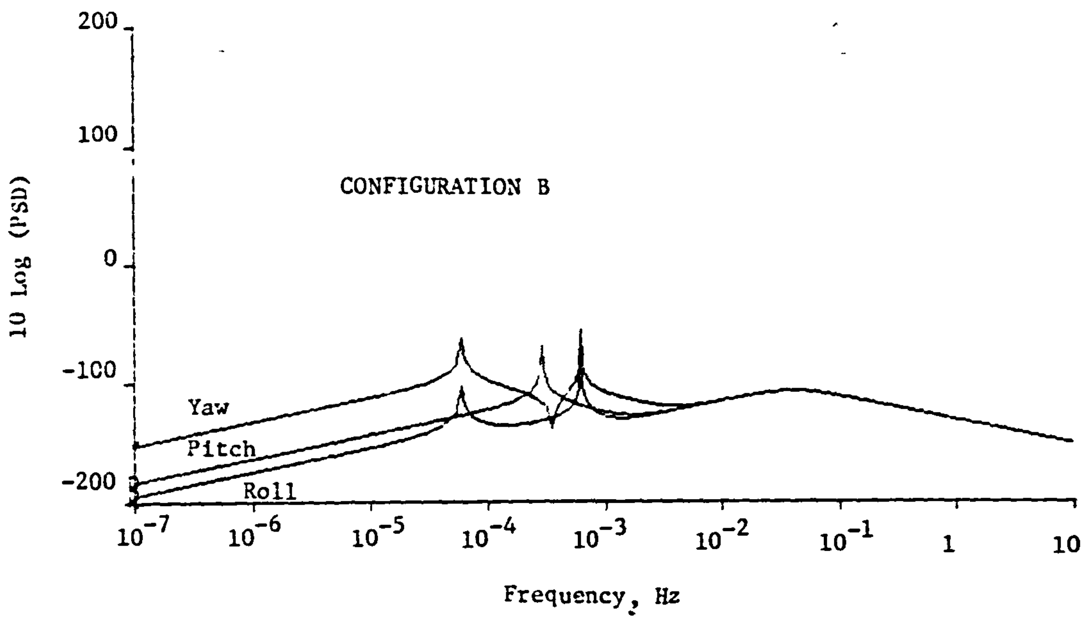

Figure 16. Instrument Pointing Rate Error, $(rad/sec)^2$-sec

Table 2. Modeled Environmental Disturbances

Sources		Static, N-m			Stochastic -- PSD, $(N\text{-}m)^2$-sec		
		X_P	Y_P	Z_P	X_P	Y_P	Z_P
Aerodynamic Drag Torques	Config. A	0	$-.68\times10^{-2}$	0	2×10^{-6}	1.2×10^{-3}	5.4×10^{-4}
	Config. B	-2.78×10^{-2}	0	-3.21×10^{-2}	6.3×10^{-4}	1.9×10^{-4}	1.2×10^{-3}
Gravity Gradient and Gyroscopic Torques		0	0	0	Proportional to attitude errors		

Table 3. Modeled Measurement Uncertainties

Sources	Performance (1σ)	Requirement (1σ)
IMU/Shuttle Misalignment	82 arc-sec	160 arc-sec
IMU Resolution	20 arc-sec	20 arc-sec
IMU Noise	(20) arc-sec	-
IMU Derived Rate	See filter dynamic model	
Rate Gyro	-	60 arc-sec/sec
Shuttle/IS Misalignment (1σ)	30 arc-sec	

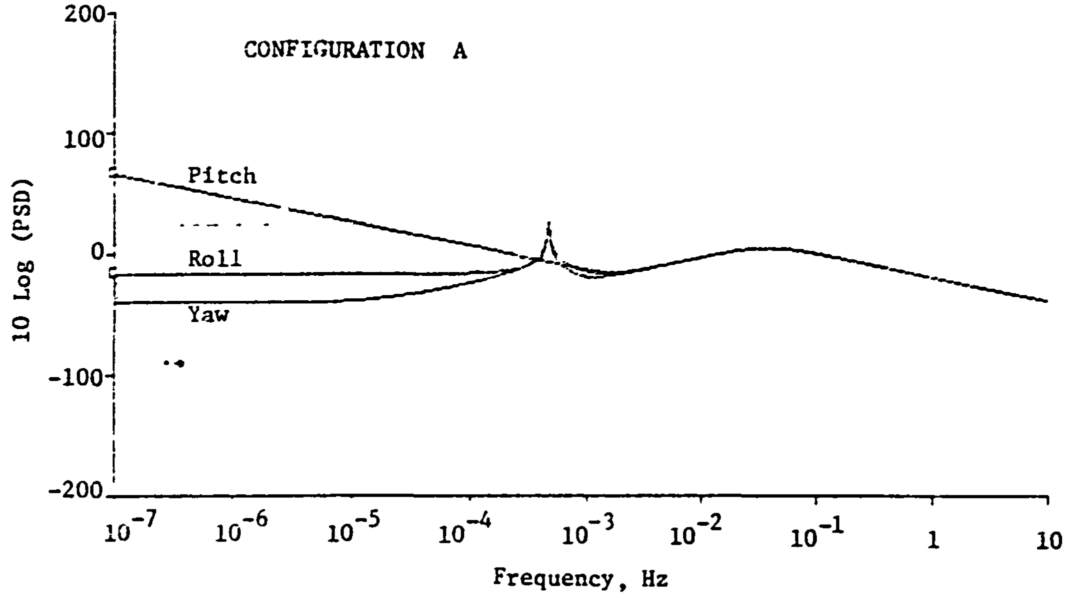

(a) IS Ground Track Error PSD, m^2-sec

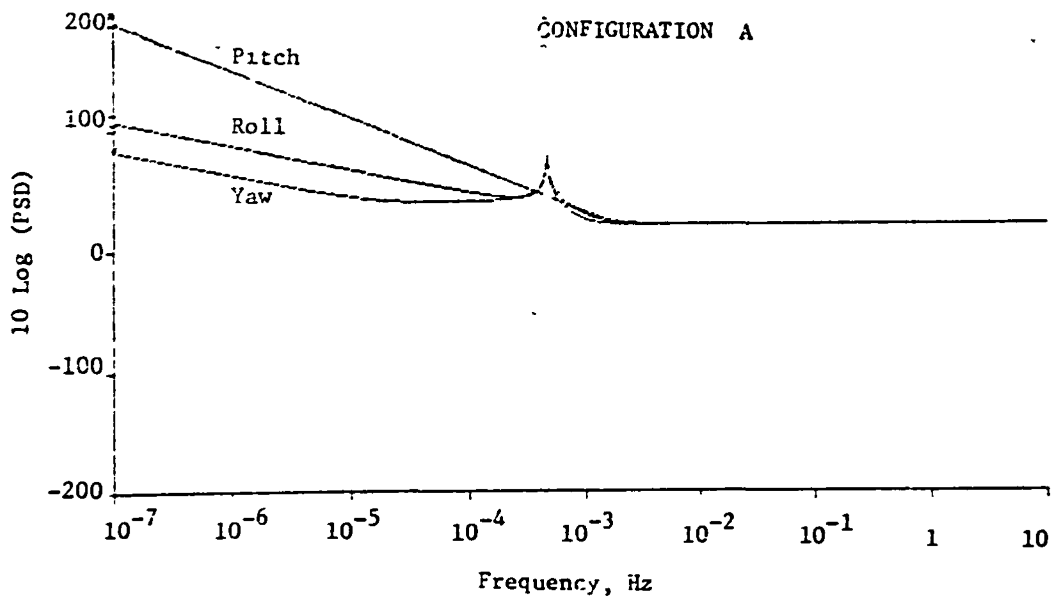

(b) IS Ground Track Rate Error PSD, $(m/sec)^2$-sec

Figure 17. IS Ground Track Error and Rate Error PSD

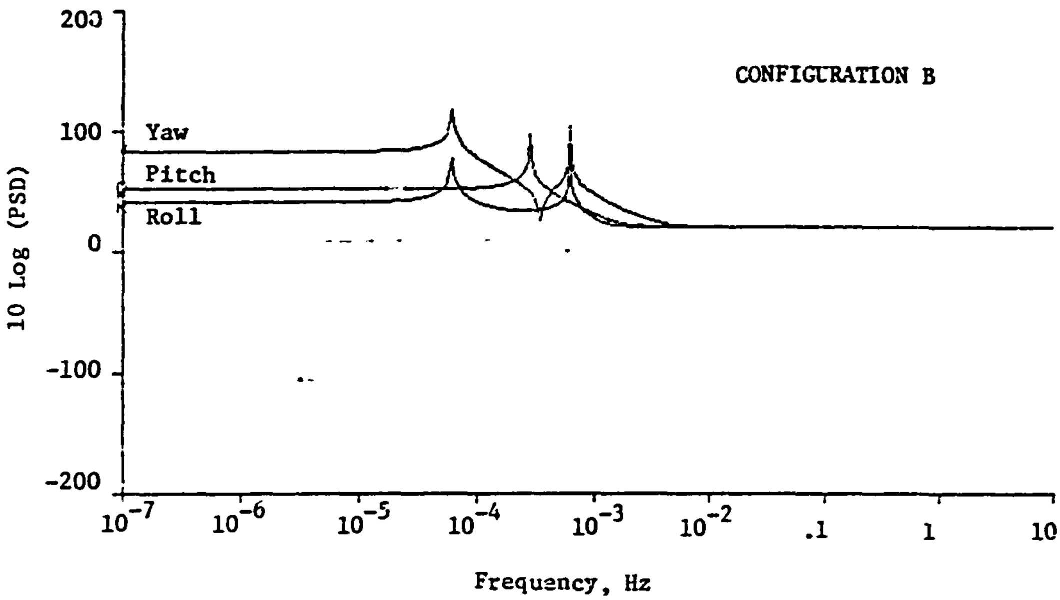

(c) IS Ground Track Error PSD, m^2-sec

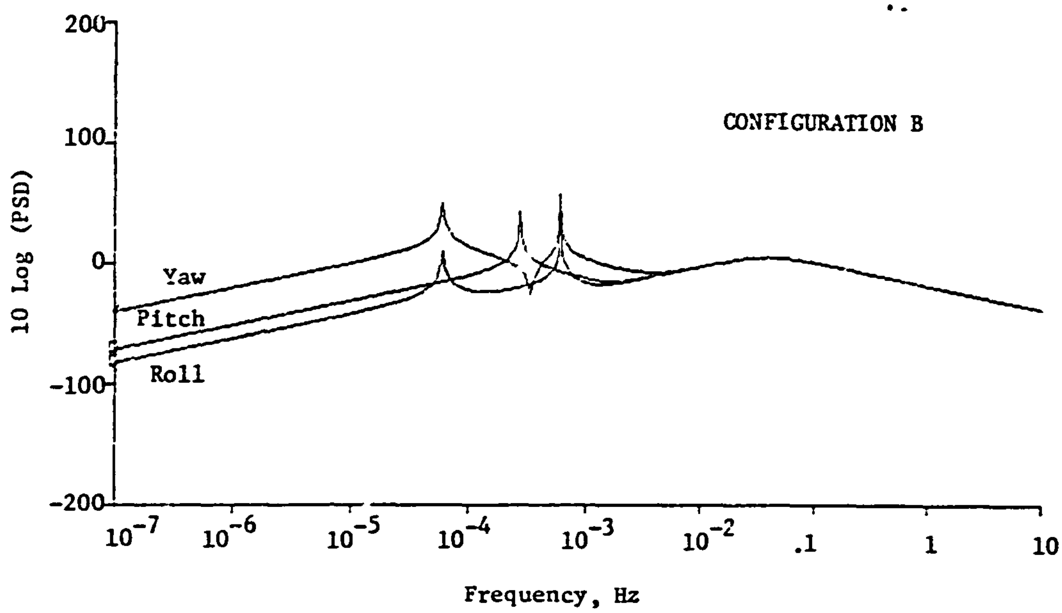

(d) IS Ground Track Rate Error PSD, $(m/sec)^2$-sec

Figure 17. (Continued)

Table 4. Expected On-Orbit Navigation Accuracies (3σ)

CASE	NAVIGATION TRACKING SYSTEM	DESCRIPTION: UNMODELED PERTURBATION	DESCRIPTION: MINIMUM PERIGEE n.mi.	POSITION, FEET: RADIAL	POSITION, FEET: DOWNTRACK	POSITION, FEET: CROSSTRACK	VELOCITY, FPS: RADIAL	VELOCITY, FPS: DOWNTRACK	VELOCITY, FPS: CROSSTRACK
1	STDN*	NOMINAL	105	5,000	34,500	5,000	38.4	5.9	9.8
	TDRSS**		105	3,600	18,500	4,000	22.1	3.3	4.0
2	STDN	SMALL	105	3,000	22,000	1,500	24.6	3.3	2.0
			150	1,200	5,500	1,000	5.8	1.3	1.8
	TDRSS		105	1,800	10,000	2,000	11.0	1.8	2.9
			150	800	2,000	1,500	2.2	0.9	2.1
3	STDN	LARGE	105	8,000	80,000	5,000	91.2	8.0	8.0
	TDRSS		105	6,000	50,000	5,000	56.0	6.2	7.8

NOTE:

The correlation between downtrack position and radial velocity is -0.95

The correlation between radial position and downtrack velocity is -0.80

* Spaceflight Tracking and Data Network

** Tracking Data Relay Satellite System

IV. PARAMETRIC ANALYSIS OF GEOMETRIC ERRORS

In section III, the steady state error dynamics of the Shuttle Imaging Spectrometer system has been analyzed with the major error sources and disturbance effects estimated. In this section, the emphasis is on the geometric error analysis. Geometric errors are consequences of the more direct errors including attitude and rate errors, ephemeris uncertainties, misalignment errors, earth rotation and curvature, etc. Figure 1 shows how the various errors propagate and how the geometric errors and the ground pattern distortions can be generated through dynamic analysis and simulation. The block that is considered in this section is II. Due to mounting and other practical considerations, only the payload-bay principal-axis nadir pointing configuration is considered (see Fig. 2).

The geometric error mapping functions due to the individual error sources as well as the aggregated errors are derived. The earth curvature effect is incorporated in all of the results. For the purpose of quick reference, the key mapping functions are tabulated in Appendix A. A list of the source code of the computer program that has been used for generating the geometric error characteristic curves is given in Appendix E.

A. COORDINATE CONFIGURATIONS

In Fig. 18, the coordinate frame (X_p,Y_p,Z_p) on the Shuttle c.m. consists of the principal body axes. For the purpose of geometric analysis, another set of coordinates is used, i.e., the (X,Y,Z) frame centered at the nadir point on the ground. This frame is the nadir projection of the orbital rotating frame centered at the Shuttle c.m. Specifically, the X-axis is in the direction of the projected motion on the ground, or the along-track direction, the Z-axis is in the nadir direction, and the Y-axis is in the cross-track direction, so that a right-hand coordinate system is formed.

For the purpose of this report, it is assumed that the Imaging Spectrometer is attached to the payload bay with its optical axis aligned with the body

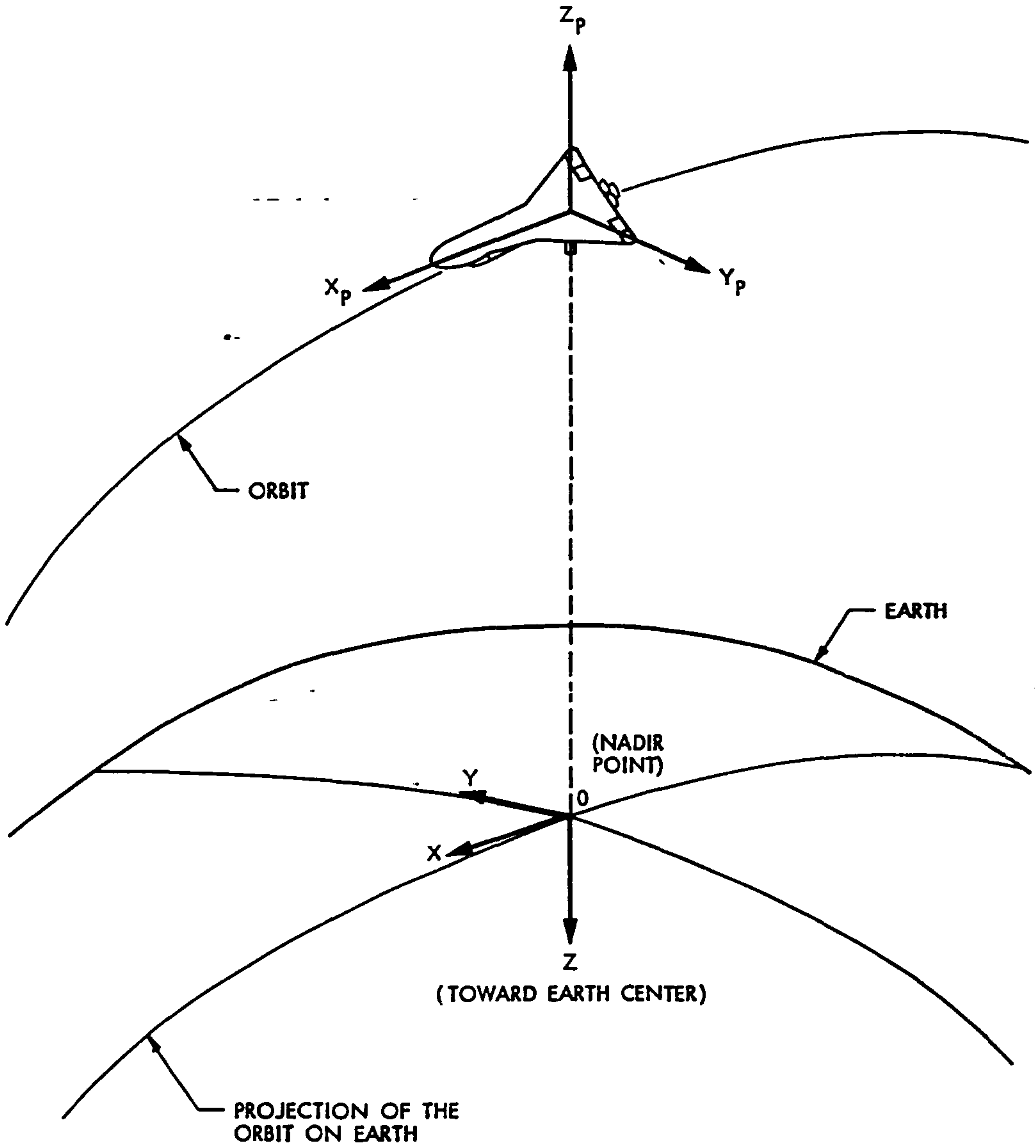

Figure 18. Payload-Bay Nadir Pointing Configuration and Coordinates

Z_p-axis. For normal IS operations, this is the desired configuration. However, for some IS experiments, such as those for assessing the atmospheric effects on the images, the IS instrument is required to point up to $\pm 45^{\circ}$ about the pitch axis (Y) from nadir (forward and backward looking) or up to $\pm 20^{\circ}$ about the roll axis (X) (side looking). For those cases, it is assumed that the instrument is gimbal mounted. However, since the analysis performed here is not primarily concerned with dynamics, no specific details are made at this time regarding mounting configurations.

B. GEOMETRIC ERRORS INDUCED BY EPHEMERIS UNCERTAINTIES

Ephemeris uncertainties include radial, along-track, and cross-track prediction errors. The geometric errors induced by ephemeris uncertainties are discussed in the following subsections.

B.1 Geometric Errors Due to Altitude Uncertainties

When the altitude of the shuttle varies, the ground point will shift in both the X and Y directions accordingly. This can be investigated in the following two ways.

B.1.1. With Fixed Viewing Angles

Referring to Figure 19, when the shuttle flies at nominal altitude h (position A), a ground point B with coordinates (Xo, Yo) corresponding to a view angle λ from the shuttle IS is located. After the shuttle elevates Δh to position A', point B' with coordinates (Xo', Yo') corresponding to the same view angle λ is located. The problem is to determine the shift of image due to the altitude change. Consider that when the altitude increases, the image of ground objects tends to move toward the nadir point, which causes reduction in image size and increase in field of view. Mathematically, the shift of image may be characterized by computing ΔX and ΔY, where

$$\Delta X = Xo - Xo'$$

$$\Delta Y = Y - Yo'$$

Starting by assuming (Xo, Yo) known, the task is to determine (Xo', Yo') by first computing the view angle λ. Figure 19b is generated by taking a side view from Fig. 19a in the direction perpendicular to Plane $A'AOC_eB'$. Apparently,

$$\sqrt{Xo^2 + Yo^2} = R \sin\beta$$

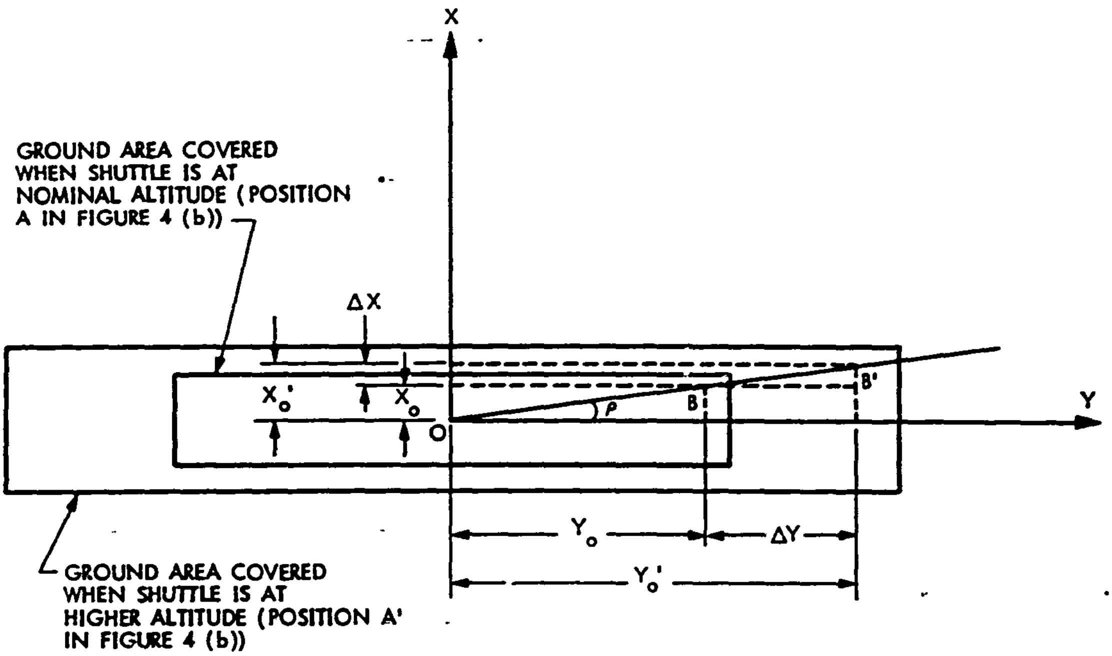

LEGEND:

B = A GROUND POINT CORRESPONDING TO VIEW ANGLE λ WHEN SHUTTLE IS AT NOMINAL ALTITUDE (POSITION A IN FIG. 4(b))

B' = THE GROUND POINT CORRESPONDING TO THE SAME VIEW ANGLE AFTER THE SHUTTLE ELEVATED Δh (POSITION A' IN FIG. 4(b))

(X_o, Y_o) = COORDINATES OF POINT B

(X_o', Y_o') = COORDINATES OF POINT B'

ΔX, ΔY = X AND Y COMPONENTS OF THE POSITION CHANGE

(a) TOP VIEW (LOOKING TOWARD NADIR)

Figure 19: Ground Point Shift in X and Y Direction due to Altitude Error

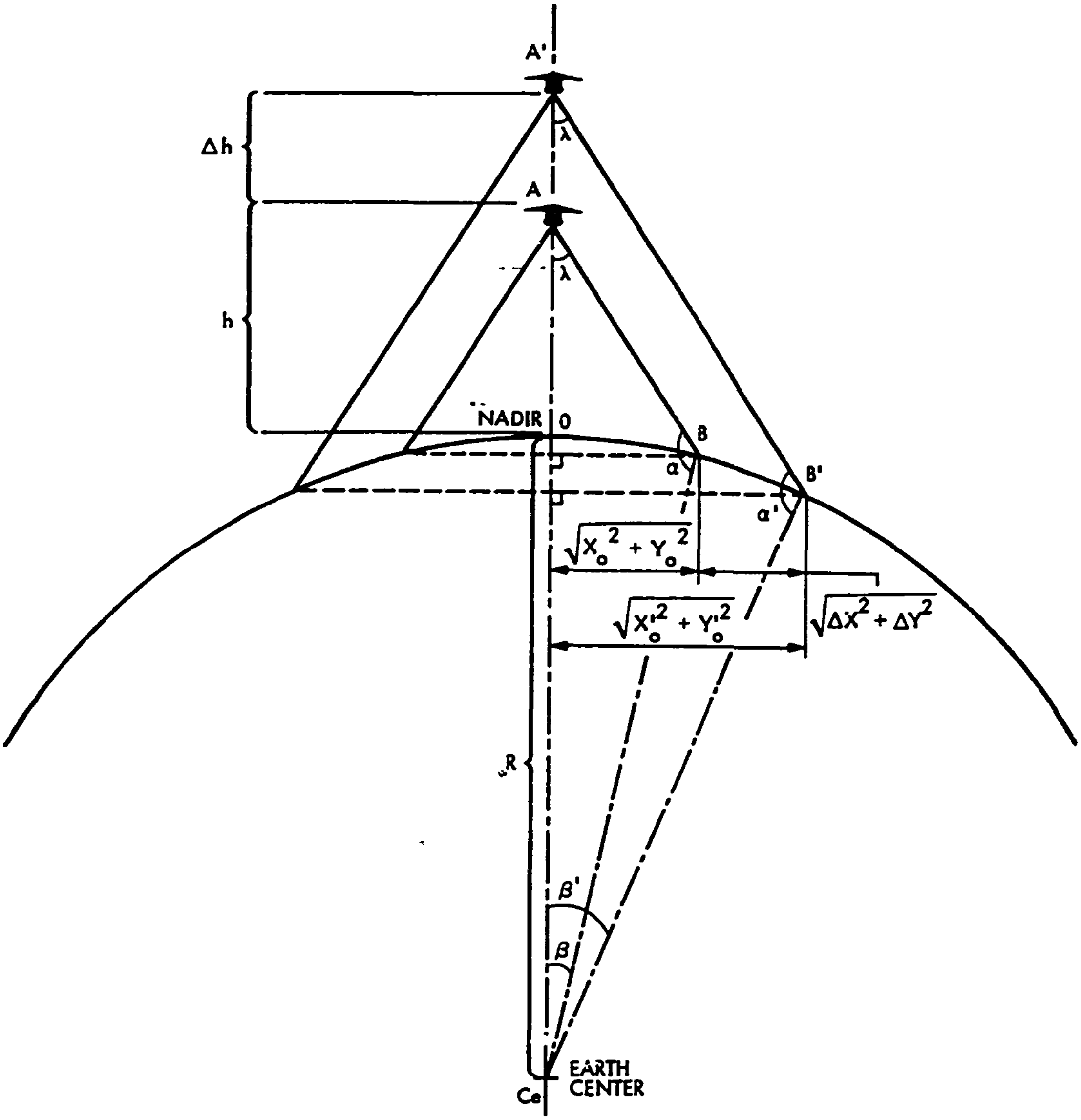

(b) SIDE VIEW

LEGEND:

- h = NOMINAL ALTITUDE
- Δh = ALTITUDE ERROR
- λ = VIEW ANGLE
- A = SHUTTLE'S POSITION AT NOMINAL ALTITUDE
- A' = SHUTTLE'S POSITION AFTER BEING ELEVATED Δh

Figure 19. (Continued)

or

$$\beta = \sin^{-1}\left(\frac{\sqrt{Xo^2 + Yo^2}}{R}\right) \tag{59}$$

and

$$\alpha = 180° - \lambda - \beta \tag{60}$$

From triangle ABC_e, we have

$$\frac{R}{\sin\lambda} = \frac{R + h}{\sin\alpha} \tag{61}$$

Substituting Eqs. (59) and (60) into (61), it becomes

$$\frac{R}{\sin\lambda} = \frac{R + h}{\sin\left[180° - \lambda - \sin^{-1}\left(\frac{\sqrt{Xo^2 + Yo^2}}{R}\right)\right]}$$

which leads to

$$\tan\lambda = \frac{\sqrt{Xo^2 + Yo^2}}{R + h - \sqrt{R^2 - Xo^2 - Yo^2}}$$

hence,

$$\lambda = \tan^{-1}\left(\frac{\sqrt{Xo^2 + Yo^2}}{R + h - \sqrt{R^2 - Xo^2 - Yo^2}}\right) \tag{62}$$

To determine $\sqrt{Xo'^2 + Yo'^2}$, triangle $A'B'C_e$ is used,

$$\frac{R}{\sin\lambda} = \frac{R + h + \Delta h}{\sin\alpha'}$$

$$\therefore \alpha' = \sin^{-1}\left[\left(1 + \frac{h + \Delta h}{R}\right)\sin\lambda\right] \tag{63}$$

and

$$\sqrt{Xo'^2 + Yo'^2} = R\sin\beta'$$

$$= R\sin(\lambda + \alpha') \tag{64}$$

Substituting Eq. (63) into (64),

$$\sqrt{Xo'^2 + Yo'^2} = R \sin\left\{\lambda + \sin^{-1}\left[\left(1 + \frac{h + \Delta h}{R}\right)\sin\lambda\right]\right\} \tag{65}$$

Expanding the right hand side of Eq.(65), and adopting the "–" sign for $\cos\left\{\sin^{-1}\left[\left(1 + \frac{h + \Delta h}{R}\right)\sin\lambda\right]\right\}$, since $90° < \sin^{-1}\left[\left(1 + \frac{h + \Delta h}{R}\right)\sin\lambda\right] < 180°$, one has

$$\sqrt{Xo'^2 + Yo'^2} = R\left[\left(1 + \frac{h + \Delta h}{R}\right)\cos\lambda - \sqrt{1 - \left(1 + \frac{h + \Delta h}{R}\right)^2 \sin^2\lambda}\right]\sin\lambda \tag{66}$$

Now, referring to Fig. 19(a), since B' is on the line OB, the angle ρ is determined by

$$\rho = \sin^{-1}\frac{Xo}{\sqrt{Xo^2 + Yo^2}} = \cos^{-1}\frac{Yo}{\sqrt{Xo^2 + Yo^2}} \tag{67}$$

Hence, from Eqs. (66) and (67),

$$Xo' = \sqrt{Xo'^2 + Yo'^2}\,\sin\rho = \frac{RXo\sin\lambda}{\sqrt{Xo^2 + Yo^2}}\left[\left(1 + \frac{h + \Delta h}{R}\right)\cos\lambda - \sqrt{1 - \left(1 + \frac{h + \Delta h}{R}\right)^2 \sin^2\lambda}\right] \tag{68}$$

$$Yo' = \sqrt{Xo'^2 + Yo'^2}\,\cos\rho = \frac{RYo\sin\lambda}{\sqrt{Xo^2 + Yo^2}}\left[\left(1 + \frac{h + \Delta h}{R}\right)\cos\lambda - \sqrt{1 - \left(1 + \frac{h + \Delta h}{R}\right)^2 \sin^2\lambda}\right] \tag{69}$$

where λ is obtained by Eq.(62).

Hence, from Eqs. (68), (69), and (62) the values for $\Delta X = Xo - Xo'$ and $\Delta Y = Yo - Yo'$ can be obtained.

When point A' is below point A, the negative value for Δh should be used in the above equations.

However, if one starts with given view angle λ and ρ, the values of Xo, Yo, Xo', and Yo' can be readily obtained using Eqs. (68) and (69) directly (set Δh to 0 for Xo and Yo).

B.1.2 With Fixed Ground Points

Referring to Fig.20, the view angle for the fixed ground point B will change as the shuttle altitude varies. Follow the same approach of paragraph B.1.1, the view angles Ω and Ω' can be found,

$$\Omega = \tan^{-1}\left(\frac{\sqrt{Xo^2 + Yo^2}}{R + h - \sqrt{R^2 - Xo^2 - Yo^2}}\right) \tag{70}$$

and

$$\Omega' = \tan^{-1}\left(\frac{\sqrt{Xo^2 + Yo^2}}{R + h + \Delta h - \sqrt{R^2 - Xo^2 - Yo^2}}\right) \tag{71}$$

Using Eqs. (70) and (71), the value of $\Delta\Omega = \Omega' - \Omega$ can be obtained. Again if point A' is below point A, the negative value for Δh should be used in the above equations.

B.2. Geometric Errors Due to Intrack and Crosstrack Prediction Errors

The intrack (along X-direction or direction of orbit) and the crosstrack (along Y-direction or "-" orbit normal direction) prediction errors will cause the ground objects to shift along the X and Y directions, respectively, as shown in Fig.21. To determine the overall geometric errors associated with ephemeris uncertainties, the intrack error ΔX^* and the crosstrack error ΔY^* can be incorporated in ΔX and ΔY found in Section B.1.1, respectively.

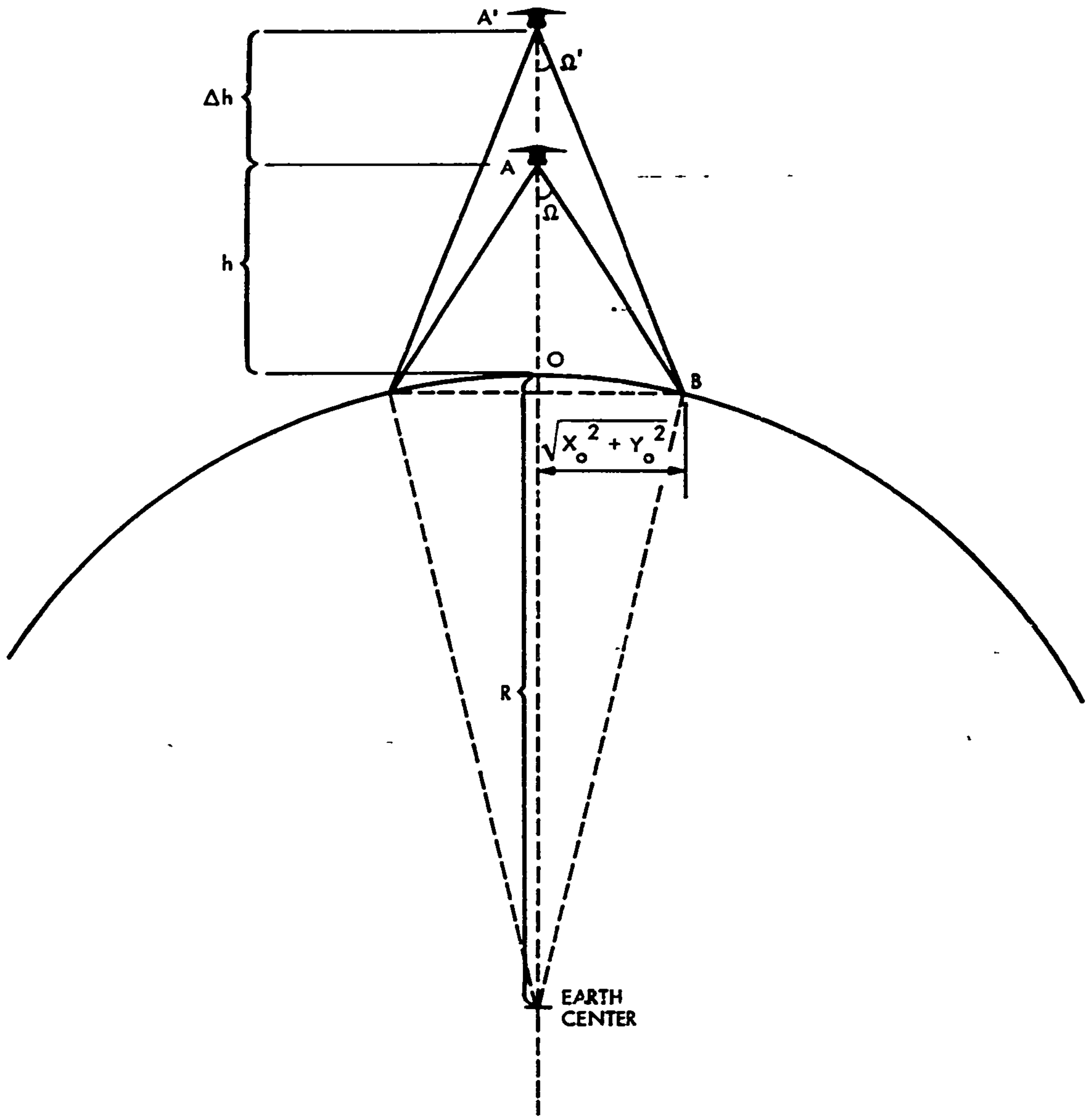

LEGEND:

Ω = VIEW ANGLE FROM SHUTTLE TO POINT B WHEN SHUTTLE IS AT NOMINAL ALTITUDE h

Ω' = VIEW ANGLE FROM SHUTTLE TO THE SAME POINT B AFTER SHUTTLE ELEVATES Δh

Figure 20. Change of View Angle of a Ground Point due to Altitude Error

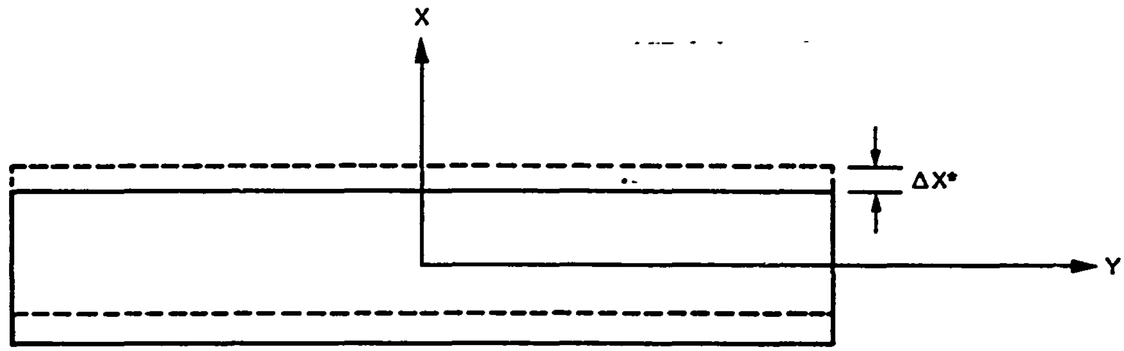

(a) INTRACK ERROR (ΔX*)

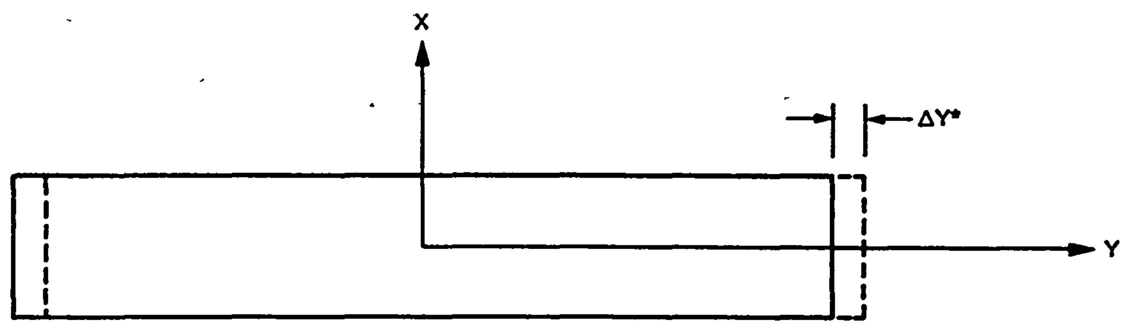

(b) CROSSTRACK ERROR (ΔY*)

Figure 21. Geometric Errors Induced by Intrack and Crosstrack Prediction Errors

C. GEOMETRIC ERRORS INDUCED BY ATTITUDE UNCERTAINTIES

Attitude uncertainties refer to the angular errors with respect to the nominal roll (ϕ), pitch (θ), and yaw (ψ) axes. The effects of these errors to the images of ground objects are studied in this subsection first on the individual error basis and then on the aggregated basis. For convenience, in the subsequent discussions, the term nominal flight condition will be used to signify the condition of the shuttle flying in a 400 km circular orbit with the attitude of payload-bay nadir pointing.

C.1 Geometric Errors Induced by Roll Error

Referring to Fig. 22, consider the nominal flight condition with ϕ_o offset angle about the roll axis. The IS slit in this case is directed at the Y-axis on the ground. For a given view angle λ, the image point (or pixel) on the ground is P_o with coordinates (0,Y*). For the same roll offset and view angle the ground point P_o' is located after a roll error ϕ is introduced. The coordinates of P_o' are (0, Y*'). Equivalently, by rotating the optical instrument to the "left," the image recorded on the film appears to move to the "right." Therefore, the geometric error may be defined as the displacement of the object image after error is introduced relative to the image before the error is introduced. Mathematically, this is $\overline{P}_o - \overline{P}_o'$ or $\overline{P}_{\phi_o,\lambda} - \overline{P}_{\phi_o+\phi,\lambda}$. Since, in the case being considered, the image is on the Y-axis, one has

$$\Delta X = 0 \tag{72}$$

$$\Delta Y = Y^* - Y^{*\prime} \tag{73}$$

where Y* and Y*' are,

$$Y^* = -R \sin(\lambda + \phi_o) \left[\left(1 + \frac{h}{R}\right)\cos(\lambda + \phi_o) - \sqrt{1 - \left(1 + \frac{h}{R}\right)^2 \sin^2(\lambda + \phi_o)}\right] \tag{74}$$

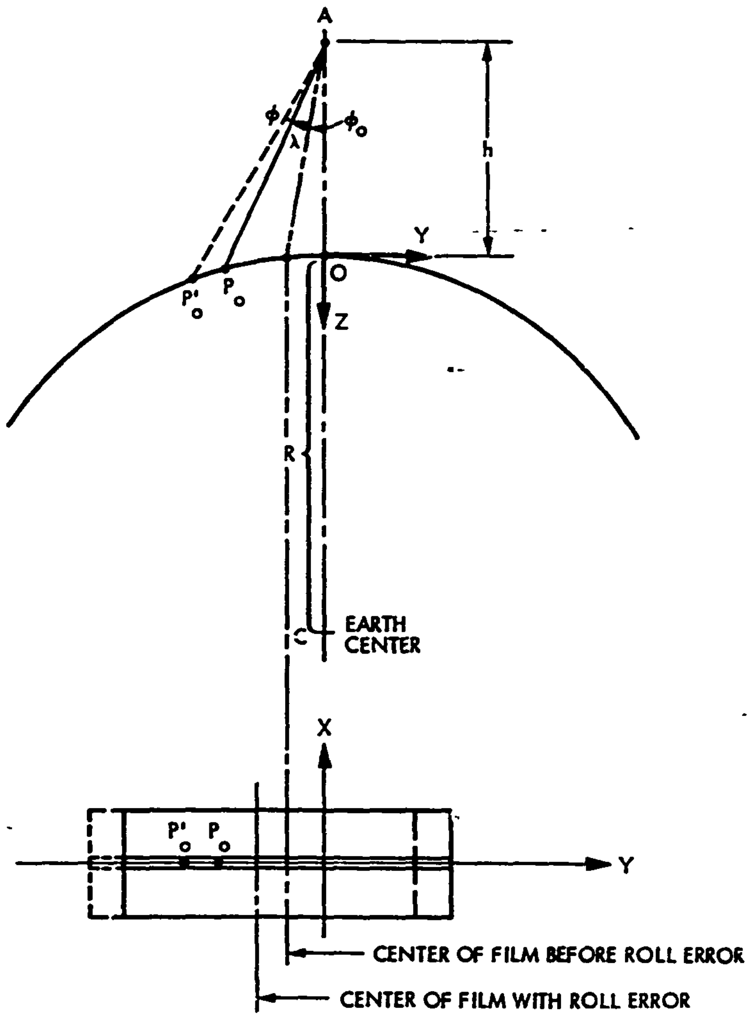

LEGEND:

λ = VIEW ANGLE

ϕ_o = ROLL OFFSET ANGLE

ϕ = ROLL ERROR

P_o = THE GROUND POINT CORRESPONDING TO VIEW ANGLE λ AND ROLL OFFSET ϕ_o

P_o = THE GROUND POINT CORRESPONDING TO THE SAME λ AND ϕ_o AFTER ROLL ERROR ϕ IS INTRODUCED

Figure 22. Shift of Ground Point Induced by Roll Error

$$Y^{*\prime} = -R \sin(\lambda + \phi_o + \phi) \left[\left(1 + \frac{h}{R}\right) \cos(\lambda + \phi_o + \phi) - \sqrt{1 - \left(1 + \frac{h}{R}\right)^2 \sin^2(\lambda + \phi_o + \phi)}\right] \tag{75}$$

C.2 Geometric Errors Induced by Pitch Error

Consider the case of pitch attitude error. Let θ_o be the offset angle about the pitch axis (desired attitude), and θ be the pitch error. Referring to Fig.23, for a given view angle λ, projecting the slit onto the XY-plane forms two line segments: $\overline{BC}$, corresponding to null pitch error ($\theta = 0$), and $\overline{B'C'}$, corresponding to arbitrary pitch error θ. Projecting along the line of view $\overline{AC}$ onto the ground, $P(X^*,Y^*)$ is obtained; similarly, $P'(X^{*\prime},Y^{*\prime})$ is obtained, corresponding to line of view $\overline{AC'}$. The geometric error here is defined the same way as that for the roll case, i.e., $\overline{P}_{\theta_o,\lambda} - P_{\theta_o+\theta,\lambda}$, or

$$\Delta X = X^* - X^{*\prime} \tag{76}$$

$$\Delta Y = Y^* - Y^{*\prime} \tag{77}$$

The formulae for computing X^*, Y^*, $X^{*\prime}$, and $Y^{*\prime}$ are derived as follows. In Fig.23, assume that h, θ, θ_o, and λ are known. The lengths of the line segments $\overline{OB}$ and $\overline{OB'}$ are

$$\overline{OB} = h \tan \theta_o \tag{78a}$$

and

$$\overline{OB'} = h \tan(\theta_o + \theta) \tag{78b}$$

and that of $\overline{AB}$ and $\overline{AB'}$ are

$$\overline{AB} = \frac{h}{\cos \theta_o} \tag{79a}$$

$$\overline{AB'} = \frac{h}{\cos(\theta_o + \theta)} \tag{79b}$$

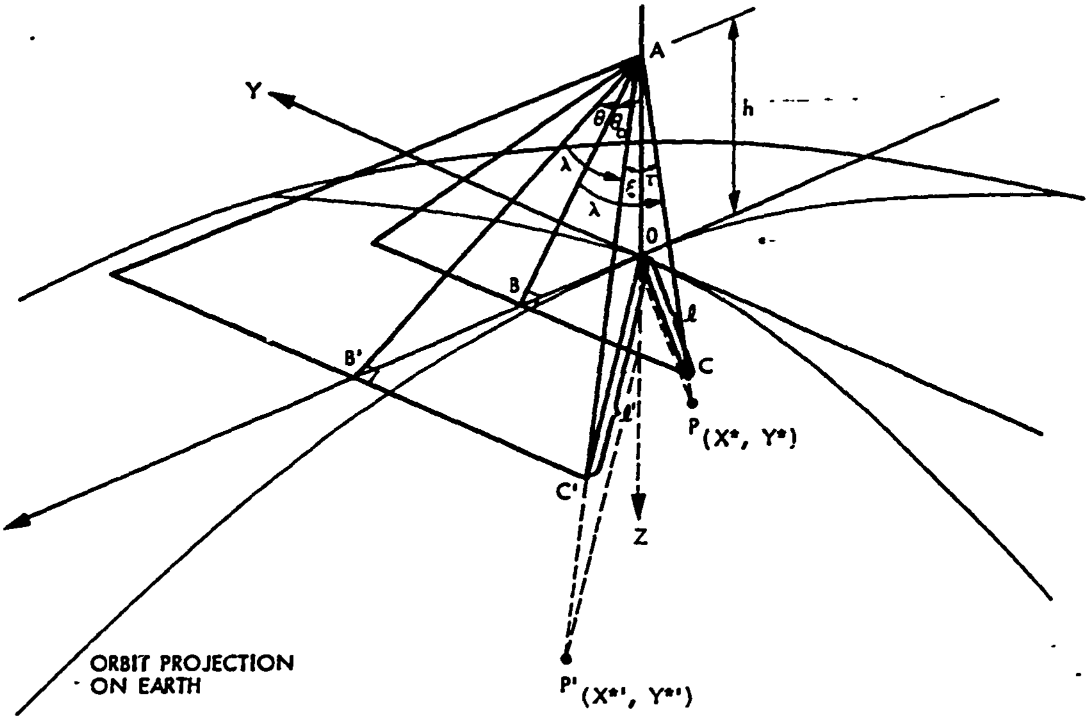

LEGEND:

λ = VIEW ANGLE

θ_o = PITCH OFFSET ANGLE

θ = PITCH ERROR

P = THE GROUND POINT CORRESPONDING TO VIEW ANGLE λ AND PITCH OFFSET θ_o

P' = THE GROUND POINT CORRESPONDING TO THE SAME λ AND θ_o AFTER PITCH ERROR θ IS INTRODUCED

Figure 23. Shift of Ground Point Induced by Pitch Error

$\overline{BC}$ and $\overline{B'C'}$, with respect to Y-axis, can be obtained as

$$\overline{BC} = -\overline{AB} \tan \lambda = \frac{-h \tan \lambda}{\cos \theta_o} \tag{80a}$$

and

$$\overline{B'C'} = -\overline{AB}' \tan \lambda = \frac{-h \tan \lambda}{\cos(\theta_o + \theta)} \tag{80b}$$

implies that the signs of $\overline{BC}$ and $\overline{B'C'}$ are opposite to that of λ. ℓ and ℓ' are, referring to Fig. 23,

$$\ell = \sqrt{\overline{OB}^2 + \overline{BC}^2} = h \sec \theta_o \sqrt{\sin^2 \theta_o + \tan^2 \lambda} \tag{81a}$$

and

$$\ell' = \sqrt{\overline{OB}'^2 + \overline{B'C'}^2} = h \sec (\theta_o + \theta) \sqrt{\sin^2 (\theta_o + \theta) + \tan^2 \lambda} \tag{81b}$$

the angles τ and ξ (see Fig. 23) can then be determined,

$$\tau = \tan^{-1} \left(\frac{\ell}{h}\right) = \tan^{-1} \left(\sec \theta_o \sqrt{\sin^2 \theta_o + \tan^2 \lambda}\right) \tag{82a}$$

and

$$\xi = \tan^{-1} \left(\frac{\ell'}{h}\right) = \tan^{-1} \left[\sec (\theta_o + \theta) \sqrt{\sin^2 (\theta_o + \theta) + \tan^2 \lambda}\right] \tag{82b}$$

Finally,

$$\begin{aligned} X^* &= \sqrt{X^{*2} + Y^{*2}}\, \frac{\overline{OB}}{\ell} \\ &= R \left[\left(1 + \frac{h}{R}\right) \cos \tau - \sqrt{1 - \left(1 + \frac{h}{R}\right)^2 \sin^2 \tau}\right] \frac{\sin \tau \sin \theta_o}{\sqrt{\sin^2 \theta_o + \tan^2 \lambda}} \end{aligned} \tag{83a}$$

$$\begin{aligned} Y^* &= \sqrt{X^{*2} + Y^{*2}}\, \frac{\overline{BC}}{\ell} \\ &= -R \left[\left(1 + \frac{h}{R}\right) \cos \tau - \sqrt{1 - \left(1 + \frac{h}{R}\right)^2 \sin^2 \tau}\right] \frac{\sin \tau \tan \lambda}{\sqrt{\sin^2 \theta_o + \tan^2 \lambda}} \end{aligned} \tag{83b}$$

$$X^{*\prime} = \sqrt{X^{*\prime 2} + Y^{\prime 2}}\,\frac{\overline{OB'}}{\ell'}$$

$$= R\left[\left(1 + \frac{h}{R}\right)\cos\xi - \sqrt{1 - \left(1 + \frac{h}{R}\right)^2 \sin^2\xi}\right]\frac{\sin\xi\,\sin(\theta_o + \theta)}{\sqrt{\sin^2(\theta_o + \theta) + \tan^2\lambda}} \tag{83c}$$

$$Y^{*\prime} = \sqrt{X^{*\prime 2} + Y^{*\prime 2}}\,\frac{\overline{B'C'}}{\ell'}$$

$$= -R\left[\left(1 + \frac{h}{R}\right)\cos\xi - \sqrt{1 - \left(1 + \frac{h}{R}\right)^2 \sin^2\xi}\right]\frac{\sin\xi\,\tan\lambda}{\sqrt{\sin^2(\theta_o + \theta) + \tan^2\lambda}} \tag{83d}$$

However, if one starts with (X^*, Y^*) given, then λ and θ_o would have to be computed. In that case,

$$\lambda = -\tan^{-1}\left[\frac{Y^*}{\left(R + h - \sqrt{R^2 - X^{*2} - Y^{*2}}\right)\sqrt{1 + \left(\frac{X^*}{R + h - \sqrt{R^2 - X^{*2} - Y^{*2}}}\right)^2}}\right] \tag{84a}$$

and

$$\theta_o = \tan^{-1}\left(\frac{X^*}{R + h - \sqrt{R^2 - X^{*2} - Y^{*2}}}\right) \tag{84b}$$

Once λ and θ_o are determined, τ and ξ can be computed using (82), and $X^{*\prime}$ and $Y^{*\prime}$ are determined using (83).

C.3 Geometric Errors Induced by Yaw Error

For a given yaw offset angle, ψ_o, and the view angle, λ, the ground point $P(X^*, Y^*)$ is located. A new point $P'(X^{*\prime}, Y^{*\prime})$ is found as yaw attitude error, ψ, is introduced (see Fig.24). The values for X^*, Y^*, $X^{*\prime}$, and $Y^{*\prime}$ can be computed as follows:

$$X^* = \left[\left(1 + \frac{h}{R}\right)\cos\lambda - \sqrt{1 - \left(1 + \frac{h}{R}\right)^2 \sin^2\lambda}\right] R\sin\lambda\,\sin\psi_o \tag{85a}$$

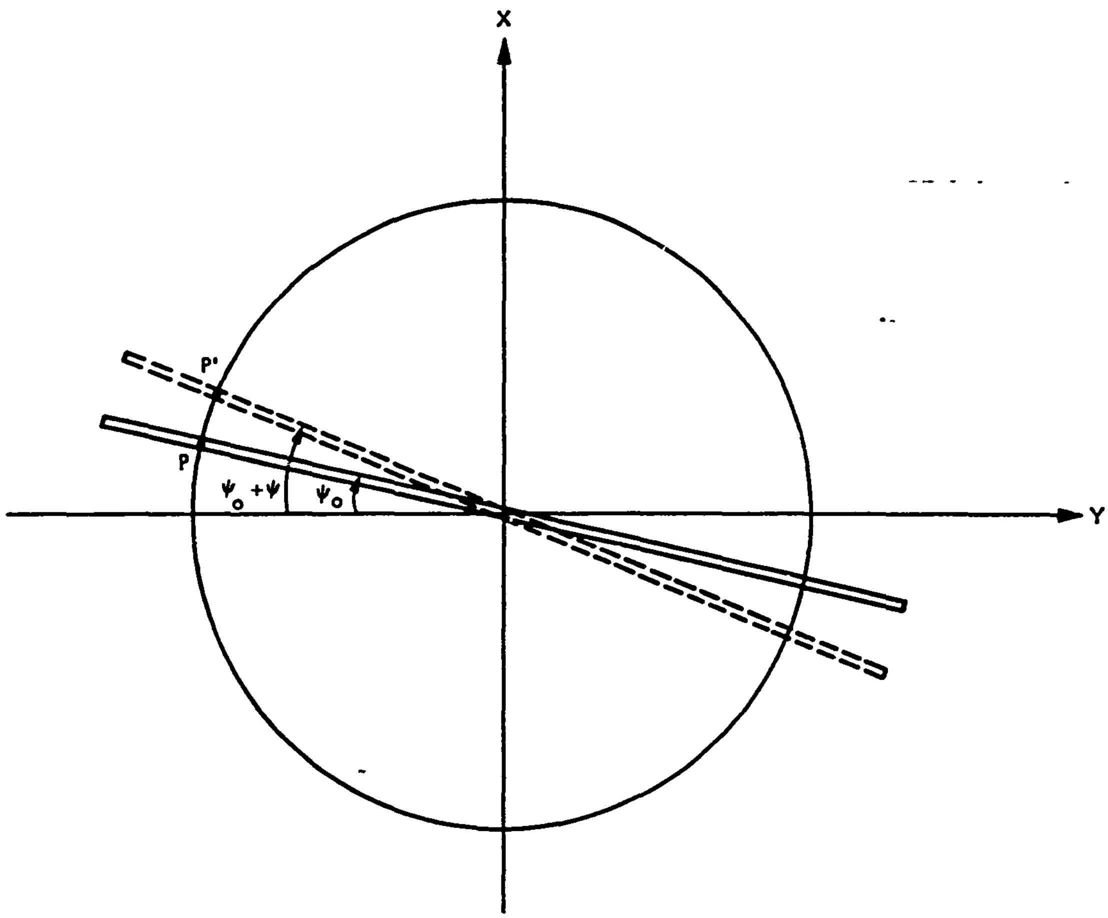

LEGEND:

ψ_o = YAW OFFSET ANGLE

ψ = YAW ERROR

P = THE GROUND POINT CORRESPONDING TO VIEW ANGLE λ AND YAW OFFSET ψ_o

P' = THE GROUND POINT CORRESPONDING TO THE SAME λ AND ψ_o AFTER YAW ERROR ψ IS INTRODUCED

Figure 24. Shift of Ground Point Induced by Yaw Error

$$Y^* = -\left[\left(1 + \frac{h}{R}\right) \cos \lambda - \sqrt{1 - \left(1 + \frac{h}{R}\right)^2 \sin^2 \lambda}\right] R \sin \lambda \cos \psi_o \quad (85b)$$

$$X^{*\prime} = \left[\left(1 + \frac{h}{R}\right) \cos \lambda - \sqrt{1 - \left(1 + \frac{h}{R}\right)^2 \sin^2 \lambda}\right] R \sin \lambda \sin (\psi_o + \psi) \quad (86a)$$

and

$$Y^{*\prime} = -\left[\left(1 + \frac{h}{R}\right) \cos \lambda - \sqrt{1 - \left(1 + \frac{h}{R}\right)^2 \sin^2 \lambda}\right] R \sin \lambda \cos (\psi_o + \psi) \quad (86b)$$

From Eqs. (85) and (86), we can obtain

$$\Delta X = X^* - X^{*\prime}$$

$$\Delta Y = Y^* - Y^{*\prime}$$

C.4 Geometric Errors Induced by Roll, Pitch, and Yaw Attitude Errors

C.4.1. The Shift of IS Line-of-Sight due to Attitude Error

Referring to Fig.25, the shuttle is flying at an arbitrary attitude (ϕ, θ, ψ). Consider the 3-2-1 sequence, i.e., the yaw, pitch, and roll rotation sequence. After yaw and pitch rotations, the Imaging Spectrometer line-of-sight will shift to $\overline{AB}$, where $B(X_1, Y_1)$ is its intersection with the XY-plane. The (X_1, Y_1) coordinates are determined as follows:

$$X_1 = X_o + h \tan \theta \cos \psi \quad (87a)$$

$$Y_1 = Y_o + h \tan \theta \sin \psi \quad (87b)$$

Through a roll angle rotation, point B will move to $C(X_2, Y_2)$ on the XY-plane, where

$$X_2 = X_o + h \tan \theta \cos \psi + \frac{h}{\cos \theta} \tan \phi \sin \psi \quad (88a)$$

$$Y_2 = Y_o + h \tan \theta \sin \psi - \frac{h}{\cos \theta} \tan \phi \cos \psi \quad (88b)$$

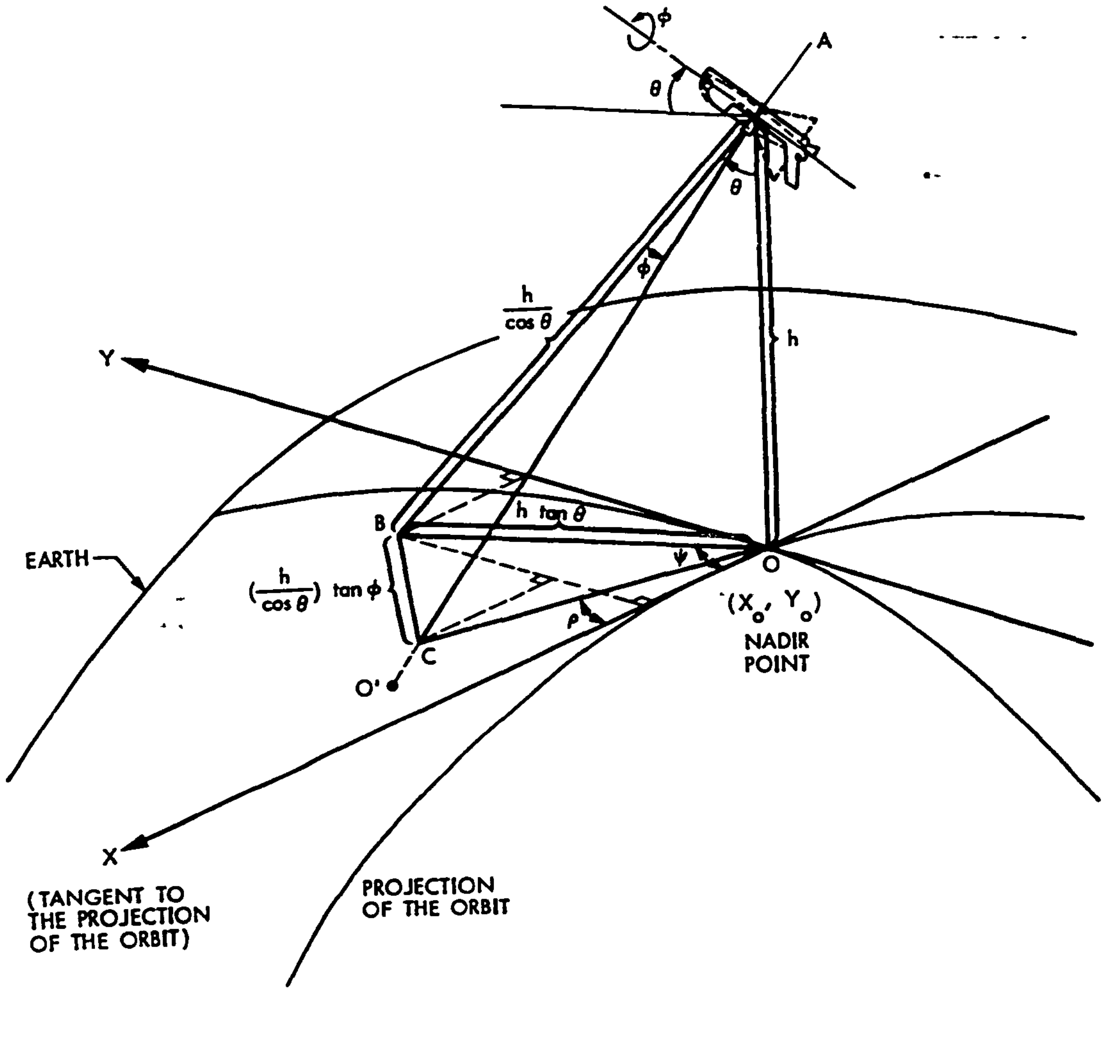

Figure 25. The Shift of Ground Projection of the IS Line-of-Sight due to Attitude Error

The interest here is to determine the coordinates of O'(X,Y) corresponding to the final line-of-sight projected onto the ground. By taking a view normal to the ACO-plane, Figure 26 is obtained. The quantities ε, ℓ, and ρ are obtained as follows,

$$\varepsilon = \tan^{-1}\left(\frac{\sqrt{X_2^2 + Y_2^2}}{h}\right) \tag{89a}$$

$$\ell = R \sin \varepsilon \left[\left(1 + \frac{h}{R}\right) \cos \varepsilon - \sqrt{1 - \left(1 + \frac{h}{R}\right)^2 \sin^2 \varepsilon}\right] \tag{89b}$$

and

$$\rho = \sin^{-1}\left(\frac{Y_2}{\sqrt{X_2^2 + Y_2^2}}\right) = \cos^{-1}\left(\frac{X_2}{\sqrt{X_2^2 + Y_2^2}}\right) \tag{89c}$$

Hence, the coordinates of X and Y are,

$$X = \ell \cos \rho = R \sin \varepsilon \left[\left(1 + \frac{h}{R}\right) \cos \varepsilon - \sqrt{1 - \left(1 + \frac{h}{R}\right)^2 \sin^2 \varepsilon}\right] \frac{X_2}{\sqrt{X_2^2 + Y_2^2}} \tag{90a}$$

$$Y = \ell \sin \rho = R \sin \varepsilon \left[\left(1 + \frac{h}{R}\right) \cos \varepsilon - \sqrt{1 - \left(1 + \frac{h}{R}\right)^2 \sin^2 \varepsilon}\right] \frac{Y_2}{\sqrt{X_2^2 + Y_2^2}} \tag{90b}$$

where X_2 and Y_2 are given in Eq. (88).

Note that this derivation is general enough so that the formulae are valid if one replaces the attitude errors with errors plus offsets, i.e., replacing ϕ, θ, and ψ by $\phi_o + \phi$, $\theta_o + \theta$, and $\psi_o + \psi$, respectively.

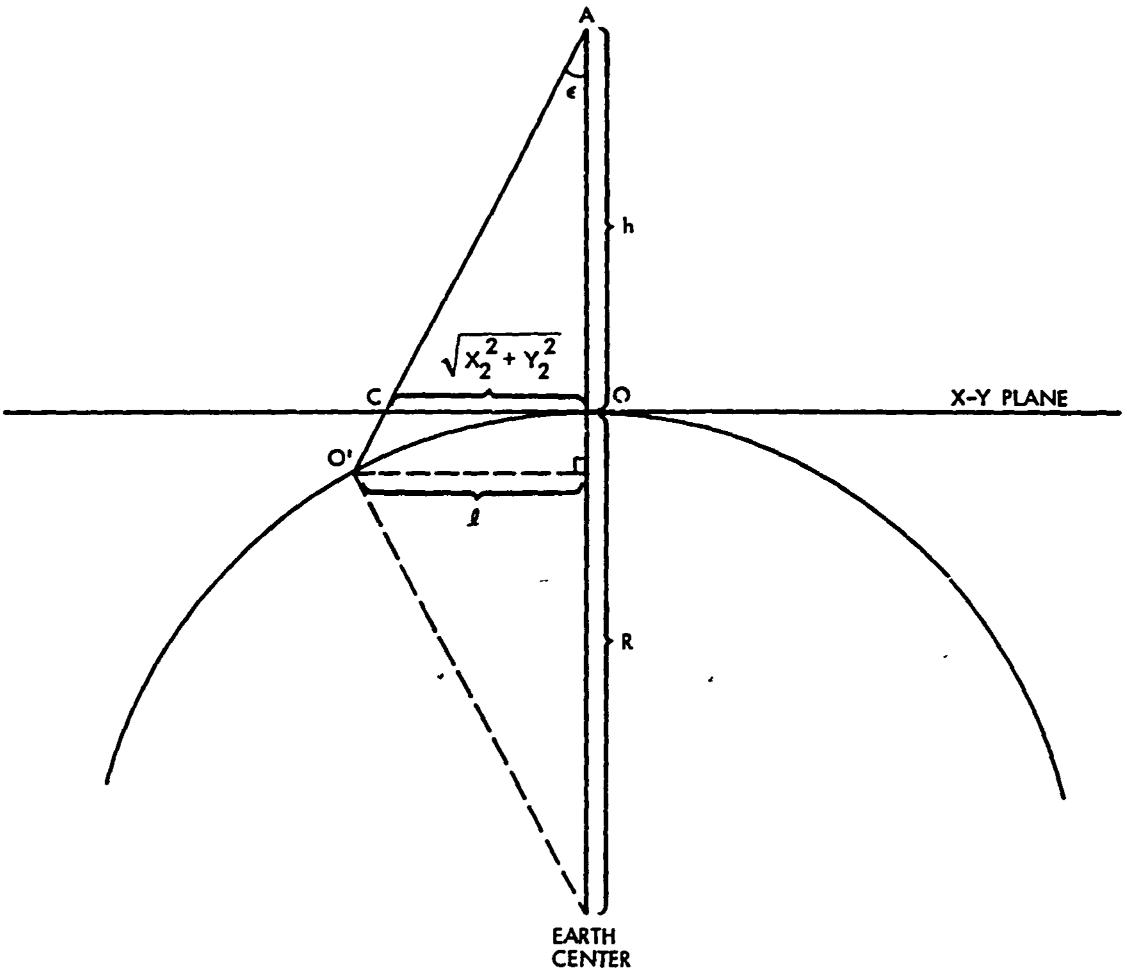

Figure 26. Side View of Figure 25

C.4.2. The Shift of Ground Image Due to Attitude Error

For simplicity, ϕ, θ, and ψ are used to represent the attitude angles as sums of attitude offsets and attitude errors. To fix the derivation, the yaw (ψ), pitch (θ), and roll (ϕ) Euler sequence is assumed.

In this subsection, the results of subsection C.4.1 are extended to cover the entire field of view of the IS slit. First consider the case of a nominal flight with zero attitude offset. Referring to Fig. 27, let O be the nadir point which is the origin of the XY-Frame and the X'Y'-Frame. The X'Y'-Frame is formed by rotating the XY-Frame through an angle ψ about the yaw axis. Let P be a point corresponding to a view angle λ (negative value shown in Fig. 27) on the Y-axis before any rotation occurs. After a ψ rotation, for the same view angle, the IS is sighting point P_1. Similarly, after a pitch (θ) and then roll (ϕ) rotation, the points P_2 and then P_3 are sighted, respectively.

The coordinates of P_2 in the X'Y'-Frame are, from the results of subsections C.1 and C.2 and Fig. 23,

$$X_2' = \frac{R \sin\theta \sin\xi_2 \left[\left(1 + \frac{h}{R}\right)\cos\xi_2 - \sqrt{1 - \left(1 + \frac{h}{R}\right)^2 \sin^2\xi_2}\right]}{\sqrt{\sin^2\theta + \tan^2\lambda}} \tag{91a}$$

$$Y_2' = -\frac{R \tan\lambda \sin\xi_2 \left[\left(1 + \frac{h}{R}\right)\cos\xi_2 - \sqrt{1 - \left(1 + \frac{h}{R}\right)^2 \sin^2\xi_2}\right]}{\sqrt{\sin^2\theta + \tan^2\lambda}} \tag{91b}$$

where the angle ξ_2 is the angle ξ defined in Fig. 23 corresponding to point P_2 here, and

$$\xi_2 = \tan^{-1}\left(\sec\theta \sqrt{\sin^2\theta + \tan^2\lambda}\right) \tag{91c}$$

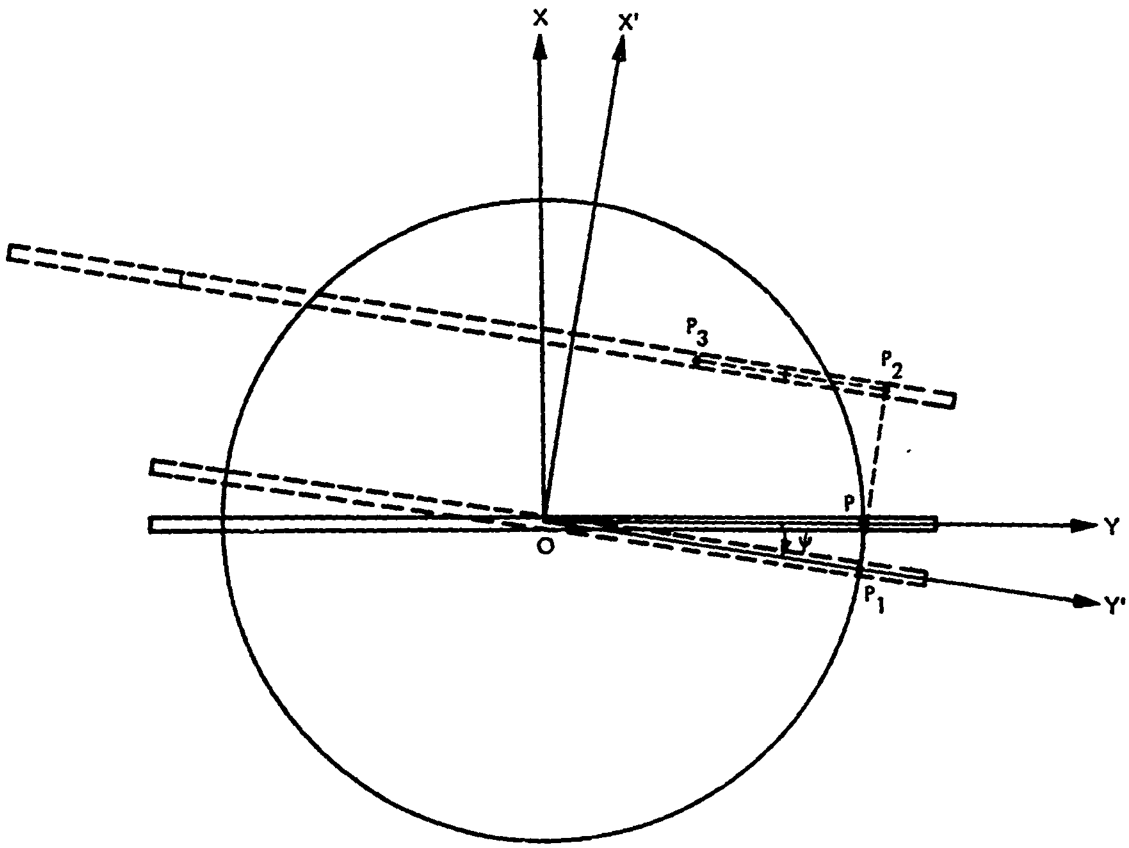

Figure 27. Shift of Ground Point Induced by Attitude Errors

The coordinates of P_3 in the X'Y'-Frame are

$$X_3' = \frac{R \sin\theta \sin\xi_3 \left[\left(1+\frac{h}{R}\right)\cos\xi_3 - \sqrt{1-\left(1+\frac{h}{R}\right)^2 \sin^2\xi_3}\right]}{\sqrt{\sin^2\theta + \tan^2(\lambda+\phi)}} \tag{92a}$$

$$Y_3' = -\frac{R \tan(\lambda+\phi) \sin\xi_3 \left[\left(1+\frac{h}{R}\right)\cos\xi_3 - \sqrt{1-\left(1+\frac{h}{R}\right)^2 \sin^2\xi_3}\right]}{\sqrt{\sin^2\theta + \tan^2(\lambda+\phi)}} \tag{92b}$$

where ξ_3 is similarly defined as ξ_2 and

$$\xi_3 = \tan^{-1}\left(\sec\theta\sqrt{\sin^2\theta + \tan^2(\lambda+\phi)}\right) \tag{92c}$$

or, finally, in the XY-Frame

$$X_3 = X_3' \cos\psi - Y_3' \sin\psi \tag{93a}$$

$$Y_3 = X_3' \sin\psi + Y_3' \cos\psi \tag{93b}$$

where X_3' and Y_3' are given in (92).

The geometric error caused by the attitude errors is therefore,

$$\Delta X = X - X_3 \tag{94a}$$

$$\Delta Y = Y - Y_3 \tag{94b}$$

where

$$X = 0$$

$$Y = -R \sin\lambda \left[\left(1+\frac{h}{R}\right)\cos\lambda - \sqrt{1-\left(1+\frac{h}{R}\right)^2 \sin^2\lambda}\right]$$

Now, consider the case of the shuttle (or the IS) flying at a nominal attitude (ϕ_o, θ_o, ψ_o) with attitude uncertainties of (ϕ, θ, ψ). Let $P_o(X_o,Y_o)$ be a ground point that is sighted by the IS with a view angle λ and attitude (ϕ_o, θ_o, ψ_o). After (ϕ, θ, ψ) attitude rotations from the nominal, the ground point $P_3(X_3,Y_3)$ is sighted with the same view angle. In this case, the geometric error is

$$\Delta X = X_o - X_3 \tag{95a}$$

$$\Delta Y = Y_o - Y_3 \tag{95b}$$

where

$$X_o = X_o' \cos \psi_o - Y_o' \sin \psi_o \tag{96a}$$

$$Y_o = X_o' \sin \psi_o + Y_o' \cos \psi_o \tag{96b}$$

$$X_3 = X_3' \cos (\psi_o + \psi) - Y_3' \sin (\psi_o + \psi) \tag{96c}$$

$$Y_3 = X_3' \sin (\psi_o + \psi) + Y_3' \cos (\psi_o + \psi) \tag{96d}$$

and

$$X_o' = \frac{R \sin \theta_o \sin \xi_o \left[\left(1 + \frac{h}{R}\right) \cos \xi_o - \sqrt{1 - \left(1 + \frac{h}{R}\right)^2 \sin^2 \xi_o}\right]}{\sqrt{\sin^2 \theta_o + \tan^2 (\lambda + \phi_o)}} \tag{97a}$$

$$Y_o' = - \frac{R \tan (\lambda + \phi_o) \sin \xi_o \left[\left(1 + \frac{h}{R}\right) \cos \xi_o - \sqrt{1 - \left(1 + \frac{h}{R}\right)^2 \sin^2 \xi_o}\right]}{\sqrt{\sin^2 \theta_o + \tan^2 (\lambda + \phi_o)}} \tag{97b}$$

where

$$\xi_o = \tan^{-1} \left(\sec \theta_o \sqrt{\sin^2 \theta_o + \tan^2 (\lambda + \phi_o)}\right) \tag{97c}$$

and

$$X_3' = \frac{R \sin (\theta_o + \theta) \sin \xi_3 \left[\left(1 + \frac{h}{R}\right) \cos \xi_3 - \sqrt{1 - \left(1 + \frac{h}{R}\right)^2 \sin^2 \xi_3}\right]}{\sqrt{\sin^2 (\theta_o + \theta) + \tan^2 (\lambda + \phi_o + \phi)}} \tag{98a}$$

$$Y_3' = - \frac{R \tan (\lambda + \phi_o + \phi) \sin \xi_3 \left[\left(1 + \frac{h}{R}\right) \cos \xi_3 - \sqrt{1 - \left(1 + \frac{h}{R}\right)^2 \sin^2 \xi_3}\right]}{\sqrt{\sin^2 (\theta_o + \theta) + \tan^2 (\lambda + \phi_o + \phi)}} \tag{98b}$$

and where

$$\xi_3 = \tan^{-1} \left[\sec (\theta_o + \theta) \sqrt{\sin^2 (\theta_o + \theta) + \tan^2 (\lambda + \phi_o + \phi)}\right] \tag{98c}$$

To include errors caused by altitude uncertainties, one can replace h by h_o in Eq. (97), and h by $h_o + \Delta h$ in Eq. (98), where h_o is the nominal or estimated altitude and $h_o + \Delta h$ is the actual altitude.

D. GEOMETRIC ERRORS INDUCED BY ATTITUDE RATE ERRORS

Attitude rates cause attitude angle changes which in turn cause geometric errors. To account for attitude rates, one integrates the rates to obtain the attitude angles, and then uses the formulae derived to obtain the corresponding time-varying geometric errors. The instantaneous attitude angles are:

$$\phi' = \phi_o + \int_{t_o}^{t} \dot{\phi} d\tau \tag{99 a}$$

$$\theta' = \theta_o + \int_{t_o}^{t} \dot{\theta} d\tau \tag{99 b}$$

$$\psi' = \psi_o + \int_{t_o}^{t} \dot{\psi} d\tau \tag{99 c}$$

E. GEOMETRIC ERRORS INDUCED BY MISALIGNMENT ERRORS

The misalignment errors can be incorporated in the attitude errors. Let $(\phi_b, \theta_b, \psi_b)$ be the attitude bias or misalignment, then the effective IS attitude angles will be

$$\phi' = \phi_o + \phi_b + \phi \tag{100a}$$

$$\theta' = \theta_o + \theta_b + \theta \tag{100b}$$

$$\psi' = \psi_o + \psi_b + \psi \tag{100c}$$

The corresponding geometric errors can be determined using the formulae derived in subsection C.

F. GEOMETRIC ERRORS INDUCED BY EARTH ROTATION

The effect of earth rotation on images varies with the position of the Shuttle relative to the earth and the Shuttle orbital elements. In general, ground images become skewed as a result of earth rotation.

Referring to Fig. 28. Let O be the nadir point at which the latitude is ζ. Let ω_e be the spin rate of the earth, where $\omega_e = \frac{2\pi}{86400} = 7.2722 \times 10^{-5}$ rad/sec. Let V_e be the linear velocity of the earth at O,

$$V_e = \omega_e R \cos \zeta \tag{101}$$

Let Γ be the orbital inclination at the equator, and let Λ be the orbital inclination to the local meridian at O. From Fig. 29 and Appendix B, one has the following spherical geometrical relation,

$$\cos \Gamma = \cos \zeta \sin \Lambda$$

or

$$\sin \Lambda = \frac{\cos \Gamma}{\cos \zeta} \tag{102a}$$

and

$$\cos \Lambda = \sqrt{1 - \sin^2 \Lambda} = \sqrt{1 - \left(\frac{\cos \Gamma}{\cos \zeta}\right)^2} \tag{102b}$$

From Fig. 29 again, Λ is also the angle between the linear velocity vector V_e and the Y-axis. Hence, velocity components V_{eX} and V_{eY} are, using (102),

$$V_{eX} = V_e \sin \Lambda = \frac{V_e \cos \Gamma}{\cos \zeta} \tag{103a}$$

and

$$V_{eY} = V_e \cos \Lambda = V_e \sqrt{1 - \left(\frac{\cos \Gamma}{\cos \zeta}\right)^2} \tag{103b}$$

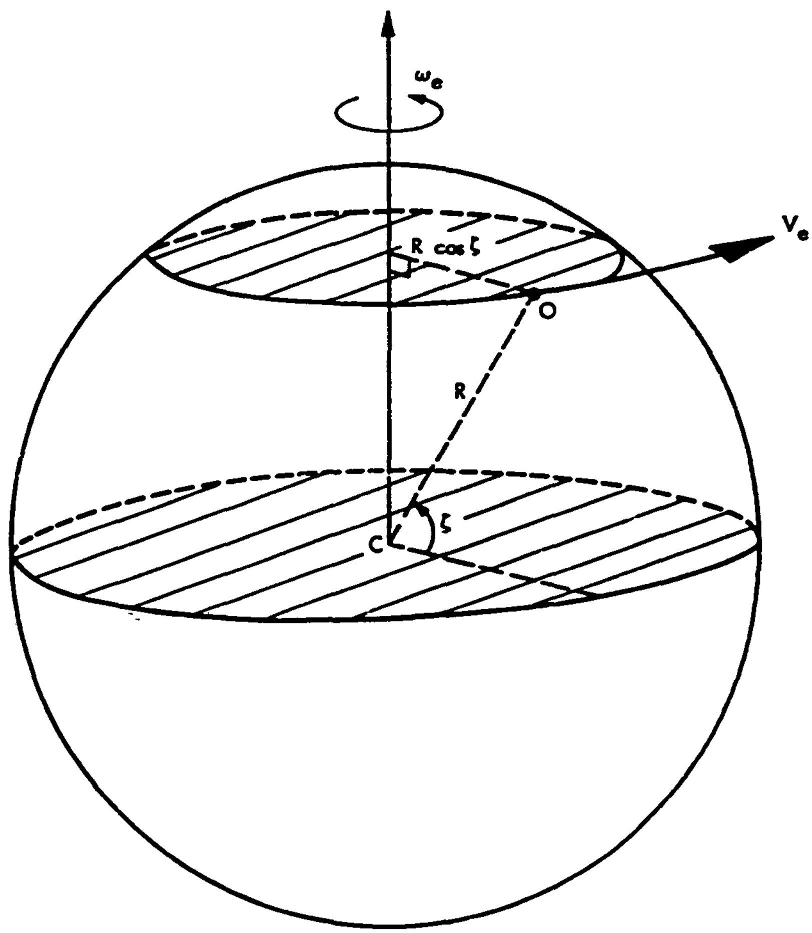

LEGEND:
ω_e = ANGULAR VELOCITY OF EARTH SPIN
ζ = LATITUDE AT POINT O
V_e = LINEAR VELOCITY OF THE EARTH AT POINT O

Figure 28. Linear Velocity of the Earth at the Nadir Point

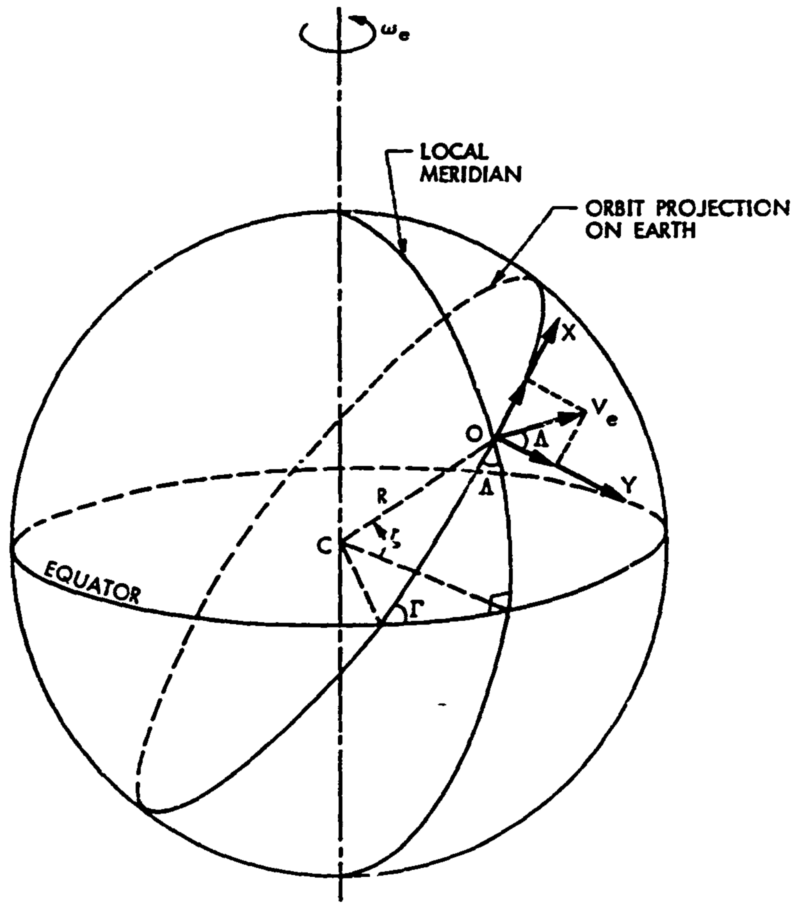

(a) INTRACK AND CROSSTRACK COMPONENTS OF EARTH LINEAR VELOCITY VECTOR AT THE NADIR POINT

(b) ORBIT INCLINATION TO THE LOCAL MERIDIAN (Λ), degrees

ORBITAL INCLINATION (degrees)	NORTH LATITUDE, degrees				
	0	20	40	60	80
0	90	–	–	–	–
18.5	71.5	–	–	–	–
40	50	54.61	90	–	–
60	30	32.15	40.75	90	–
85	5	5.32	6.53	10.04	30.13
90	0	0	0	0	0

Figure 29. Earth Sperical Geometry

During the time interval from t_1 to t_2, the ground point has moved from P(X, Y) to P'(X', Y'), the corresponding position changes are,

$$\Delta X = \int_{t_1}^{t_2} V_{eX} dt = \int_{t_1}^{t_2} \frac{Ve \cos \Gamma}{\cos \zeta} dt \qquad (104a)$$

$$\Delta Y = \int_{t_1}^{t_2} V_{eY} dt = \int_{t_1}^{t_2} Ve \sqrt{1 - \left(\frac{\cos \Gamma}{\cos \zeta}\right)^2} dt \qquad (104b)$$

Note that for small time intervals, ζ may be considered constant and (104) may be approximated as

$$\Delta X \cong \frac{\cos \Gamma}{\cos \zeta} V_e \ (t_2 - t_1) \qquad (105a)$$

$$\Delta Y \cong \sqrt{1 - \left(\frac{\cos \Gamma}{\cos \zeta}\right)^2} \ V_e (t_2 - t_1) \qquad (105b)$$

and

$$X' = X + \Delta X \qquad (106a)$$

$$Y' = Y + \Delta Y \qquad (106b)$$

G. NUMERICAL RESULTS: GEOMETRIC ERRORS AND ERROR SENSITIVITIES

Numerical results of error sensitivities and geometric errors due to various direct errors have been generated. These data are summarized in Tables 5-10 and discussed in the following subsections.

G.1 Geometric Errors Due to Altitude Uncertainties

Table 5 shows the geometric error for a 1 km altitude change and error sensitivity caused by altitude uncertainty. The nominal altitude of 400 km was used to generate these data. This result is also plotted in Fig. 30 as a function of view angles for altitude changes ranging from 1 km to 4 km. As indicated in this figure, the geometric errors are quite linear with the view angles and the altitude errors for the range shown.

For the Imaging Spectrometer illustrated in Fig. 4, the view angles are limited by the field of view of $\pm .825^{o}$. Using the various expected on-orbit navigation accuracies shown in Table 4, and the sensitivity data of Table 5, the corresponding geometric error can be determined. For instance, from Table 4, the 3σ altitude uncertainty, with TDRSS in the tracking system for the 150 nmi. orbit, if the small unmodeled perturbation is used, is 800 feet (or ~244 m) and with the STDN system and large unmodeled perturbation and 105 nmi. orbit, the 3σ altitude uncertainty is 8000 feet (or ~2440 m). From Table 5, the corresponding 3σ geometric errors for the largest view angle ($.825^{o}$) are 3.51 m and 35.1 m, respectively. Note that the nominal pixel size is 30 m.

G.2 Geometric Errors Due to Roll Uncertainties

The geometric errors for view angles ranging from -9^{o} to $+9^{o}$ due to a roll error of 1^{o} are tabulated in Table 6. The error sensitivity at the nominal attitude is also tabulated in Table 6. By comparing the errors for 1^{o} and the sensitivity for the same view angle, it is found that the differences are .2% or less. That is, for small angles, the error sensitivity data can be used to compute errors. Fig. 31 shows the plots of geometric errors for roll errors of up to 5^{o}. Unlike the errors corresponding to altitude uncertainties, these curves are relatively flat. The geometric error is about 7 km per 1^{o} of roll error.

It is noted from Fig. 31, that for small roll errors, the geometric errors are nearly symmetrical with the view angles. For larger roll angles, the geometric errors are greater for view angles that have the same sign of ϕ. This is more visible from Fig. 32 which shows the plots of geometric errors corresponding to roll errors of 1^{o} and 2^{o} from a roll offset of 20^{o}.

G.3 Geometric Errors Due to Pitch Uncertainties

Table 7 shows the error sensitivity and the geometric errors corresponding to the 1° pitch error for the view angles of up to $\pm 9^\circ$. The geometric errors caused by pitch errors are about the same in amplitude as those caused by roll errors. Fig. 33 shows that pitch curves are rather flat, unlike the corresponding roll curves. Figs. 34 and 35 show the 1° and 2° pitch uncertainty induced geometric error curves with 22.5° and 45° pitch offsets, respectively. These curves, especially those in Fig. 35, are more similar to the roll curves in shape.

G.4 Geometric Errors Due to Yaw Uncertainties

Geometric errors due to rotations about the yaw or the local vertical axis (assuming zero offsets) are tabulated in Table 8 for 1° and plotted in Fig. 36 for up to 5°. Linearity applies for both the view angles and the yaw angles for the ranges covered here. Unlike roll and pitch errors, yaw errors induce much smaller geometric errors.

G.5 Geometric Errors Due to Attitude Uncertainties

Table 9 shows the geometric errors due to 1° error in each of the roll, pitch, and yaw axes. The error magnitude for a given view angle is approximately the vector sum of the roll and pitch induced errors.

Fig. 37 shows the plots of geometric errors caused by up to 5° roll, pitch, and yaw errors. Fig. 38 shows two curves, one corresponding to 1° pitch error and the other, 1° yaw error, with the roll offset of 20°.

Comparing pitch curve with that of Fig. 33, the 20° roll offset has no noticeable effects on the geometric errors. On the other hand, the effects on the yaw curve are quite pronounced, as a large bias of approximately 2.5 km results due to the 20° roll.

Fig. 39 shows the 1° roll and 1° yaw curves for a pitch offset of 22.5°. Fig. 40 shows the same curves for 45° pitch offset.

With the large angular pitch offsets, the yaw curves appear quite different from those without pitch offset, as noted in Figs. 36, 39, and 40. With these offsets, yaw-induced error curves look quite similar to those induced by roll errors in shape. By offsetting the pitch angle to 45°, the yaw-induced geometric errors increase to about sevenfold from zero pitch offset, and more than twofold over the 22.5° pitch offset.

The roll-induced geometric errors were less drastically affected by pitch angular offsets. For instance, for 22.5° pitch offset, the error has increased about 7% from that with zero offset, and about 46% for 45° pitch offset.

G. 6 Ground Point Shift Due to Shuttle Motion and Earth Rotation

The earth rotation effect on the shift of the ground image varies with the latitude of the shuttle, and the combined effects of the earth rotation and shuttle motion vary with the orbital inclination in addition to the latitude. Table 10 shows the tabulation with latitude ranging from 0° to 80°. The largest earth rotation effect occurs at the equator, .46 km in one second, and diminishes to .08 km in one second at the latitude of 80° as shown in Fig. 41.

The combined effects are dominated by the motion of the shuttle since at 400 km altitude the projected ground speed is much greater than the earth rotation speed. In a one-second period, the image will shift more than 7 km for any latitude.

Table 5. Geometric Errors and Error Sensitivity Due to Altitude Uncertainties

- Nominal Earth Radius = 6356.785 km (Polar)
- Nominal Altitude = 400 km

View Angle, deg.	0	1	2	3	4	5	6	7	8	9
Geometric Error Induced by 1 km Altitude Error, km	0	0.01746	0.03492	0.05242	0.06995	0.08753	0.1052	0.1229	0.1407	0.1586
Geometric Error Sensitivity, km/km	0	0.01746	0.03492	0.05242	0.06995	0.08753	0.1052	0.1229	0.1407	0.1586

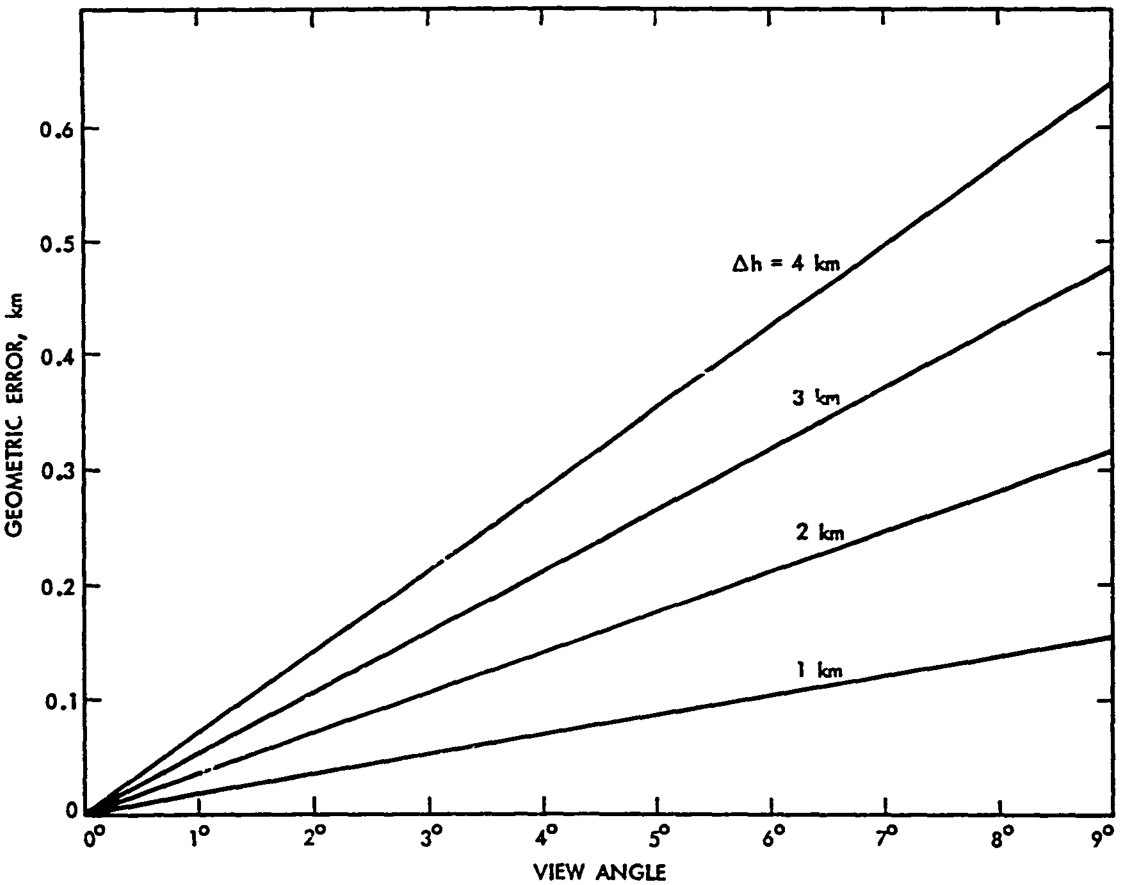

Figure 30. Geometric Error due to Altitude Uncertainties (Δh)

Table 6. Geometric Errors and Error Sensitivity Due to Roll Attitude Error

- Nominal Earth Radius = 6356.785 km (Polar)
- Nominal Altitude = 400 km

View Angle, deg.	-9	-8	-7	-6	-5	-4	-3	-2	-1	0
Geometric Error Induced by +1° Roll Error, km	7.153	7.114	7.081	7.052	7.029	7.010	6.996	6.987	6.982	6.982
Geometric Error Sensitivity, km/deg.	7.173	7.133	7.097	7.066	7.040	7.019	7.002	6.991	6.984	6.981

View Angle, deg.	1	2	3	4	5	6	7	8	9	
Geometric Error Induced by +1° Roll Error, km	6.987	6.996	7.010	7.029	7.052	7.081	7.114	7.153	7.196	
Geometric Error Sensitivity, km/deg.	6.984	6.991	7.002	7.019	7.040	7.066	7.097	7.133	7.173	

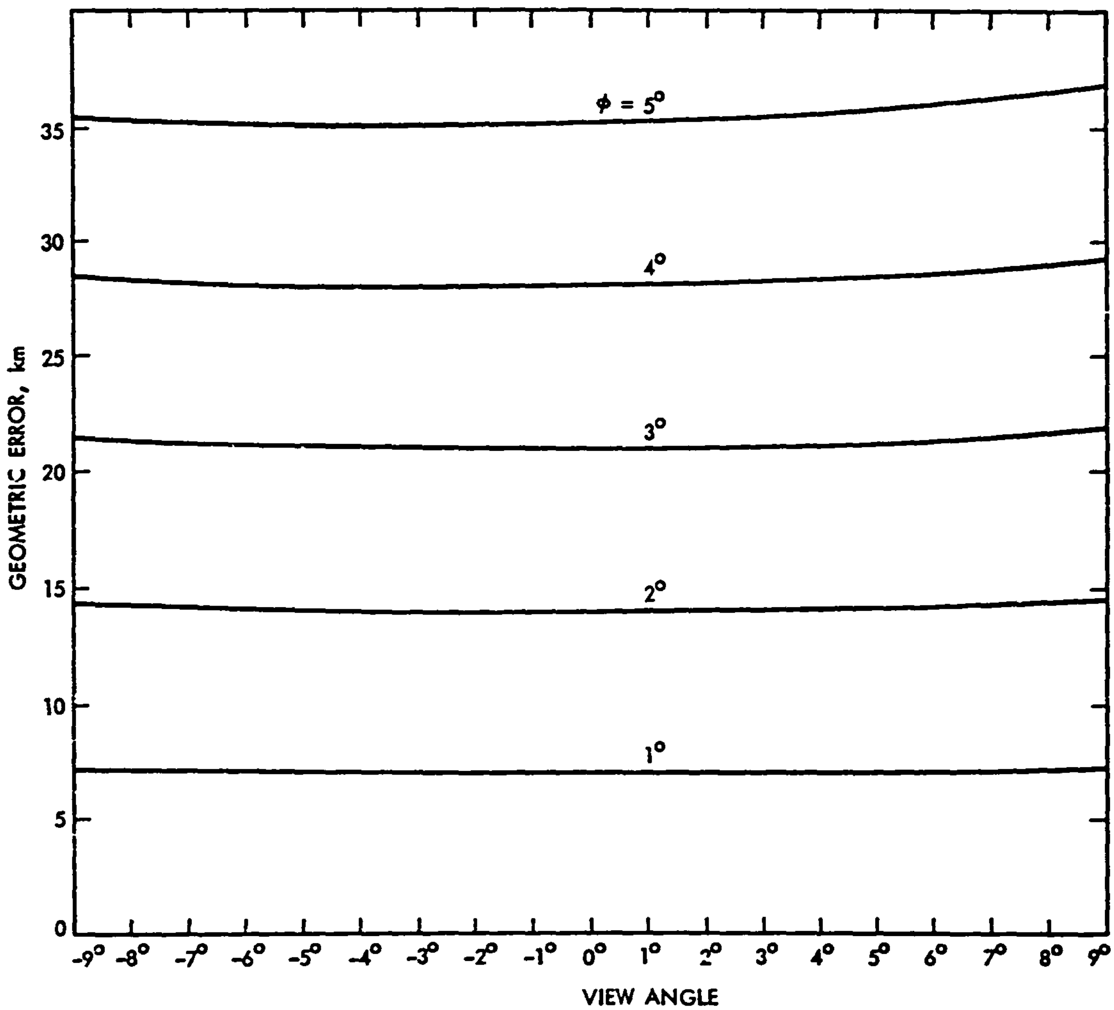

Figure 31. Geometric Error due to Roll Attitude Error (ϕ)

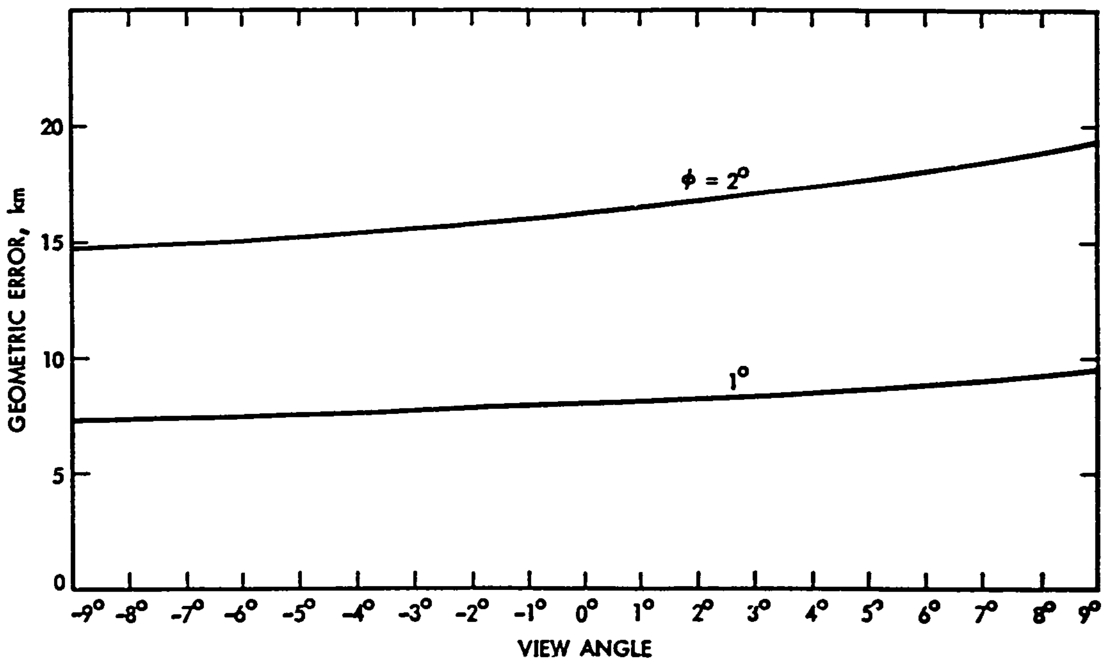

Figure 32. Geometric Error due to Roll Uncertainty (ϕ) About 20° Roll Offset

Table 7. Geometric Errors and Error Sensitivity
Due to Pitch Attitude Error

- Nominal Earth Radius = 6356.785 km (Polar)
- Nominal Altitude = 400 km

View Angle, deg.	-9	-8	-7	-6	-5	-4	-3	-2	-1	0
Geometric Error Induced by 1° Pitch Error, km	6.988	6.986	6.985	6.985	6.984	6.983	6.983	6.982	6.982	6.982
Geometric Error Sensitivity, km/deg.	6.987	6.986	6.985	6.984	6.983	6.982	6.982	6.982	6.981	6.981
View Angle, deg.	1	2	3	4	5	6	7	8	9	
Geometric Error Induced by 1° Pitch Error, km	6.982	6.982	6.983	6.983	6.984	6.985	6.985	6.986	6.988	
Geometric Error Sensitivity, km/deg.	6.981	6.982	6.982	6.982	6.983	6.984	6.985	6.986	6.987	

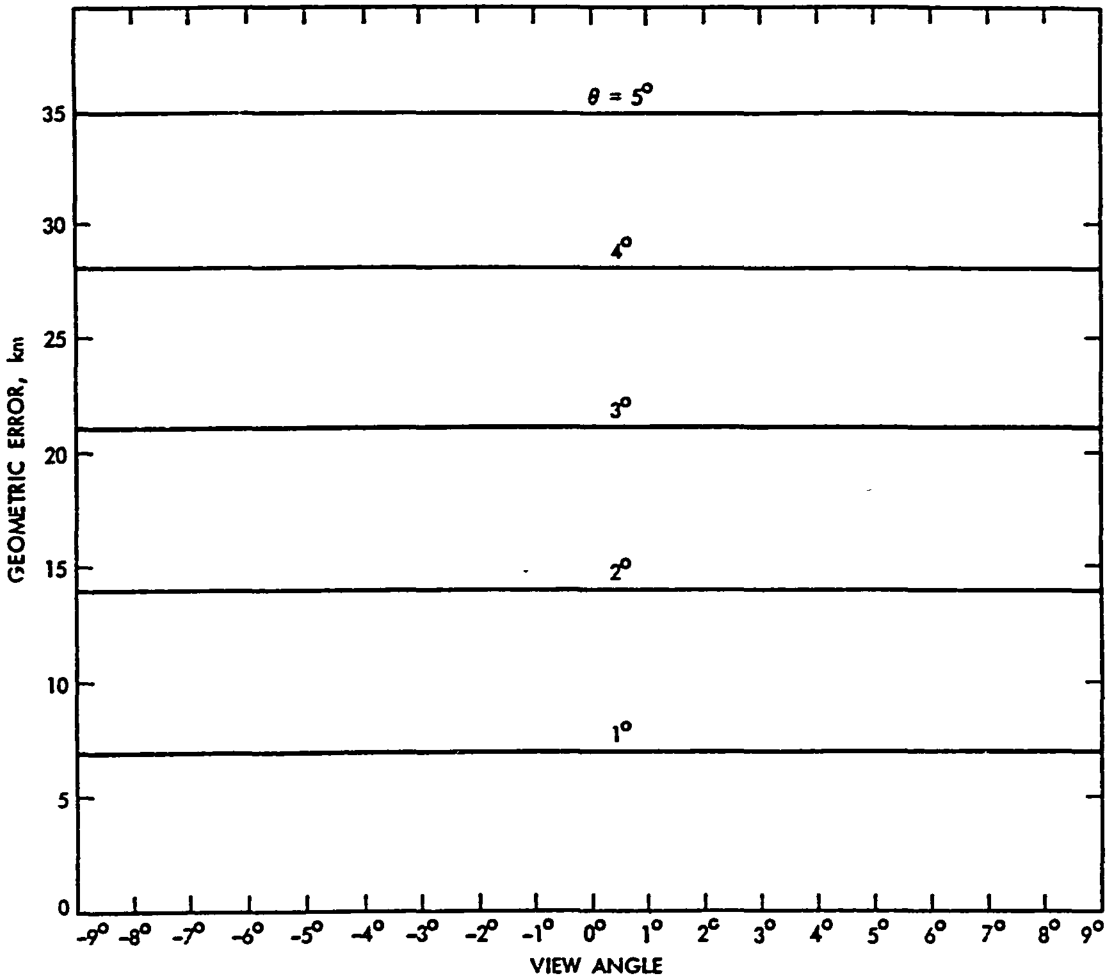

Figure 33. Geometric Error due to Pitch Attitude Error (θ)

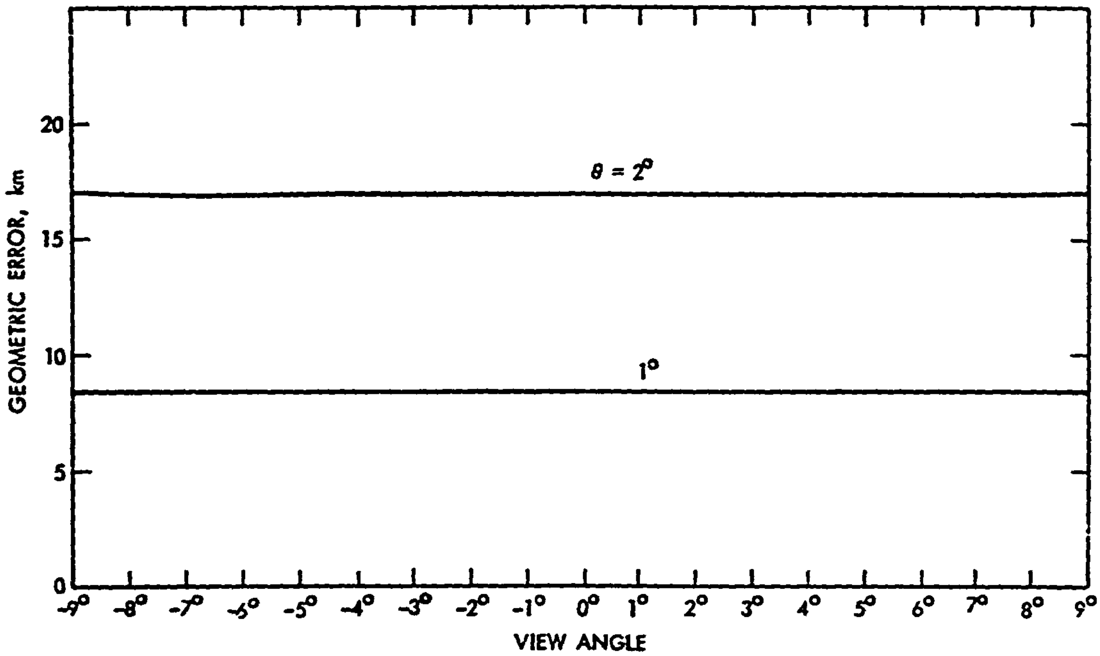

Figure 34. Geometric Error due to Pitch Uncertainty (θ) About 22.5° Pitch Offset

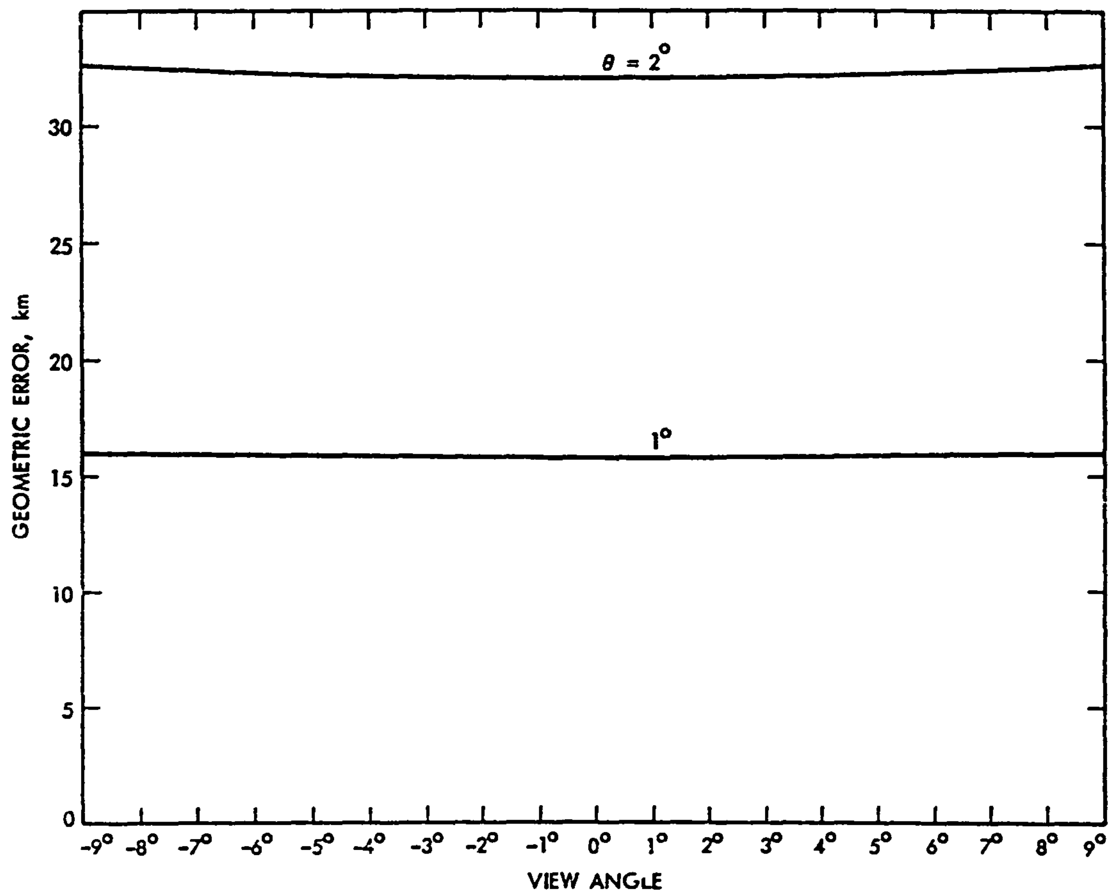

Figure 35. Geometric Error due to Pitch Uncertainty (θ) About 45° Pitch Offset

Table 8. Geometric Errors and Error Sensitivity Due to Yaw Attitude Error

- Nominal Earth Radius = 6356.785 km (Polar)
- Nominal Altitude = 400 km

View Angle, deg.	0	1	2	3	4	5	6	7	8	9
Geometric Error Induced by 1 Yaw Error, km	0	0.1219	0.2438	0.3659	0.4883	0.6109	0.7340	0.8576	0.9818	1.107
Geometric Error Sensitivity, km/deg.	0	0.1219	0.2438	0.3659	0.4883	0.6109	0.7340	0.8576	0.9818	1.107

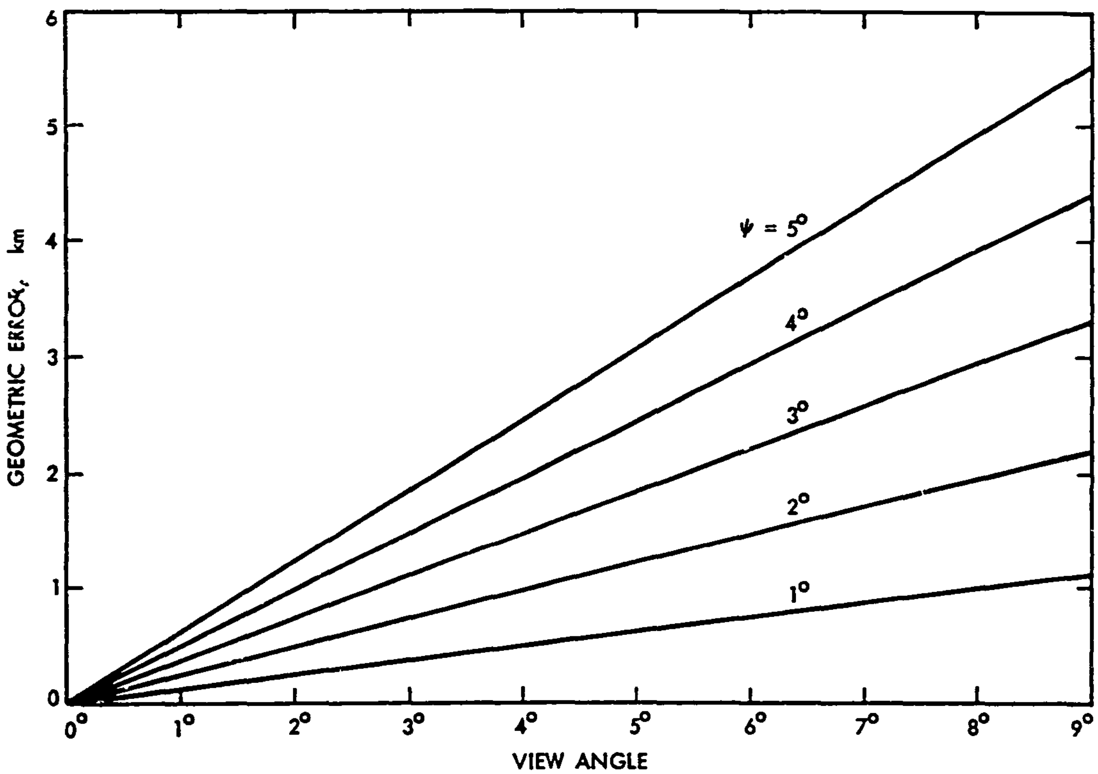

Figure 36. Geometric Error due to Yaw Attitude Error (ψ)

Table 9. Geometric Errors Induced by Yaw, Pitch, and Roll Errors

- Nominal Earth Radius = 6356.785 km (Polar)
- Nominal Altitude = 400 km
- Yaw Error = $+1^{\circ}$
- Pitch Error = $+1^{\circ}$
- Roll Error = $+1^{\circ}$

View Angle, deg.	-9	-8	-7	-6	-5	-4	-3	-2	-1	0
Error, km	9.245	9.296	9.353	9.414	9.480	9.551	9.625	9.704	9.788	9.875
View Angle, deg.	1	2	3	4	5	6	7	8	9	
Error, km	9.966	10.06	10.16	10.27	10.37	10.48	10.60	10.72	10.85	

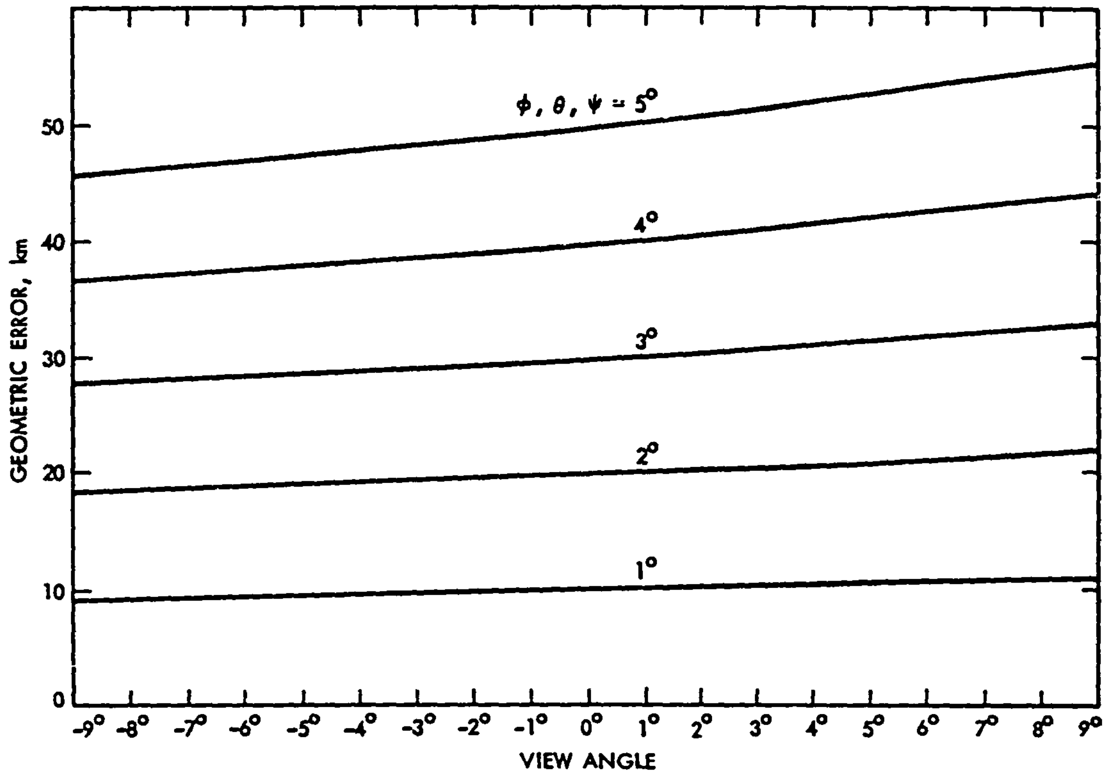

Figure 37. Geometric Error due to Roll (ϕ), Pitch (θ), and Yaw (ψ) Errors

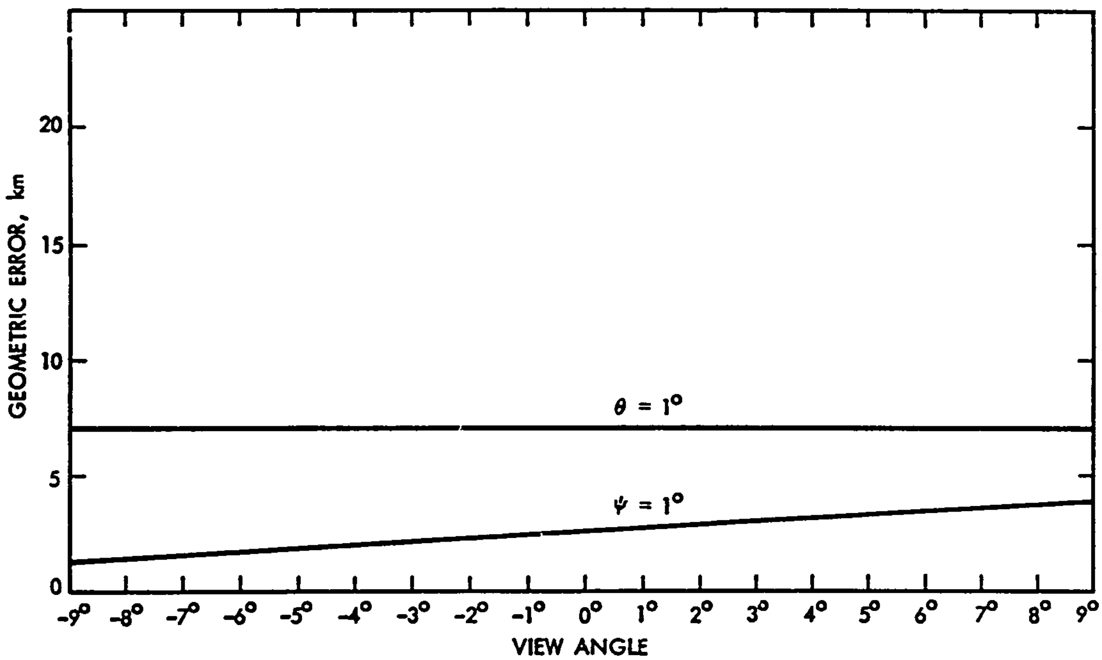

Figure 38. Geometric Error due to Pitch (θ) and Yaw (ψ) Uncertainties About 20° Roll Offset

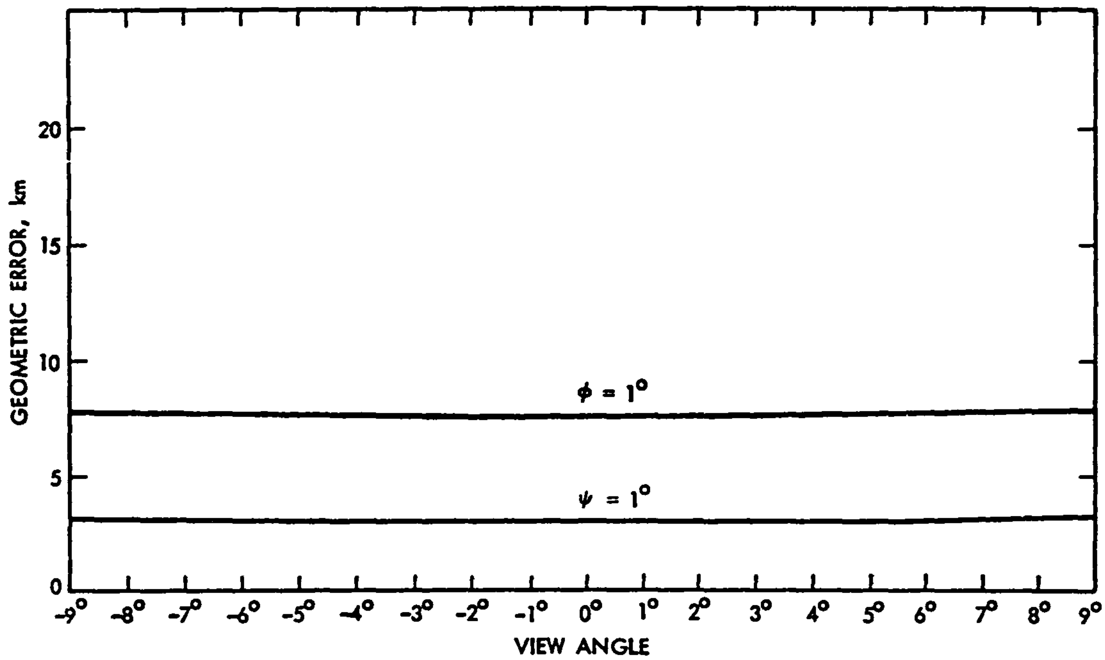

Figure 39. Geometric Error due to Roll (ϕ) and Yaw (ψ) Uncertainties About 22.5° Pitch Offset

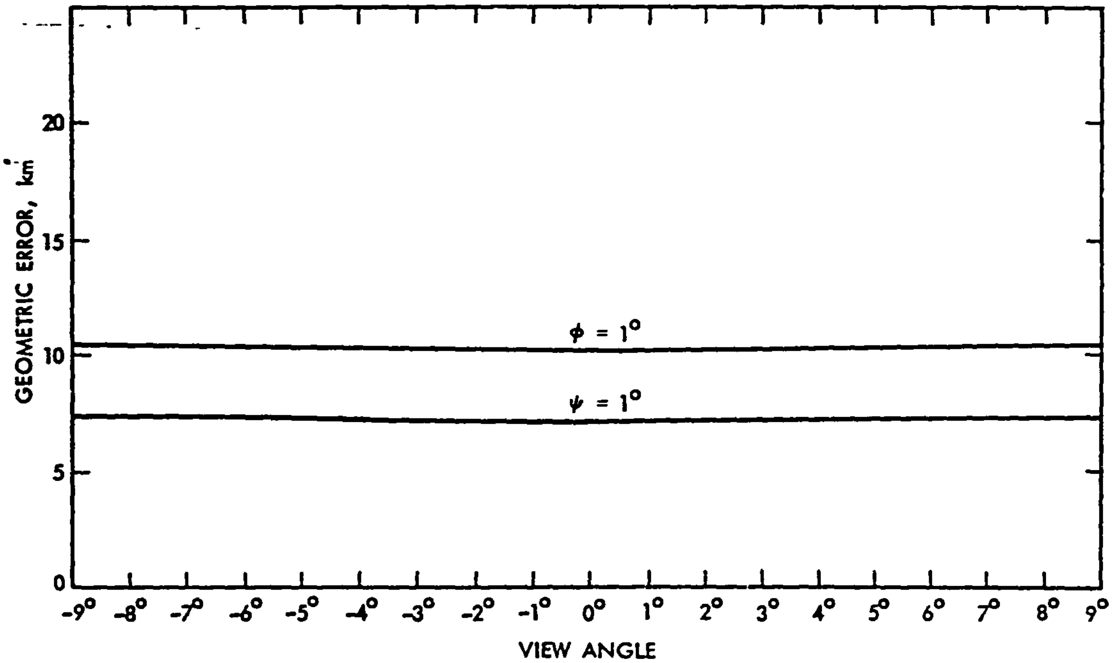

Figure 40. Geometric Error due to Roll (φ) and Yaw (ψ) Uncertainties About 45° Pitch Offset

Table 10. Ground Point Shift Induced by Shuttle Motion and Earth Rotation

- Nominal Earth Radius = 6356.785 km (Polar)
- Nominal Orbit Inclination = 85°
- Nominal Shuttle Ground Speed = 7.202 km/sec

Latitude, deg.	0	20	40	60	80
Ground Point Shift Velocity due to Earth Rotation, km/sec	0.4623	0.4344	0.3541	0.2311	0.08027
Ground Point Shift Velocity Relative to Nadir Point, km/sec	7.177	7.175	7.171	7.166	7.162
Angle of Velocity Vector with Y-axis, deg.	-86.32	-86.54	-87.19	-88.18	-89.44
Shift in 0.1 sec, km	0.7177	0.7175	0.7171	0.7166	0.7162

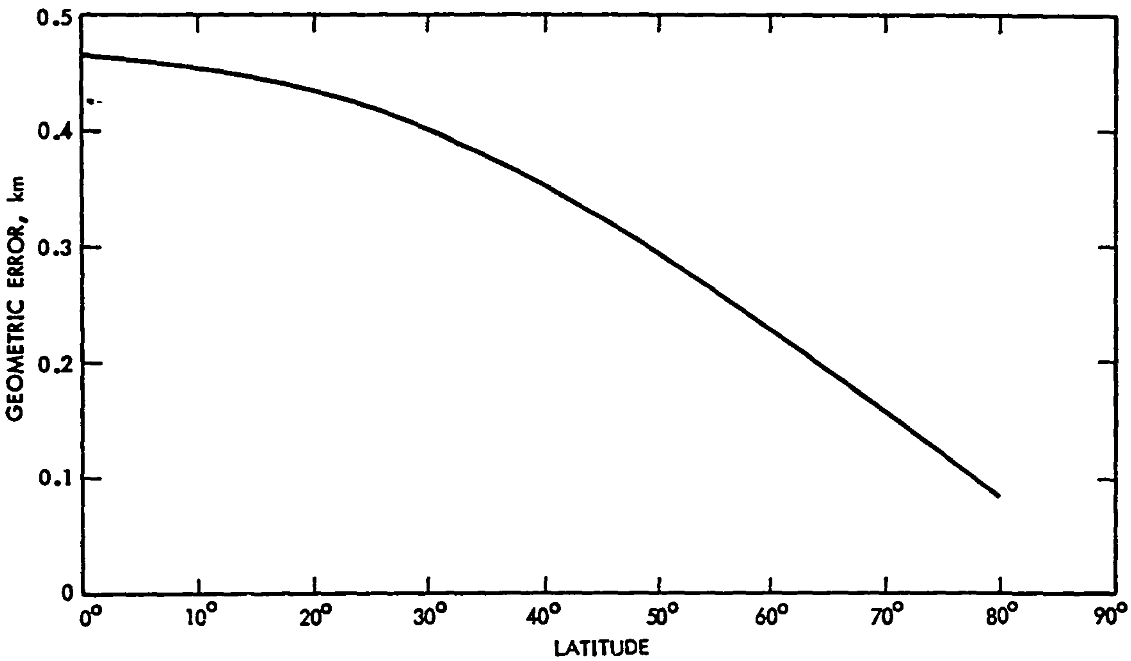

Figure 41. Geometric Error Caused by Earth Rotation for the Time Period of 1 Second

H. SUMMARY OF MAJOR FINDINGS

In this section geometric errors caused by the "direct error sources" are analyzed. Equations that map the direct errors onto the geometric errors are derived in Subsections B through G. Extensive illustrations of geometry are used to assist the derivations. Direct error effects included here are those of pointing errors and angular rates, ephemeris prediction errors including altitude, intrack, and crosstrack uncertainties, earth rotation and curvature, and shuttle and instrument misaligment. For quick reference the key error mapping functions are listed in Appendix A. A program list is given in Appendix E.

The numerical results for both the geometric errors and error sensitivities are tabulated in Tables 5 through 10 and also plotted in Figs. 30 through 41. To illustrate the effects of view angles and linearity, an extended range of $\pm 9^{\circ}$ is used. For the push broom imaging spectrometer studied here, the field of view is limited by $\pm .825^{\circ}$ (see Fig. 4). The following are the specific findings resulting from further analysis:

1. The effects of earth curvature are very small for the applications here. For instance, the linear displacement of a 10 km arc is 9.9999...km. Fig. 42 illustrates several cases of earth curvature effects.

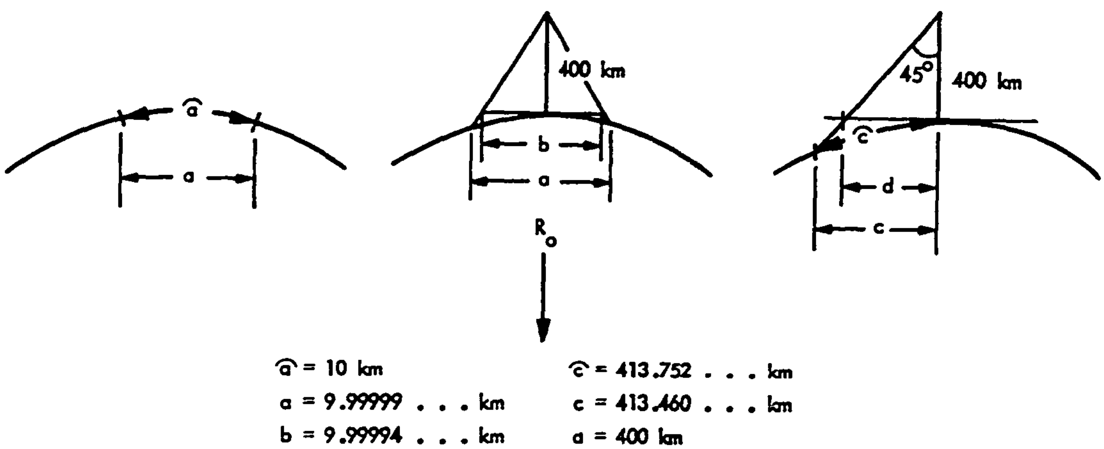

Figure 42. Effects of Earth Curvature

2. Altitude uncertainties cause only moderate geometric errors. Table 11 shows that the worst 1σ geometric error is 11.71 m and the corresponding rate is .133 m/sec. The worst case associates with the STDN system and large unmodeled perturbation and 200 km orbit. The least 1σ errors are .22 m and .0032 m/sec corresponding to the TDRSS system and small unmodeled perturbation and 300 km orbit. The effects of other navigation uncertainties such as downtrack and crosstrack position errors are not small, however. Table 12 shows the 3σ uncertainties in feet. Downtrack and crosstrack position errors are mapped directly to the geometric errors.

3. Geometric errors caused by altitude uncertainties are, within the range of interest here, proportional to the view angle and altitude error (see Table 5 and Fig. 30).

4. The effects of roll and pitch attitude errors are relatively large compared with those of altitude errors and yaw attitude errors. Table 13 shows that, for nominal flight conditions, the error sensitivity is approximately 1.94 m/arc sec, or ~7000 m/degree. The yaw sensitivity is very small, from 0 for 0° view angle to .0279 m/arc sec for maximum IS view angle ±.825°.

The effects of attitude errors increase significantly for large attitude offsets. For instance, for 20° roll offset (side looking), the roll sensitivity increases to 2.28 m/arc sec from 1.94 and yaw sensitivity increases to .75 m/arc sec from .0279. The pitch sensitivity, in this case, is nearly unaffected. By offsetting the pitch angle to 45° (forward looking), the roll sensitivity increases to 2.83 m/arc sec, the pitch to 4.36 m/arc sec, and the yaw to 1.97 m/arc sec. Table 13 shows the error sensitivities and 1° geometric errors for many combinations of interest.

5. Without attitude offsets and within the IS field of view, the geometric errors are almost proportional to roll errors (Fig.31), pitch errors (Fig.33), and yaw errors (Fig.36), and are independent of the view angle except for the yaw cases (for which the error is proportional to the view angle). For the cases of large roll or pitch angular offset, most of the properties change only slightly (see Figs. 32, 34, 35, 38, 39, and 40).

6. The performance of the Imaging Spectrometer is limited by the shuttle Inertial Measuring Unit accuracy, the shuttle reference misalignment, and the misalignment between the shuttle and the Imaging Spectrometer, unless means of error reduction, such as using ground control points and a precision point mount between the shuttle and the IS instruments, are employed.

On top of these uncertainties, the shuttle deadband is another source of error that can cause gross geometric errors. This problem, of course, can be resolved by using a precision point mount.

Table 14 shows geometric errors caused by the IMU/shuttle misalignment, IMU resolution, IMU noise, rate gyro drift, and combined shuttle/IS misalignment, for nominal attitude and attitude offsets. Single axis geometric errors corresponding to the combined shuttle/IS misalignment are 169 m, 198 m, and 379 m, respectively, for nominal, 20° roll offset, and 45° pitch offset, for instance. Other cases are shown in detail in Table 14.

7. Earth rotation causes images to shift toward the direction of rotation. The magnitude of this shift depends on the latitude of the object (see Fig. 41). For instance, at the equator, the object moves approximately 462 m in 1 second, while at 60° latitude, it moves only 231 m in one second.

Table 11. Geometric Errors Due to Expected On-orbit Navigation Uncertainty

Navigation Tracking System	Unmodeled Perturbation	Minimum Perigee, km	1σ Altitude Error, m	Max. Geom. Error in FOV, m	1σ Radial Velocity, m/s	Max. Geom. Error in FOV, m/s
STDN	Nominal	200	508	7.32	3.87	.056
TDRSS	Nominal	200	366	5.27	2.25	.032
STDN	Small	200	305	4.39	2.50	.036
		300	122	1.76	.59	.0085
TDRSS		200	183	2.63	1.12	.016
		300	81	1.17	.22	.0032
STDN	Large	200	813	11.71	9.27	.133
TDRSS	Large	200	610	8.78	5.69	.082

STDN — Spaceflight Tracking and Data Network
TDRSS — Tracking Data Relay Satellite System

Table 12. Expected On-Orbit Navigation Accuracies (Ref. 12)

Navigation Tracking System	Unmodeled Perturbation	Minimum Perigee, n.mi.	3σ Position, Feet			3σ Velocity, FPS		
			Radial	Down Track	Cross Track	Radial	Down Track	Cross Track
STDN	Nominal	105	5,000	34,500	5,000	38.4	5.9	9.8
TDRSS		105	3,600	18.500	4,000	22.1	3.3	4.0
STDN	Small	105	3,000	22,000	1,500	24.6	3.3	2.0
		150	1,200	5,500	1,000	5.8	1.3	1.8
TDRSS		105	1,800	10,000	2,000	11.0	1.8	2.9
		150	800	2,000	1,500	2.2	0.9	2.1
STDN	Large	105	8,000	80,000	5,000	91.2	8.0	8.0
TDRSS		105	6,000	50,000	5,000	56.0	6.2	7.8

NOTE:

The correlation between downtrack position and radial velocity is -0.95.
The correlation between radial position and downtrack velocity is -0.80.

STDN - Spaceflight Tracking and Data Network
TDRSS - Tracking Data Relay Satellite System

Table 13. Geometric Error Sensitivity

Nominal Orbit: 400 km Circular

Error Source	Attitude Offset	Error Sensitivity, m/arc sec: For View Angle = 0°	Error Sensitivity, m/arc sec: For View Angle = ±.825°	Geometric Error for 1° Angular Error, m
Roll angle	No offset	1.939	1.940	6,987
Pitch angle		1.939	1.939	6,982
Yaw angle		0	.0279	101
Roll angle	20° roll offset	2.25	2.28 2.22	8,200
Pitch angle		1.94	1.94	7,000
Yaw angle		.72	.75 .70	2,683
Roll angle	22.5° pitch offset	2.11	2.11	7,600
Pitch angle		2.31	2.31	8,300
Yaw angle		.83	.83	3,000
Roll angle	45° pitch offset	2.82	2.83	10,200
Pitch angle		4.33	4.36	15,700
Yaw angle		1.94	1.97	7,100
Altitude uncertainty		0	.0144 m/m	14.4 m per 1 km altitude change max in FOV

Table 14. Geometric Error Induced by Shuttle and Imaging Spectrometer Measurement Uncertainties

Nominal Orbit: 400 km Circular

Source	Attitude Offset	Per Axis, arc • sec	Per Axis Geometric Error, m	2 Axes,† Geometric Error, m
IMU/Shuttle Misalignment	No Offset	82	159	225
IMU Resolution•		20	39	55
IMU Noise		20	39	55
Rate Gyro		60 arc sec/sec	116 m/s	165 m/s
Combined Shuttle/IS Misalignment		87	169	239
IMU/Shuttle Misalignment	20° Roll Offset	82	187	245
IMU Resolution		20	46	60
IMU Noise		20	46	60
Rate Gyro		60 arc sec/sec	137 m/s	180 m/s
Combined Shuttle/IS Misalignment		87	198	260
IMU/Shuttle Misalignment	45° Pitch Offset	82	358	426
IMU Resolution		20	87	104
IMU Noise		20	87	104
Rate Gyro		60 arc sec/sec	262 m/s	312 m/s
Combined Shuttle/IS Misalignment		87	379	452

†Combined roll and pitch axes.

V. GROUND PATTERNS AND IMAGE DISTORTIONS

The extent that direct errors and earth geometric properties affect the performance of the Shuttle Imaging Spectrometer are analyzed and extensively illustrated with charts and tables in section IV. The advantages of tables and charts are that they carry precise and specific information which is invaluable for design and performance prediction. However, it is difficult to relate this information directly to images of ground objects by human brains. To compensate for this and to make direct observation of how errors in the system affect ground images, selected ground patterns as seen through this optical system are studied here.

The patterns that are readily generated and, most importantly, suitable for exhibiting imaging distortions are square grid patterns.

To cover a large ground that is comparable to the field of view of the imaging spectrometer, a 10 km field is selected and the field is evenly divided into 10 segments of 1 km each. Since the imaging spectrometer employs a push broom principle, each field is then 10 km wide (cross track) and 30 m "long" (along track). However, to see a large ground area, a 10 km x 10 km field is employed with the along track grids tagged with time. Considering a perfectly spherical earth, an imaginary 10 x 10 grid is painted on the ground. As the satellite flies through this region, in the direction from the bottom to the top of the paper, a push broom camera should see a pattern just like that of Fig. 43(a). This pattern is referred to as the nominal ground pattern.

Fig. 43 shows how the ground pattern changes when simple attitude error occurs without considering the effect of Earth rotation. To show the effect of errors, the solid pattern (actual) is overlayed with the "+" pattern (the undistorted nominal pattern). Fig. 43(b) shows that when a 0.1° roll attitude error occurs, the IS instrument points 0.1° left of the object field and the image on

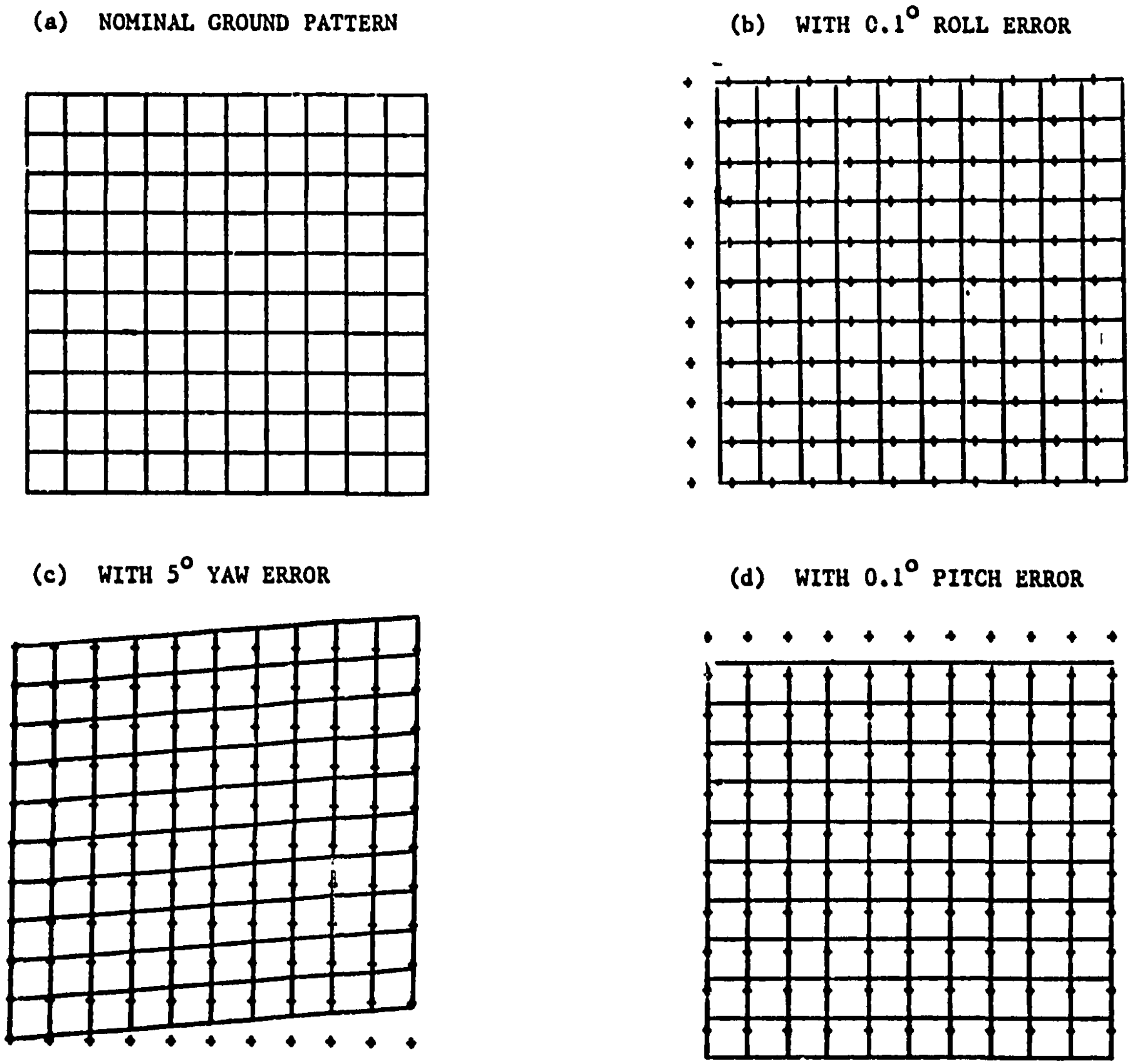

Fig. 43. Ground Pattern Distortions With No Earth Rotation Effect

the "film" has shifted to the right; therefore, the solid pattern has shifted to the right of the "+" pattern. The same explanation applies also to the 0.1° pitch error as shown in Fig. 43(d), except that, for pitch, the pattern image has shifted to the "-along track" direction. A 5° yaw error (clockwise rotation) will make the pattern appear skewed as shown in Fig. 43(c).

Fig. 44 shows the effects of simple attitude errors with 20° roll offset. With the large roll angle, the nominal pattern itself has suffered cross track distortions, i.e., the pattern image appears shrunk cross-trackwise as shown in Fig. 44(a). In Fig. 44(b), (c), and (d), the "+" patterns represent the distorted nominal patterns due to roll offset alone and the solid patterns represent those due to attitude errors on top of roll offset. The distortions are similar to those found in Fig. 43 except that with the 20° roll offset the images appear narrower.

The effects of simple attitude errors with 45° pitch offset are shown in Fig. 45. The effect of pitch offset is similar to roll offset, i.e., the nominal pattern image has shrunk cross-trackwise. One might expect also along-track shrinkage. The reason that there is no along-track shrinkage is because of the push-broom effect. Shrinkage will occur for a frame camera, however. It is noted that the pattern images associated with the 45° pitch offset are narrower than those of the 20° roll offset. This is due to the fact that 20° is a lot less than 45°.

The effects of constant attitude rate errors are shown in Fig. 46. Rate errors cause accumulation of attitude errors, i.e., the attitude errors grow with time t. Take the 0.1 deg/sec rate error for the roll axis for instance, the roll error is 0.1 t; whereas, the 0.1° roll error (Fig. 43(b)) at t = 0 is 0; therefore, the "+" pattern image coincides with the solid one at a very

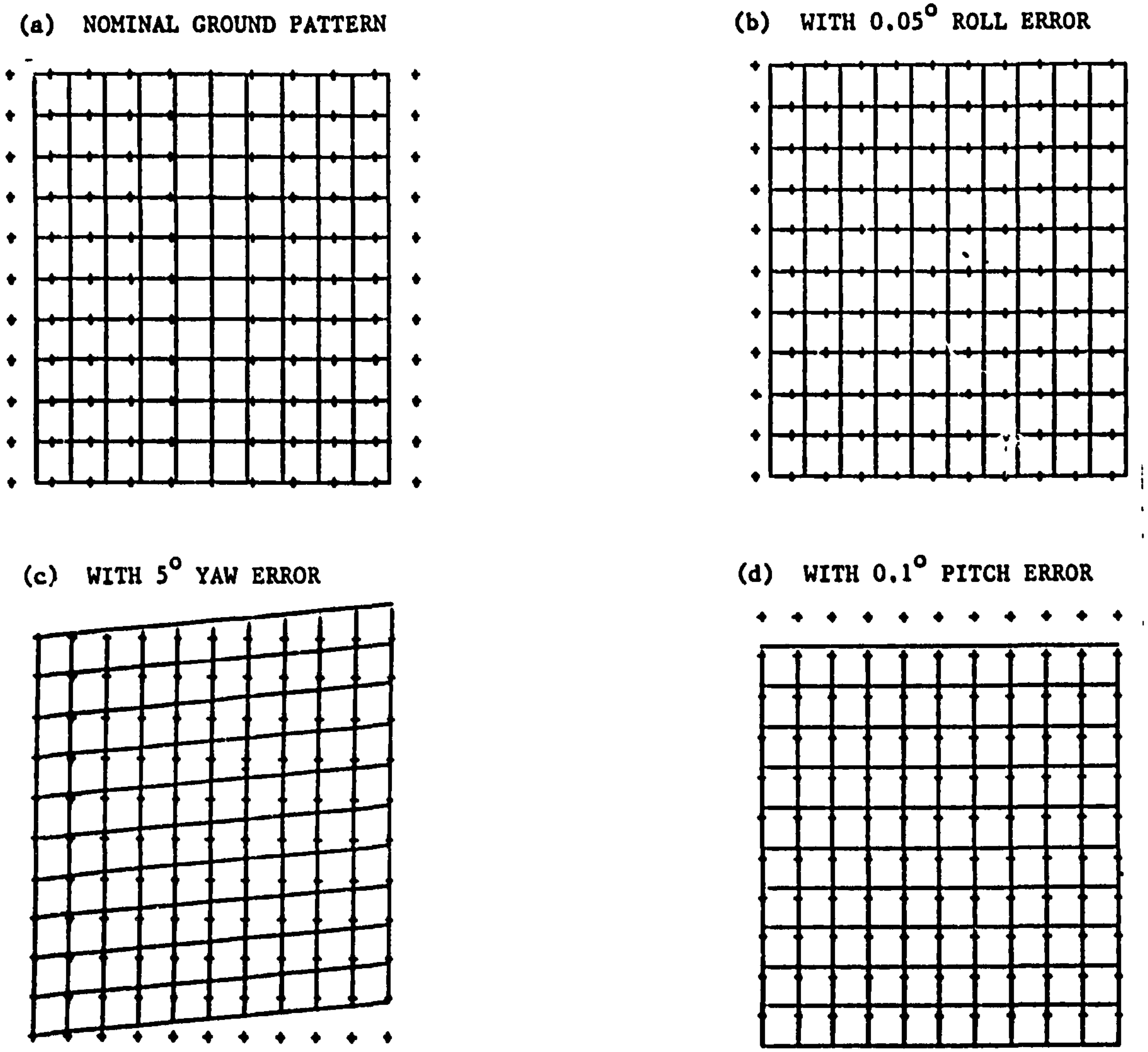

Fig. 44. Ground Pattern Distortions With 20° Roll Offset and No Earth Rotation Effect

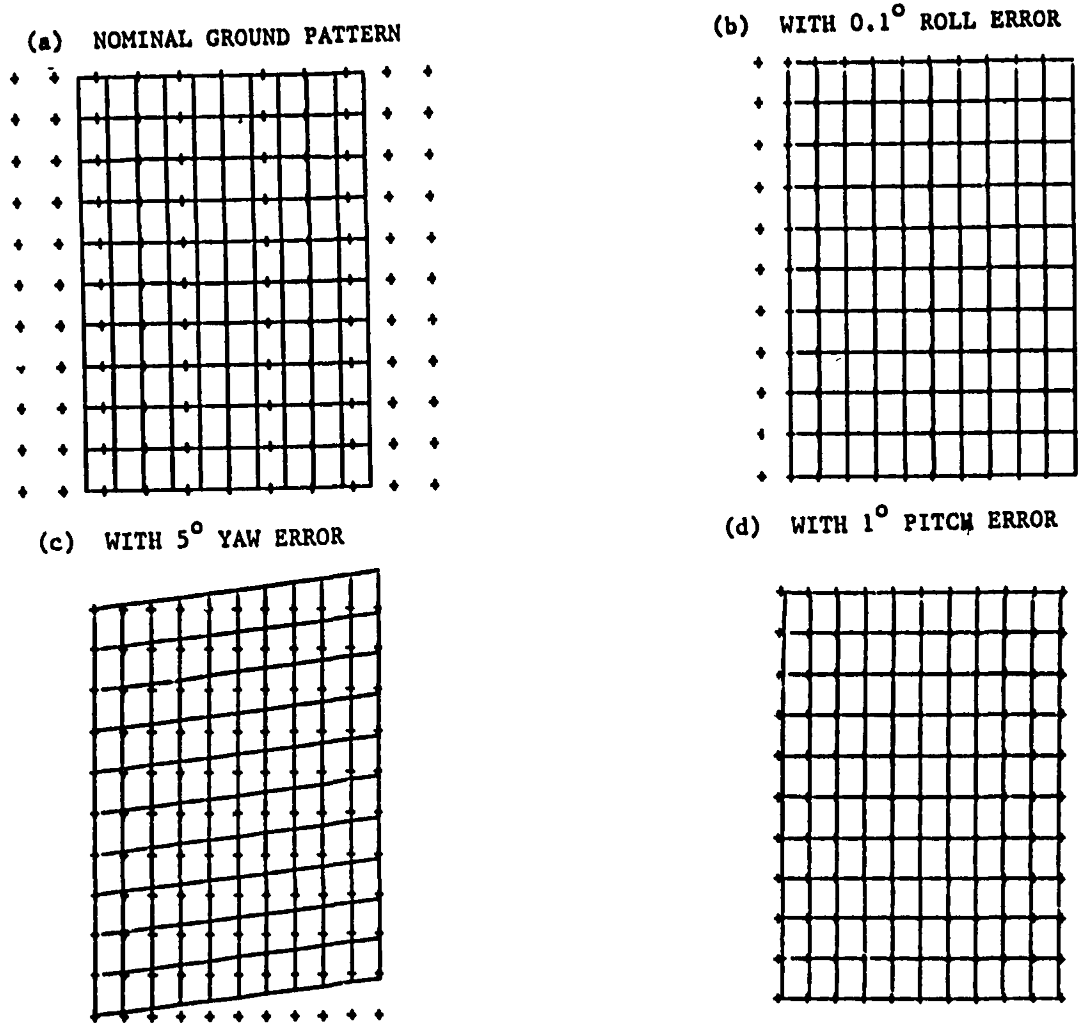

Fig. 45. Ground Pattern Distortions With 45° Pitch Offset and No Earth Rotation Effect

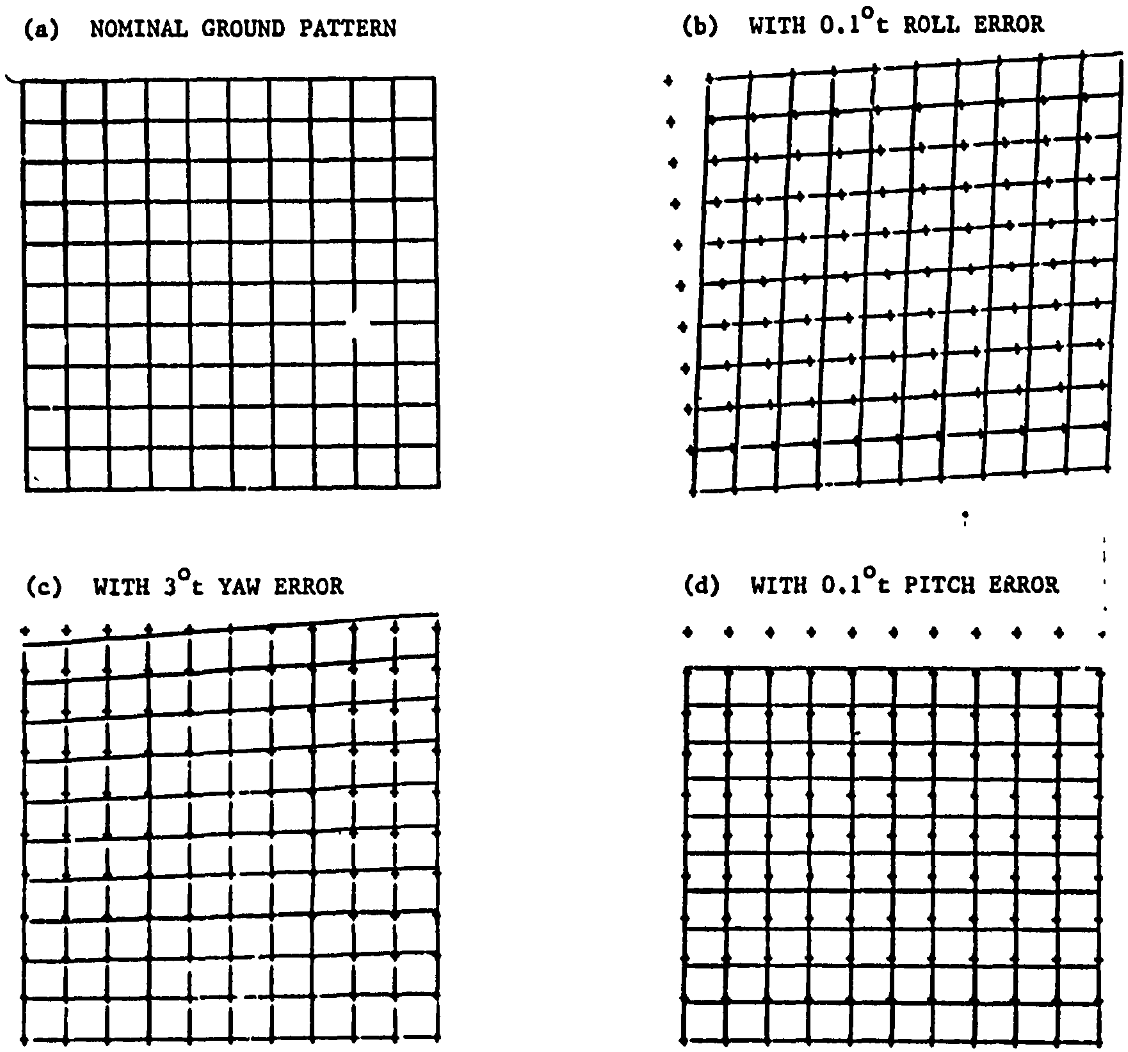

Fig. 46. Ground Pattern Distortions With Constant Rotation Rate and No Earth Rotation Effect

small t. Shown in Fig. 46(b) is the solid pattern shift to the right at a constant slope with time, which is quite different from Fig. 43(b). Similar comment applies to Fig. 46(c) and (d).

The effects of sinusoidal attitude rates on the pattern images are shown in Fig. 47. For instance, the sinusoidal rate causing a 0.2 sin (4.51378t) degree roll error will make the image appear as the shape "S", as shown in Fig. 47(b). The same function applied to the pitch axis will cause along-track distortions with densely packed grid lines followed by loosely packed ones, etc., as illustrated in Fig. 47(d).

Altitude change causes images to vary in size. Again, it affects the cross-track much more than the along-track due to the push-broom principle. As shown in Fig. 48, the solid image has shrunk cross-trackwise but expanded along-trackwise. The former is due to the altitude increase of 40 km which has no amplification effect on push-broom camera; the latter is due to the fact that, at higher altitude, the orbital rate is decreased, i.e., it will take a longer period of time to fly through the same ground area.

Finally, the effects of earth rotation are shown in Fig. 49. Earth rotation will cause the image to skew toward the direction of earth rotation. As discussed in section IV, the effect of the image shift is most pronounced when the satellite flies through the equator, and reduces as the latitude increases. Earth rotation will not cause along-track distortions.

Computer programs that are used to generate these patterns and distortions are listed in Appendix F.

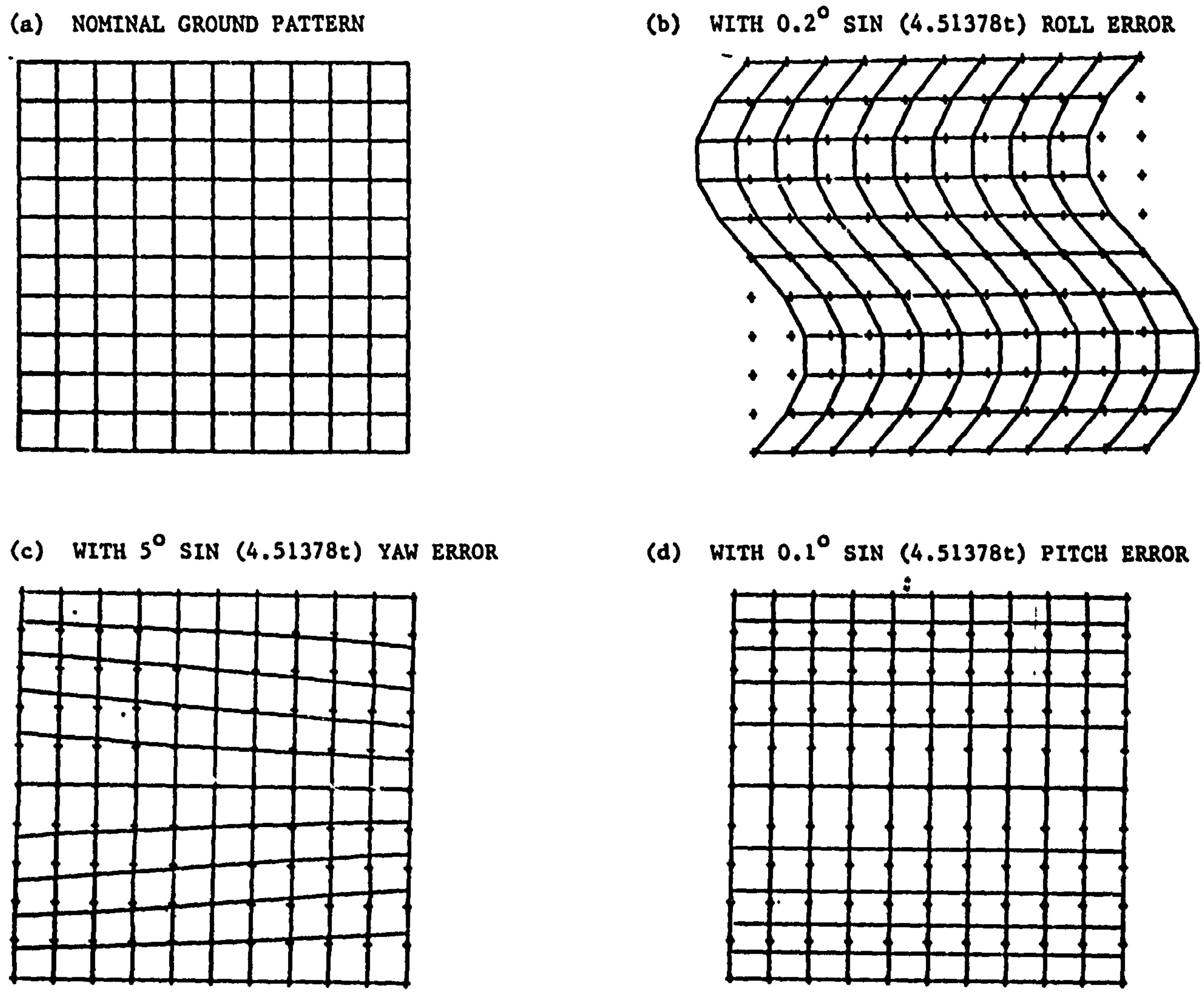

Fig. 47. Ground Pattern Distortions With Sinusoidal Rotation Rate and No Earth Rotation Effect

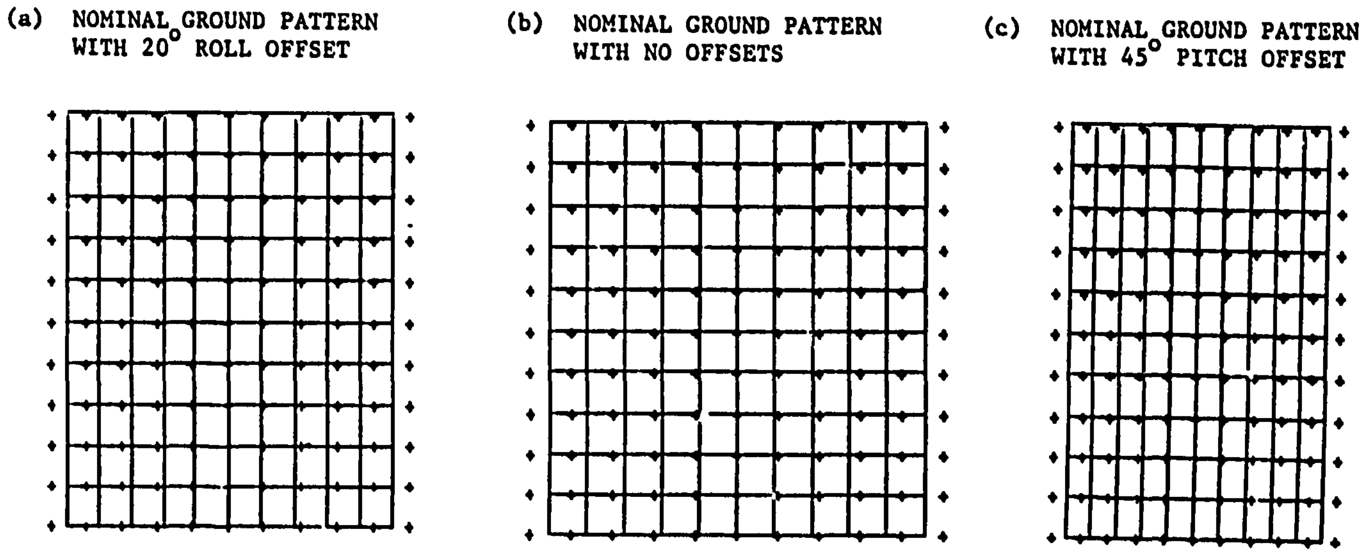

Fig. 48. Ground Pattern Distortions With Effect of Altitude Change (increase) of 40 km and No Earth Rotation Effect

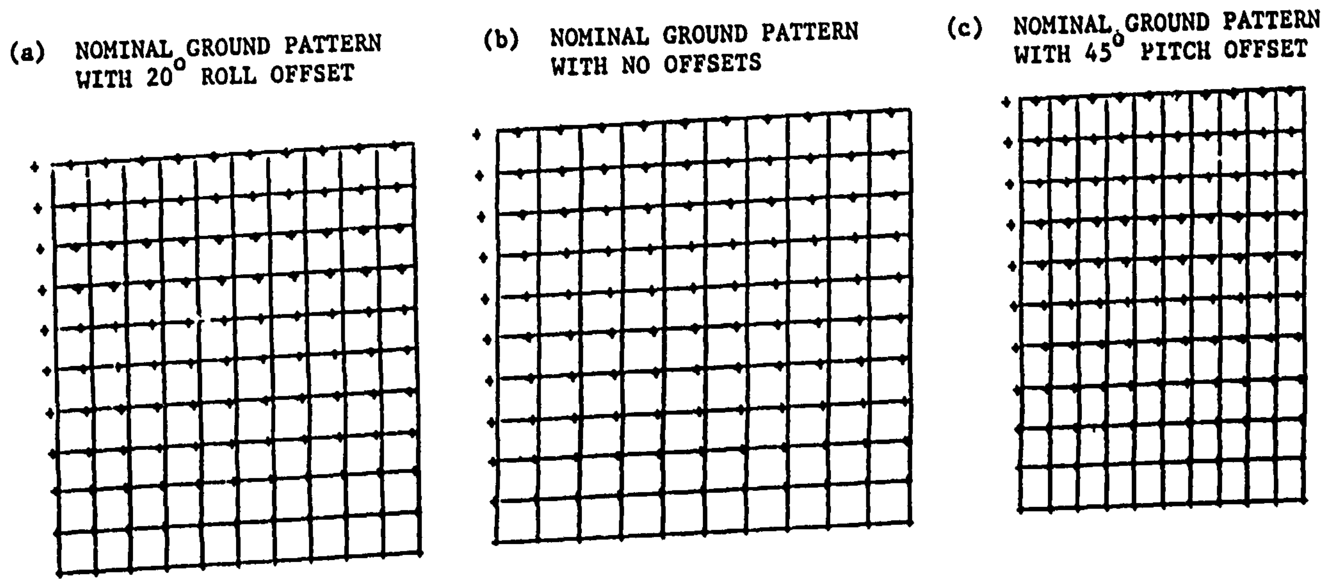

Fig. 49. Ground Pattern Distortions With Effect of Earth Rotation for 40° Latitude and Orbit Inclination of 85°

VI. CONCLUSIONS

1. The effects of earth curvature are very small for the application here (see Fig. 42).

2. Altitude uncertainties cause only moderate geometric errors. The worst 1σ geometric errors are 11.71 m in position and 0.133 m/sec in rate with STDN and large unmodeled perturbations at 200 km orbit. The performance improves with TDRSS. For the 300 km orbit and with small unmodeled perturbations, the 1σ geometric errors will reduce to 0.22 m and 0.0032 m/sec (see Table 11).

3. The effects of other navigation errors are significantly greater. The 1σ downtrack errors range from 203 m (300 km orbit) to 8128 m (200 km orbit); and those for the cross track are 152 m to 508 m (see Table 12).

4. The effects of roll and pitch attitude errors are relatively large compared with, for instance, those caused by yaw errors and altitude uncertainties. The error sensitivity is 1.94 m/arc sec or approximately 7000 m/degree. The yaw sensitivity is 0 for a 0° view angle and 0.028 m/arc sec for the maximum view angle of $\pm$ 0.825° (see Table 12).

5. The error sensitivities of attitude errors increase significantly for large attitude offsets. For 20° side looking, the sensitivity increases to 2.28 m/arc sec for roll errors and to 0.75 m/arc sec for yaw errors, and the pitch error sensitivity is almost unaffected. For the 45° forward looking case, the sensitivities for the pitch, roll, and yaw errors increase to 2.83, 4.36, and 1.97 m/arc sec, respectively (see Table 13).

6. The performance of the Shuttle Imaging Spectrometer is limited by the Shuttle IMU (Inertial Measuring Unit) accuracy, instrument misalignment, Shuttle RCS (Reaction Control Subsystem) deadband, etc. unless some means of error reduc-

tion are employed. For instance, ground control points may be used to reduce navigation prediction errors; and precision point mounts, such as AGS (ASPS[+] Gimbal System) and IPS (Instrument Pointing System), may be used to reduce the attitude errors. The single axis geometric errors due to the combined Shuttle/IS misalignment, for instance, for normal nadir pointing, 20° side looking, and 45° forward looking are 169 m, 198 m, and 379 m, respectively (refer to Table 14).

7. Earth rotation causes shifts of images toward the direction of rotation. The magnitude of these shifts depends on the latitude of the object. For instance, at the equator the object moves approximately 462 m in one second (for 400 km orbit), and at 60° latitude it moves only 231 m in one second.

8. Distorted images for selected ground patterns provide revealing information of the effects of system errors to the images of ground objects.

[+] Annular Suspension Pointing System

REFERENCES

1. "LANDSAT D Position Determination and Correction Study," Final Report prepared for NASA Goddard Space Flight Center by General Electric-Space Division, GE DOC #76SDS4277, NASA CR-144829, 22 Nov. 1976.

2. "Shuttle Imaging Spectrometer Experiment, Vol. I: Investigation and Technical Plan," Proposal submitted to NASA, JPL internal document D-755, July 18, 1983.

3. Wellman, J.B., Breckinridge, J.B., Kupferman, P.N., and Salazar, R., "Imaging Spectrometer: An Advanced Multispectral Imaging Concept," Vol. I, Digest of 1982 International Geoscience and Remote Sensing Symposium, Munich, West Germany, June 1-4, 1982.

4. Shuttle Operational Data Book, JSC-08934, Vol. II, Rev. B, August 1980; Amendment 46, January 6, 1982.

5. Space Shuttle System Payload Accomodations, JSC-07700, Vol. XIV, Rev. G, September 26, 1980, Change No. 35, August 21, 1981.

6. "Three-Plate On-Orbit Aerodynamic Torque Model," SSFS Doc. Series AER037, JSC-12604 (LEC-10294) Johnson Space Center, Houston, TX, March 1977.

7. "General Consideration of Control Disturbances for Large Space Structures," Final Report for JPL, contract #955345, prepared by Lockheed Missiles and Space Co., Sunnyvale, CA, January 18, 1980.

8. Space Transportation System User Handbook, N77-82346, NASA, Washington, D.C., June 1977.

9. "LANDSAT D Position Determination and Correction Study," Final Report prepared for NASA Goddard Space Flight Center by General Electric-Space Division, CR-144829, November 22, 1978.

10. Space Shuttle Orbiter Flight Test, Level C, Functional Subsystem Software Requirements, Guidance, Navigation, and Control, Part C, Flight Control, Part 2, SD 76-SH-0009 Book 2B, September 15, 1980.

11. Sackett, L.L., and Kirchway, C.B., "Dynamic Interaction of the Shuttle On-Orbit Flight Control System with Deployed Flexible Payload," Paper #82-1535, AIAA Guidance and Control Conference, San Diego, CA, August 9-11, 1982.

12. Osborne, D., Update of JSC-07700, Vol. XIV, July 1982.

13. Wertz, J.R., Spacecraft Attitude Determination and Control, D. Reidel Publishing Co., Dordrecht, Holland, pp. 730-731, 1978.

APPENDICES

APPENDIX A

GEOMETRIC ERROR MAPPING FUNCTION TABLE

Part A: Given the attitude offsets and a view angle, find the coordinates of the corresponding ground points before and after the errors are introduced.

Error Sources	Geometric Error Mapping Function	Comments
Altitude Error, Δh	At nominal altitude h, a view angle λ is given which sights a ground point $P(0, Y_o)$. After elevating Δh, the same view angle will sight another ground point $P'(0, Y_o')$. The following equations are for obtaining Y_o and Y_o': $$Y_o = -R \sin\lambda \left[\left(1 + \frac{h}{R}\right)\cos\lambda - \sqrt{1 - \left(1 + \frac{h}{R}\right)^2 \sin^2\lambda}\right]$$ $$Y_o' = -R \sin\lambda \left[\left(1 + \frac{h + \Delta h}{R}\right)\cos\lambda - \sqrt{1 - \left(1 + \frac{h + \Delta h}{R}\right)^2 \sin^2\lambda}\right]$$	R = Earth Radius
Yaw Error, ψ	Given: a yaw offset ψ_o and a view angle λ which sights a ground point $P(X^*, Y^*)$. The same view angle will sight another ground point $P'(X^{*\prime}, Y^{*\prime})$ after yaw error ψ is introduced. The following equations are for obtaining X^*, Y^*, $X^{*\prime}$, and $Y^{*\prime}$: $$X^* = \left[\left(1 + \frac{h}{R}\right)\cos\lambda - \sqrt{1 - \left(1 + \frac{h}{R}\right)^2 \sin^2\lambda}\right] R \sin\lambda \sin\psi_o$$ $$Y^* = -\left[\left(1 + \frac{h}{R}\right)\cos\lambda - \sqrt{1 - \left(1 + \frac{h}{R}\right)^2 \sin^2\lambda}\right] R \sin\lambda \cos\psi_o$$	R = Earth Radius h = Nominal Altitude

Error Sources	Geometric Error Mapping Function	Comments
	$X^{*\prime} = \left[\left(1 + \frac{h}{R}\right) \cos \lambda - \sqrt{1 - \left(1 + \frac{h}{R}\right)^2 \sin^2 \lambda}\right] R \sin \lambda \sin (\psi_o + \psi)$ $Y^{*\prime} = -\left[\left(1 + \frac{h}{R}\right) \cos \lambda - \sqrt{1 - \left(1 + \frac{h}{R}\right)^2 \sin^2 \lambda}\right] R \sin \lambda \cos (\psi_o + \psi)$	
Roll Error, ϕ	Given: a roll offset ϕ_o and a view angle λ which sights a ground point P(0, Y*). The same view angle will sight another ground point P'(0, Y*') after roll error ϕ is introduced. The following equations are for obtaining Y* and Y*': $Y^* = -R \sin (\lambda + \phi_o) \left[\left(1 + \frac{h}{R}\right) \cos (\lambda + \phi_o) - \sqrt{1 - \left(1 + \frac{h}{R}\right)^2 \sin^2 (\lambda + \phi_o)}\right]$ $Y^{*\prime} = -R \sin (\lambda + \phi_o + \phi) \left[\left(1 + \frac{h}{R}\right) \cos (\lambda + \phi_o + \phi) - \sqrt{1 - \left(1 + \frac{h}{R}\right)^2 \sin^2 (\lambda + \phi_o + \phi)}\right]$	R = Earth Radius h = Nominal Altitude
Pitch Error, θ	Given: a pitch offset θ_o and a view angle λ which sights a ground point P(X*, Y*). The same view angle will sight another ground point P'(X*', Y*') after pitch error θ is introduced. The following equations are for obtaining X*, Y*, X*', and Y*': $X^* = R \left[\left(1 + \frac{h}{R}\right) \cos \tau - \sqrt{1 - \left(1 + \frac{h}{R}\right)^2 \sin^2 \tau}\right] \frac{\sin \tau \sin \theta_o}{\sqrt{\sin^2 \theta_o + \tan^2 \lambda}}$ $Y^* = -R \left[\left(1 + \frac{h}{R}\right) \cos \tau - \sqrt{1 - \left(1 + \frac{h}{R}\right)^2 \sin^2 \tau}\right] \frac{\sin \tau \tan \lambda}{\sqrt{\sin^2 \theta_o + \tan^2 \lambda}}$	R = Earth Radius h = Nominal Altitude For τ and ξ, refer to Fig. 23.

Error Sources	Geometric Error Mapping Function	Comments
	$X^{*\prime} = R\left[\left(1+\frac{h}{R}\right)\cos\xi - \sqrt{1-\left(1+\frac{h}{R}\right)^2\sin^2\xi}\right]\frac{\sin\xi\sin(\theta_o+\theta)}{\sqrt{\sin^2(\theta_o+\theta)+\tan^2\lambda}}$ $Y^{*\prime} = -R\left[\left(1+\frac{h}{R}\right)\cos\xi - \sqrt{1-\left(1+\frac{h}{R}\right)^2\sin^2\xi}\right]\frac{\sin\xi\tan\lambda}{\sqrt{\sin^2(\theta_o+\theta)+\tan^2\lambda}}$ $\tau = \tan^{-1}\left(\sec\theta_o\sqrt{\sin^2\theta_o+\tan^2\lambda}\right)$ $\xi = \tan^{-1}\left[\sec(\theta_o+\theta)\sqrt{\sin^2(\theta_o+\theta)+\tan^2\lambda}\right]$	
Yaw Error ψ, Followed by pitch error θ, then roll error ϕ	Given a yaw offset ψ_o, followed by a pitch offset θ_o, then a roll offset ϕ_o. A view angle λ is also given which sights a ground point $P_o(X_o,Y_o)$. After the errors ψ, θ, and ϕ are introduced, the same view angle will sight another ground point $P_3(X_3, Y_3)$. The following equations are for obtaining X_o, Y_o, X_3, and Y_3: $X'_o = \frac{R\sin\theta_o\sin\xi_o\left[\left(1+\frac{h}{R}\right)\cos\xi_o - \sqrt{1-\left(1+\frac{h}{R}\right)^2\sin^2\xi_o}\right]}{\sqrt{\sin^2\theta_o+\tan^2(\lambda+\phi_o)}}$ $Y'_o = -\frac{R\tan(\lambda+\phi_o)\sin\xi_o\left[\left(1+\frac{h}{R}\right)\cos\xi_o - \sqrt{1-\left(1+\frac{h}{R}\right)^2\sin^2\xi_o}\right]}{\sqrt{\sin^2\theta_o+\tan^2(\lambda+\phi_o)}}$;	R = Earth Radius h = Nominal Altitude For ξ_o and ξ_3, refer to Fig. 23.

Error Sources	Geometric Error Mapping Function	Comments
	$X_3' = \dfrac{R \sin(\theta_o + \theta) \sin \xi_3 \left[\left(1 + \frac{h}{R}\right) \cos \xi_3 - \sqrt{1 - \left(1 + \frac{h}{R}\right)^2 \sin^2 \xi_3}\right]}{\sqrt{\sin^2(\theta_o + \theta) + \tan^2(\lambda + \phi_o + \phi)}}$	
	$Y_3' = -\dfrac{R \tan(\lambda + \phi_o + \phi) \sin \xi_3 \left[\left(1 + \frac{h}{R}\right) \cos \xi_3 - \sqrt{1 - \left(1 + \frac{h}{R}\right)^2 \sin^2 \xi_3}\right]}{\sqrt{\sin^2(\theta_o + \theta) + \tan^2(\lambda + \phi_o + \phi)}}$	
	$\xi_o = \tan^{-1}\left(\sec \theta_o \sqrt{\sin^2 \theta_o + \tan^2(\lambda + \phi_o)}\right)$	
	$\xi_3 = \tan^{-1}\left[\sec(\theta_o + \theta)\sqrt{\sin^2(\theta_o + \theta) + \tan^2(\lambda + \phi_o + \phi)}\right]$	
	$X_o = X_o' \cos \psi_o - Y_o' \sin \psi_o$	
	$Y_o = X_o' \sin \psi_o + Y_o' \cos \psi_o$	
	$X_3 = X_3' \cos(\psi_o + \psi) - Y_3' \sin(\psi_o + \psi)$	
	$Y_3 = X_3' \sin(\psi_o + \psi) + Y_3' \cos(\psi_o + \psi)$	

Part B: Given the coordinates of a ground point, find the attitude offsets, the corresponding view angle and the coordinates of the point with the same view angle after the errors are introduced.

Error Sources	Geometric Error Mapping Function	Comments
Altitude Error, Δh	At nominal altitude h, a ground point $P(X_o, Y_o)$ corresponding to view angle λ is given. After elevating Δh, the same view angle λ will aim at another ground point $P'(X_o', Y_o')$. The following equations are for obtaining X_o' and Y_o': $\lambda = \tan^{-1}\left(\frac{\sqrt{X_o^2 + Y_o^2}}{R + h - \sqrt{R^2 - X_o^2 - Y_o^2}}\right)$ $X_o' = \frac{RX_o \sin \lambda}{\sqrt{X_o^2 + Y_o^2}}\left[\left(1 + \frac{h + \Delta h}{R}\right) \cos \lambda - \sqrt{1 - \left(1 + \frac{h + \Delta h}{R}\right)^2 \sin^2 \lambda}\right]$ $Y_o' = \frac{RY_o \sin \lambda}{\sqrt{X_o^2 + Y_o^2}}\left[\left(1 + \frac{h + \Delta h}{R}\right) \cos \lambda - \sqrt{1 - \left(1 + \frac{h + \Delta h}{R}\right)^2 \sin^2 \lambda}\right]$	R = Earth Radius

Error Sources	Geometric Error Mapping Function	Comments
Roll Error, ϕ	A ground point P(0, Y*) corresponding to roll offset ϕ_o and view angle λ is given. After roll error ϕ is introduced, the same view angle λ will aim at another ground point P'(0, Y*'). The following equations are for obtaining Y*': $\lambda + \phi_o = -\text{sgn}(Y^*) \; \tan^{-1}\left(\frac{\lvert Y^*\rvert}{R + h - \sqrt{R^2 - Y^{*2}}}\right)$ $Y^{*\prime} = -R \sin (\lambda + \phi_o + \phi) \left[\left(1 + \frac{h}{R}\right) \cos (\lambda + \phi_o + \phi) - \sqrt{1 - \left(1 + \frac{h}{R}\right)^2 \sin^2 (\lambda + \phi_o + \phi)}\right]$	R = Earth Radius h = Nominal Altitude

Error Sources	Geometric Error Mapping Function	Comments
Pitch Error, θ	A ground point $P(X^*, Y^*)$ corresponding to pitch offset θ_o and view angle λ is given. After pitch error θ is introduced, the same view angle λ will aim at another ground point $P'(X^{*\prime}, Y^{*\prime})$. The following equations are for obtaining $X^{*\prime}$ and $Y^{*\prime}$: $\lambda = \tan^{-1}\left[\frac{Y^*}{\left(R + h - \sqrt{R^2 - X^{*2} - Y^{*2}}\right)\left(\sqrt{1 + \left(\frac{X^*}{R + h - \sqrt{R^2 - X^{*2} - Y^{*2}}}\right)^2}\right)}\right]$ $\theta_o = \tan^{-1}\left[\frac{X^*}{R + h - \sqrt{R^2 - X^{*2} - Y^{*2}}}\right]$ $\xi = \tan^{-1}\left[\sec(\theta_o + \theta)\sqrt{\sin^2(\theta_o + \theta) + \tan^2\lambda}\right]$ $X^{*\prime} = \frac{R \sin(\theta_o + \theta) \sin\xi \left[\left(1 + \frac{h}{R}\right)\cos\xi - \sqrt{1 - \left(1 + \frac{h}{R}\right)^2 \sin^2\xi}\right]}{\sqrt{\sin^2(\theta_o + \theta) + \tan^2\lambda}}$ $Y^{*\prime} = -\frac{R \tan\lambda \sin\xi \left[\left(1 + \frac{h}{R}\right)\cos\xi - \sqrt{1 - \left(1 + \frac{h}{R}\right)^2 \sin^2\xi}\right]}{\sqrt{\sin^2(\theta_o + \theta) + \tan^2\lambda}}$	R = Earth Radius h = Nominal Altitude For ξ, refer to Fig.23.

Error Sources	Geometric Error Mapping Function	Comments
Yaw Error, ψ	A ground point $P(X^*,Y^*)$ corresponding to yaw offset ψ_o and a certain view angle is given. After yaw error ψ is introduced, the same view angle will aim at another ground point $P'(X^{*\prime},Y^{*\prime})$. The following equations are for obtaining $X^{*\prime}$ and $Y^{*\prime}$: $\psi_o = -\tan^{-1}\left(\frac{X^*}{Y^*}\right)$ $\lambda = -\,\mathrm{sgn}\,(Y^*)\tan^{-1}\left(\frac{\sqrt{X^{*2}+Y^{*2}}}{R+h-\sqrt{R^2-X^{*2}-Y^{*2}}}\right)$ $X^{*\prime} = \left[\left(1+\frac{h}{R}\right)\cos\lambda - \sqrt{1-\left(1+\frac{h}{R}\right)^2\sin^2\lambda}\right] R\sin\lambda\sin(\psi_o+\psi)$ $Y^{*\prime} = -\left[\left(1+\frac{h}{R}\right)\cos\lambda - \sqrt{1-\left(1+\frac{h}{R}\right)^2\sin^2\lambda}\right] R\sin\lambda\cos(\psi_o+\psi)$	R = Earth Radius h = Nominal Altitude
Earth Rotation	Let Γ be the shuttle orbital inclination at the equator, and ζ be the latitude of the nadir point. A given point $P(X,Y)$, after time period Δt, will move to $P'(X',Y')$. The following equations are for obtaining X' and Y': $V_e = \omega R\cos\zeta$ $\omega = \frac{2\pi}{86{,}400}$ radians/sec $X' = X + \frac{\cos\Gamma}{\cos\zeta} V_e\Delta t$ $Y' = Y = \sqrt{1-\left(\frac{\cos\Gamma}{\cos\zeta}\right)^2}\, V_e\Delta t$	V_e = Linear Velocity of Ground Point at Latitude ζ ω = Angular Velocity of Earth Rotation Δt is assumed small.

Error Sources	Geometric Error Mapping Function	Comments
Yaw Error ψ followed by Pitch Error θ then Roll Error ϕ	A ground point P(0,Y*) corresponding to view angle λ (with no attitude offset) is given. A yaw error ψ is introduced first, then a pitch error θ, finally a roll error ϕ. The same view angle λ will then aim at another ground point P'(X*',Y*'). The following equations are for obtaining X*' and Y*': $\lambda = -\operatorname{sgn}(Y^*)\ \tan^{-1}\left(\frac{\lvert Y^* \rvert}{R + h - \sqrt{R^2 - Y^{*2}}}\right)$ $\xi = \tan^{-1}\left[\sec\theta\sqrt{\sin^2\theta + \tan^2(\lambda + \phi)}\right]$ $X = \frac{R \sin\theta \sin\xi \left[\left(1 + \frac{h}{R}\right)\cos\xi - \sqrt{1 - \left(1 + \frac{h}{R}\right)^2 \sin^2\xi}\right]}{\sqrt{\sin^2\theta + \tan^2(\lambda + \phi)}}$ $Y = \frac{-R \tan(\lambda + \theta) \sin\xi \left[\left(1 + \frac{h}{R}\right)\cos\xi - \sqrt{1 - \left(1 + \frac{h}{R}\right)^2 \sin^2\xi}\right]}{\sqrt{\sin^2\theta + \tan^2(\lambda + \phi)}}$ $X^{*\prime} = X\cos\psi - Y\sin\psi$ $Y^{*\prime} = X\sin\psi + Y\cos\psi$	R = Earth Radius h = Nominal Altitude For ξ, refer to Fig. 23.

APPENDIX B

NAPIER'S RULES FOR RIGHT SPHERICAL TRIANGLES*

A right spherical triangle has five variable parts. If these components and their complements (complement of $\Gamma \equiv 90° - \Gamma$) are arranged in a circle, as illustrated below

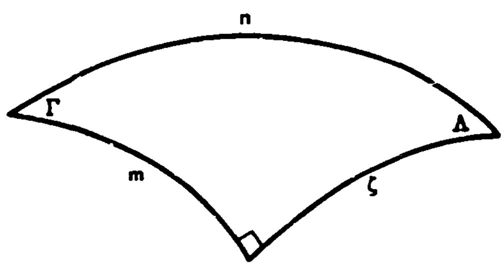

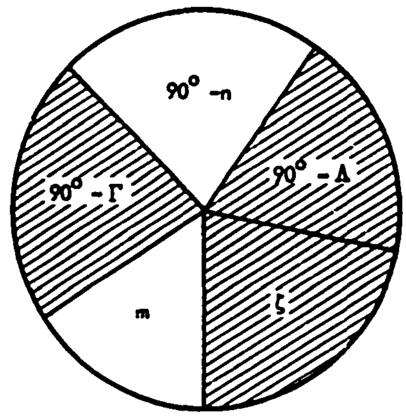

then, the following relationships hold between the five components in the circle:

The sine of any component equals the product of either:

1. The tangents of the adjacent components, or
2. The cosines of the opposite components

For our case, from 2:

$$\sin (90° - \Gamma) = \cos \zeta \cos (90° - \Lambda)$$

i.e.,

$$\cos \Gamma = \cos \zeta \sin \Lambda$$

---

*See Ref. 13

APPENDIX C

COMPUTER PROGRAM FOR SHUTTLE IMAGING SPECTROMETER POINTING ERROR POWER SPECTRAL DENSITIES FOR CONFIGURATION A — PAYLOAD-BAY NADIR POINTING

```
ELT  WED-10/20/82-10:23:28-(52,)
12537*IS(1).SRMA/PROG(52)
PROGRAM IMAGING SPECTROMETER SHUTTLE RIGID MOUNT - A
INITIAL
VARIABLE T=0.0
        INTEGER FNUM,NPOINT


COMMENT INITIALIZE SOME PARAMETERS
        CONSTANT NPOINT=641
        CONSTANT FNUM=39
        CALL FOPEN(FNUM)
        TFINAL=1.0*NPOINT-1.0
        CONSTANT FACTOR=0.0
        CONSTANT SCAFAC=1.0E+5
        SCFAC2=SCAFAC*SCAFAC
        SCF2DB=10.0*ALOG10(SCFAC2)

COMMENT SET VARIOUS MATHMATICAL CONSTANTS
        PI=3.14159265
        ASRCC=PI/(180.0*3600.0)
        RSHZCC=1.0/(2.0*PI)

COMMENT DEFINE MOMENTS OF INERTIA
        CONSTANT IX=1.38E+6
        CONSTANT IY=1.00E+7
        CONSTANT IZ=1.05E+7
        IX2=IX*IX
        IY2=IY*IY
        IZ2=IZ*IZ
        IXYZ=IX-IY+IZ
        IXYZ2=IXYZ*IXYZ

COMMENT DEFINE WO
        CONSTANT WO=0.0011315
        WO2=WO*WO
        WO4=WO2*WO2

COMMENT DEFINE INITIAL ANGLES AND RATES
        CONSTANT THO=0.0
        CONSTANT PHIO=0.0
        CONSTANT PSIO=0.0
        CONSTANT THOD=0.0
        CONSTANT PHIOD=0.0
        CONSTANT PSIOD=0.0
        THO2=THO*THO
        THOD2=THOD*THOD
        PHIO2=PHIO*PHIO
        PHIOD2=PHIOD*PHIOD
        PSIO2=PSIO*PSIO
        PSIOD2=PSIOD*PSIOD

COMMENT DEFINE Q'S
        CONSTANT QX=2.014E-6
        CONSTANT QY=1.251E-3
        CONSTANT QZ=5.438E-4

COMMENT DEFINE RATE FILTER PARAMETERS
        CONSTANT WD=0.2513
        CONSTANT ZETAD=0.8
        WD2=WD*WD
        WD4=WD2*WD2
        ZD2=ZETAD*ZETAD

COMMENT DEFINE VARIOUS CONSTANTS
        CONSTANT R=8.55E-10
```

```
        CONSTANT SIGBO=87.32
        SIGBO=SIGBO*ASRCC
        SIGBO2=SIGBO*SIGBO
        CONSTANT TAU=0.023
        TAU2=TAU*TAU
        DELW=1.0

COMMENT DEFINE W CONSTANTS AND INITIALIZE W
        CONSTANT WLO=6.28318531E-7
        CONSTANT WFACT=1.02920U527
        W=WLO/WFACT

END
DYNAMIC
CINTERVAL CI=1.0

COMMENT COMPUTE W
        W=W*WFACT
        PROCEDURAL(DELW=W)
          DELW=0.0
          IF(W.LE.0.) DELW=1.0
        END
        WHZ=W*RSHZCC
        FREQ=ALOG10(WHZ)
        W2=W*W
        W4=W2*W2

COMMENT COMPUTE HW2 AND DW2
        HW2=1.0/(TAU2*W2+1.0)
        HDW2=WD4*W2/((W2-WD2)**2+4.0*ZD2*WD2*W2)
        DW2=IX*IZ*W4-WO2*(IX*IZ+IY2+3.C IY*IZ-3.0*IZ2)*W2
COMMENT DW2=DW2+4.0*WO4*(IY-IX)*(IY-IZ)
        DW2=DW2/SCAFAC
        DW2=DW2*DW2

COMMENT COMPUTE F'S
COMMENT FTHW2=HW2*SCFAC2/((IY*W2+3.0*WO2*(IZ-IX))**2)
COMMENT FRW2=(IZ*W2-WO2*(IY-IX))**2*HW2/DW2
COMMENT FYW2=(IX*W2+4.0*WO2*(IZ-IY))**2*HW2/DW2
        FTHW2=HW2*SCFAC2/((IY*W2)**2)
        FRW2=(IZ*W2)**2*HW2/DW2
        FRYW2=WO2*IXYZ2*W2*HW2/DW2
        FYW2=(IX*W2)**2*HW2/DW2

COMMENT COMPUTE PSD'S

COMMENT PITCH PSD COMPUTATIONS
        PPW1=FTHW2*IY2*THOD2
        PPW2=FTHW2*IY2*THO2*W2
        PPW3=FTHW2*QY
        PPW=R+SIGBO2*DELW+(PPW1+PPW2+PPW3)/SCFAC2
        PPWD=PPW*HDW2

COMMENT ROLL PSD COMPUTATIONS
        PRW1=FRW2*IX2*PHIOD2
        PRW2=FRW2*IX2*PHIO2*W2
        PRW3=FRW2*WO2*IXYZ2*PSIO2
        PRW4=FRW2*QX
        PRW5=FRYW2*IZ2*PSIOD2
        PRW6=FRYW2*IZ2*PSIO2*W2
        PPW7=FRYW2*WO2*IXYZ2*PHIO2
        PRW8=FRYW2*QZ
        RS=R+SIGBO2*DELW
        PRW=RS+(PRW1+PRW2+PRW3+PRW4+PRW5+PRW6+PRW7+PRW8)/SCFAC2
        PRWD=PRW*HDW2

```

```
COMMENT YAW PSD COMPUTATIONS
        PYW1=FYW2*IZ2*PSIOD2
        PYW2=FYW2*IZ2*PSIO2*W2
        PYW3=FYW2*WO2*IXYZ2*PHIO2
        PYW4=FYW2*OZ
        PYW5=FRYW2*IX2*PHIOD2
        PYW6=FRYW2*IX2*PHIO2*W2
        PYW7=FRYW2*WO2*IXYZ2*PSIO2
        PYW8=FRYW2*OX
        PYW=RS*(PYW1+PYW2+PYW3+PYW4+PYW5+PYW6+PYW7+PYW8)/SCFAC2
        PYWD=PYW*HDW2


COMMENT PREPARE VARIABLES FOR OUTPUT
        RSIG=P*SIGBO2*DELW
        RSIGDB=10.0*ALOG10(RSIG)+FACTOR
        PPW3DB=10.0*ALOG10(PPW3)-SCF2DB+FACTOR
        PPWDB=10.0*ALOG10(PPW)+FACTOR
        PRW4DB=10.0*ALOG10(PRW4)-SCF2DB+FACTOR
        PRW8DB=10.0*ALOG10(PRW8)-SCF2DB+FACTOR
        PRWDB=10.0*ALOG10(PRW)+FACTOR
        PYW4DB=10.0*ALOG10(PYW4)-SCF2DB+FACTOR
        PYW8DB=10.0*ALOG10(PYW8)-SCF2DB+FACTOR
        PYWDB=10.0*ALOG10(PYW)+FACTOR

        PPWDDB=10.0*ALOG10(PPWD)+FACTOR
        PRWDDB=10.0*ALOG10(PPWD)+FACTOR
        PYWDDB=10.0*ALOG10(PYWD)+FACTOR

COMMENT SAVE NUMBERS IN FILE
        CALL FSAVE(FREQ,PPWDB,PRWDB,PYWDB,FNUM)


        TERMT(T.GE.TFINAL)
DERIVATIVE
ALGORITHM IALG=3
        QQ=INTEG(1.0,0.0)
END
END
TERMINAL

COMMENT CLOSE FILE
        CALL FCLOSE(FNUM)
END
END
EOF:175
```

```
O:>ELT  WED-10/20/82-10:30:02-(3,)
12537*IS(1).SRMA/FSUBS(3)
@FOR,IS FF.FOPEN
        SUBROUTINE FOPEN(N)
        REWIND N
        RETURN
        END
@FOR,IS FF.FSAVE
        SUBROUTINE FSAVE(W,P1,P2,P3,N)
        WRITE(N,100)W,P1,P2,P3
  100   FORMAT(4G14.8)
        RETURN
        END
@FOR,IS FF.FCLOSE
        SUBROUTINE FCLOSE(N)
        ENDFILE N
        RETURN
        END
EOF:16
```

APPENDIX D

COMPUTER PROGRAM FOR SHUTTLE IMAGING SPECTROMETER POINTING ERROR POWER SPECTRAL DENSITIES FOR CONFIGURATION B -- NOSE-DOWN NADIR POINTING

```
ELT  WED-10/20/82-10:36:41-(14,)
12537*IS(1).SRMB/PROG(14)
PROGRAM IMAGING SPECTROMETER SHUTTLE RIGID MOUNT - B
INITIAL
VARIABLE T=0.0
        INTEGER FNUM,NPOINT


COMMENT INITIALIZE SOME PARAMETERS
        CONSTANT NPOINT=641
        CONSTANT FNUM=39
        CALL FOPEN(FNUM)
        TFINAL=1.0*NPOINT-1.0
        CONSTANT FACTOR=0.0
        CONSTANT SCAFAC=1.0E+10
        SCFAC2=SCAFAC*SCAFAC
        SCF2DB=10.0*ALOG10(SCFAC2)

COMMENT SET VARIOUS MATHMATICAL CONSTANTS
        PI=3.14159265
        ASRCC=PI/(180.0*3600.0)
        RSHZCC=1.0/(2.0*PI)

COMMENT DEFINE MOMENTS OF INERTIA
        CONSTANT IX=1.00E+7
        CONSTANT IY=1.05E+7
        CONSTANT IZ=1.38E+6
        IX2=IX*IX
        IY2=IY*IY
        IZ2=IZ*IZ
        IXYZ=IX-IY+IZ
        IXYZ2=IXYZ*IXYZ

COMMENT DEFINE WO
        CONSTANT WO=0.0011315
        WO2=WO*WO
        WO4=WO2*WO2

COMMENT DEFINE.INITIAL ANGLES AND RATES
        CONSTANT THO=0.0
        CONSTANT PHIO=0.0
        CONSTANT PSIO=0.0
        CONSTANT THOD=0.0
        CONSTANT PHIOD=0.0
        CONSTANT PSIOD=0.0
        THO2=THO*THO
        THOD2=THOD*THOD
        PHIO2=PHIO*PHIO
        PHIOD2=PHIOD*PHIOD
        PSIO2=PSIO*PSIO
        PSIOD2=PSIOD*PSIOD

COMMENT DEFINE Q'S
        CONSTANT QX=1.970E-4
        CONSTANT QY=1.286E-3
        CONSTANT QZ=6.320E-4

COMMENT DEFINE RATE FILTER PARAMETERS
        CONSTANT WD=0.2513
        CONSTANT ZETAD=0.8
        WD2=WD*WD
        WD4=WD2*WD2
        ZD2=ZETAD*ZETAD

COMMENT DEFINE VARIOUS CONSTANTS
        CONSTANT R=8.55E-10
```

```
        CONSTANT SIGBO=87.32
        SIGBO=SIGBO*ASRCC
        SIGBO2=SIGBO*SIGBO
        CONSTANT TAU=0.023
        TAU2=TAU*TAU
        DELW=1.0
COMMENT DEFINE W CONSTANTS AND INITIALIZE W
        CONSTANT WLO=6.28318531E-7
        CONSTANT WFACT=1.029200527
        W=WLO/WFACT
END
DYNAMIC
CINTERVAL CI=1.0
COMMENT COMPUTE W
        W=W*WFACT
        PROCEDURAL(DELW=W)
          DELW=0.0
          IF(W.LE.0.) DELW=1.0
        END
        WHZ=W*RSHZCC
        FREQ=ALOG10(WHZ)
        W2=W*W
        W4=W2*W2
COMMENT COMPUTE HW2 AND DW2
        HW2=1.0/(TAU2*W2+1.0)
        HDW2=WD4*W2/((W2-WD2)**2+4.0*ZD2*WD2*W2)
        DW2=IX*IZ*W4-WO2*(IX*IZ+IY2+3.0*IY*IZ-3.0*IZ2)*W2
        DW2=DW2+4.0*WO4*(IY-IX)*(IY-IZ)
        DW2=DW2/SCAFAC
        DW2=DW2*DW2
COMMENT COMPUTE F'S
        FTHW2=HW2*SCFAC2/((IY*W2+3.0*WO2*(IZ-IX))**2)
        FRW2=(IZ*W2-WO2*(IY-IX))**2*HW2/DW2
        FYW2=(IX*W2+4.0*WO2*(IZ-IY))**2*HW2/DW2
        FRYW2=WO2*IXYZ2*W2*HW2/DW2
COMMENT COMPUTE PSD'S
COMMENT PITCH PSD COMPUTATIONS
        PPW1=FTHW2*IY2*THOD2
        PPW2=FTHW2*IY2*THO2*W2
        PPW3=FTHW2*QY
        PPW=R+SIGBO2*DELW+(PPW1+PPW2+PPW3)/SCFAC2
        PPWD=PPW*HDW2
COMMENT ROLL PSD COMPUTATIONS
        PRW1=FRW2*IX2*PHIOD2
        PRW2=FRW2*IX2*PHIO2*W2
        PRW3=FRW2*WO2*IXYZ2*PSIO2
        PRW4=FRW2*QX
        PRW5=FRYW2*IZ2*PSIOD2
        PRW6=FRYW2*IZ2*PSIO2*W2
        PRW7=FRYW2*WO2*IXYZ2*PHIO2
        PRW8=FRYW2*QZ
        RS=R+SIGBO2*DELW
        PRW=RS+(PRW1+PRW2+PRW3+PRW4+PRW5+PRW6+PRW7+PRW8)/SCFAC2
        PRWD=PRW*HDW2
COMMENT YAW PSD COMPUTATIONS
        PYW1=FYW2*IZ2*PSIOD2
        PYW2=FYW2*IZ2*PSIO2*W2
```

```
        PYW3=FYW2*WO2*IXYZ2*PHIO2
        PYW4=FYW2*OZ
        PYW5=FRYW2*IX2*PHIOD2
        PYW6=FRYW2*IX2*PHIO2*W2
        PYW7=FRYW2*WO2*IXYZ2*PSIO2
        PYW8=FRYW2*OX
        PYW=RS+(PYW1+PYW2+PYW3+PYW4+PYW5+PYW6+PYW7+PYW8)/SCFAC2
        PYWD=PYW*HDW2


COMMENT PREPARE VARIABLES FOR OUTPUT
        RSIG=R+SIGBOZ*DELW
        RSIGDB=10.0*ALOG10(RSIG)+FACTOR
        PPW3DB=10.0*ALOG10(PPW3)-SCF2DB+FACTOR
        PPWDB=10.0*ALOG10(PPW)+FACTOR
        PRW4DB=10.0*ALOG10(PRW4)-SCF2DB+FACTOR
        PRW8DB=10.0*ALOG10(PRW8)-SCF2DB+FACTOR
        PRWDB=10.0*ALOG10(PRW)+FACTOR
        PYW4DB=10.0*ALOG10(PYW4)-SCF2DB+FACTOR
        PYW8DB=10.0*ALOG10(PYW8)-SCF2DB+FACTOR
        PYWDB=10.0*ALOG10(PYW)+FACTOR

        PPWDDB=10.0*ALOG10(PPWD)+FACTOR
        PRWDDB=10.0*ALOG10(PRWD)+FACTOR
        PYWDDB=10.0*ALOG10(PYWD)+FACTOR

COMMENT SAVE NUMBERS IN FILE
        CALL FSAVE(FREQ,PPWDB,PRWDB,PYWDB,FNUM)


        TERMT(T.GE.TFINAL)
DERIVATIVE
ALGORITHM IALG=3
        QQ=INTEG(1.0,0.0)
END
END
TERMINAL

COMMENT CLOSE FILE
        CALL FCLOSE(FNUM)
END
END
EOF:172
```

```
ELT  WED-10/20/82-10:50:42-(G,)
12537*IS(1).SRMB/FSUBS(0)
@FOR,IS FF.FOPEN
        SUBROUTINE FOPEN(N)
        REWIND N
        RETURN
        END
@FOR,IS FF.FSAVE
        SUBROUTINE FSAVE(W,P1,P2,P?,N)
        WRITE(N,100)W,P1,P2,P3
  100   FORMAT(4G14.8)
        RETURN
        END
@FOR,IS FF.FCLOSE
        SUBROUTINE FCLOSE(N)
        ENDFILE N
        RETURN
        END
EOF:16
```

APPENDIX E

GEOMETRIC ERROR ANALYSIS PROGRAM LISTINGS

```
100 D 004552 DOLTA     0000 R 000263 DPITCH    0000 R 000156 DPSA      0000 R 000067
100 R 000064 DPSI2     0000 R 000244 DROLL     0000 D 002262 DSXY      0000 R 000170
100 R 000125 DTETA1    0000 R 000130 DTETA2    0000 R 000213 DTHETA    0000 D 003214
100 D 001240 DY        0000 R 000225 DYAW      0000 D 022676 ERR       0000 D 023102
100 D 013626 FI        0000 D 000352 FI1       0000 D 000360 FI2       0000 R 000000
100 I 030711 J         0000 I 030706 K         0000 D 000302 LAMDA     0000 D 000626
100 D 001536 PDXY      0000 D 013640 PDY       0000 R 030710 PI        0000 D 017166
100 D 004252 PSI       0000 D 001776 PSXY      0000 D 003264 PXY       0000 D 000742
100 D 004266 RA        0000 D 006520 RHO       0000 D 010254 RHO1      0000 D 010836
100 D 026522 RO1       0000 D 002522 S         0000 R 000047 SDH       0000 D 013350
100 D 013166 SHFT      0000 D 022532 SLUMDA    0000 D 015576 SQURT     0000 D 010620
100 D 027614 SOUT1     0000 D 002236 SXY       0000 D 003240 T         0000 D 022502
100 R 000052 TDH2      0000 D 007314 TETA1     0000 D 007322 TETA2     0000 D 014732
100 D 007526 TII2      0000 D 007330 TI1       0000 D 007336 TI2       0000 D 003144
100 D 015552 T1        0000 D 025372 T11       0000 D 005130 T2        0000 D 023206
100 D 022750 VP        0000 D 022736 VPX       0000 D 022734 VS        0000 D 022556
100 D 014756 XI        0000 R 000075 XO        0000 D 000326 XY        0000 R 000133
100 D 012074 X2        0000 D 011530 X22       0000 D 017224 X3        0000 D 000674
100 D 014136 YI        0000 D 005062 YO        0000 D 023140 YO        0000 D 011346
100 D 011712 Y22       0000 D 020316 Y3
```

```
C      THIS PROGRAM COMPUTES THE ERROR SENSITIVITIES AND GEOMETRIC
C      ERRORS OF GROUND POINTS INDUCED BY ALTITUDE,ROLL,YAW AND
C      PITCH ERRORS AS WELL AS EARTH ROTATION AND SHUTTLE MOTION



       PARAMETER NLAMDA=10,NLOMDA=19,NDH=8,NFI=3,NPSI=3,NTETA=3
      $,NDT=3,NDETA=5,NDFI=5,NDPSA=10,NDTHE=10,NCOM=15,NSDH=2
       REAL H,R,DH(NDH),DLAMDA(NLAMDA),DLOMDA(NLOMDA),SDH(NSDH),
      $TDH1,TDH2,DFI1(NFI),DFI2(NFI),DPSI1(NPSI),DPSI2(NPSI),
      $DPSI(NPSI),DBETA(NPSI),XO(NLOMDA),DFI(NDFI),
      $DTETA1(NTETA),DTETA2(NTETA),XO(NLOMDA),DPSA(NDPSA)
      $,DT(NDT),DTAU,DETA(NDETA),DALFA(NDPSA),DTHETA(NDTHE)
      $,DYAW(NCOM),DROLL(NCOM),DPITCH(NCOM)
       DOUBLE PRECISION LAMDA(NLAMDA),XY(NLAMDA),FI1(NFI),FI2(NFI)
      $,DXY(NDH,NLAMDA),LOMDA(NLOMDA),Y(NLOMDA),PY(NDF;,NLOMDA)
      $,DY(NDFI,NLOMDA),PDXY(NDH,NLAMDA),PSXY(NLAMDA,NDH),
      $SXY(NLAMDA),DSXY(NLAMDA,NDH),S(NLAMDA,NDH),BY1(NFI,NLOMDA),
      $TXY1(NLAMDA),TXY2(NLAMDA),DTXY(NLAMDA),T(NLAMDA),PXY(NDH,NLAMD
      $A),BY2(NFI,NLOMDA),DBY(NFI,NLOMDA),B(NFI,NLOMDA),PSI(NPSI),
      $BETA(NPSI),RA(NLAMDA),DELTA(NPSI,NLAMDA),D(NPSI,NLAMDA),
      $PSA(NDPSA),ALFA(NDPSA),DOLTA(NDPSA,NLAMDA),YO(NLOMDA),
      $T2(NDTHE,NLOMDA),DEL(NDTHE,NLOMDA),RHO(NDTHE,NLOMDA)
      $,TETA1(NTETA),TETA2(NTETA),TI1(NTETA),TI2(NTETA),
      $TII1(NTETA,NLOMDA),TII2(NTETA,NLOMDA),DEL1(NTETA,NLOMDA),
      $DEL2(NTETA,NLOMDA),RHO1(NTETA,NLOMDA),RHO2(NTETA,NLOMDA),
      $SQURT1(NTETA,NLOMDA),SQURT2(NTETA,NLOMDA),X11(NTETA,NLOMDA),
      $Y11(NTETA,NLOMDA),X22(NTETA,NLOMDA),Y22(NTETA,NLOMDA)
       DOUBLE PRECISION X2(NCOM,NLOMDA),
      $SHFT(NTETA,NLOMDA),SEN(NTETA,NLOMDA),YAW(NCOM),ROLL(NCOM),
      $FI(NDFI),PDY(NDFI,NLOMDA),YI(NDTHE,NLOMDA),THETA(NDTHE),
      $XI(NDTHE,NLOMDA),T1(NDTHE),SQURT(NDTHE,NLOMDA),
      $SHF(NDTHE,NLOMDA),PITCH(NCOM),
```

ORIGINAL PAGE IS
OF POOR QUALITY

```
          $X3(NCOM,NLOMDA),Y3(NCOM,NLOMDA)
          $,DIFF(NCOM,NLOMDA),TAU,OMEGA,ETA(NDETA),
          $V(NDETA),SLUMDA(NDETA),CLUMDA(NDETA),VX(NDETA),VY(NDETA),
          $DEX(NDETA,NDT),DEY(NDETA,NDT),ERR(NDETA,NDT),VS,VPX(NDETA),
          $VP(NDETA),ANGL(NDETA),DANGL(NDETA),DELX(NDETA,NDT)
          $,DELY(NDETA,NDT),ERRO(NDETA,NDT),Y0(NLOMDA)
          $,T33(NCOM,NLOMDA),DE1(NCOM,NLOMDA),T11(NCOM),
          $Y2(NCOM,NLOMDA),RO1(NCOM,NLOMDA),SOUT1(NCOM,NLOMDA)
           DATA (DH(K),K=1,NDH)/1.,-1.,2.,-2.,3.,-3.,4.,-4./
           DATA H,R,DTAU/400.,6356.785,85./
           DATA (DFI(K),K=1,NDFI)/18.,19.,20.,21.,22./
           DATA (DPSA(K),K=1,NDPSA)/.5,1.,1.5,2.,2.5,3.,3.5,4.,4.5,5./
           DATA (DTHETA(K),K=1,NDTHE)/20.5,21.5,22.5,23.5,24.5,43.,44.,
          $45.,46.,47./
           DATA (DYAW(K),K=1,NCOM)/0.,0.,0.,1.,-1.,0.,0.,0.,1.,-1.,0.,
          $0.,0.,1.,-1./
           DATA (DPITCH(K),K=1,NCOM)/0.,1.,-1.,0.,0.,22.5,22.5,22.5,22.5,
          $22.5,45.,45.,45.,45.,45./
           DATA (DROLL(K),K=1,NCOM)/20.,20.,20.,20.,20.,0.,1.,-1.,0.,0.,
          $0.,1.,-1.,0.,0./
           DATA (DLAMDA(I),I=1,NLAMDA)/0.,1.,2.,3.,4.,5.,6.,7.,8.,9./
           DATA (DLOMDA(I),I=1,NLOMDA)/-9.,-8.,-7.,-6.,-5.,-4.,-3.,-2.,
          $-1.,0.,1.,2.,3.,4.,5.,6.,7.,8.,9./
           DATA (SDH(I),I=1,NSDH)/.01,.02/
           DATA TDH1,TDH2/.01,-.01/
           DATA (DFI1(K),K=1,NFI),(DFI2(K),K=1,NFI)/.01,.02,.05,-.01,
          $-.02,-.05/
           DATA (DPSI1(K),K=1,NPSI),(DPSI2(K),K=1,NPSI)/.01,.02,.05,
          $-.01,-.02,-.05/
           DATA (DTETA1(K),K=1,NTETA),(DTETA2(K),K=1,NTETA)/.01,.02,
          $.05,-.01,-.02,-.05/
           DATA (XO(K),K=1,NLOMDA)/19*0./
           DATA (XO(K),K=1,NLOMDA)/19*0./
           DATA (DT(K),K=1,NDT)/1.,.1,.01/
           DATA (DETA(K),K=1,NDETA)/0.,20.,40.,60.,80./
           PI=3.14159265


           DO 100 K=1,NDH
           DO 90 I=1,NLAMDA
           LAMDA(I)=DLAMDA(I)*PI/180.
           XY(I)=R*((1+H/R)*DCOS(LAMDA(I))-DSQRT(1-(1+H/R)*(1+H/R)*
          $DSIN(LAMDA(I))*DSIN(LAMDA(I))))*DSIN(LAMDA(I))
           PXY(K,I)=R*((1+(H+DH(K))/R)*DCOS(LAMDA(I))-DSQRT(1-(1+(H+DH(K
          $))/R)*(1+(H+DH(K))/R)*DSIN(LAMDA(I))*DSIN(LAMDA(I))))*DSIN
          $(LAMDA(I))
           DXY(K,I)=PXY(K,I)-XY(I)
           IF(DXY(K,I).EQ.0.) GO TO 80
           PDXY(K,I)=DABS(DXY(K,I))*100./DABS(XY(I))
           GO TO 90
        80 PDXY(K,I)=0.
        90 CONTINUE
       100 CONTINUE


           DO 102 J=1,NSDH
           DO 101 I=1,NLAMDA
```

```
      LAMDA(I)=DLAMDA(I)*PI/180.
      SXY(I)=R*((1+H/R)*DCOS(LAMDA(I))-DSQRT(1-(1+H/R)*(1+H/R)*
     $DSIN(LAMDA(I))*DSIN(LAMDA(I))))*DSIN(LAMDA(I))
      PSXY(I,J)=R*((1+(H+SDH(J))/R)*DCOS(LAMDA(I))-DSQRT(1-(1+(H+SDH(J))
     $/R)*(1+(H+SDH(J))/R)*DSIN(LAMDA(I))*DSIN(LAMDA(I))))*DSIN(
     $LAMDA(I))
      DSXY(I,J)=PSXY(I,J)-SXY(I)
      S(I,J)=DSXY(I,J)/SDH(J)
  101 CONTINUE
  102 CONTINUE


      DO 103 I=1,NLAMDA
      LAMDA(I)=DLAMDA(I)*PI/180.
      TXY1(I)=R*((1+(H+TDH1)/R)*DCOS(LAMDA(I))-DSQRT(1-(1+(H+TDH1)/R)*
     $(1+(H+TDH1)/R)*DSIN(LAMDA(I))*DSIN(LAMDA(I))))*DSIN(LAMDA(I))
      TXY2(I)=R*((1+(H+TDH2)/R)*DCOS(LAMDA(I))-DSQRT(1-(1+(H+TDH2)/R)*
     $(1+(H+TDH2)/R)*DSIN(LAMDA(I))*DSIN(LAMDA(I))))*DSIN(LAMDA(I))
      DTXY(I)=TXY1(I)-TXY2(I)
      T(I)=DTXY(I)/(TDH1-TDH2)
  103 CONTINUE


      DO 111 K=1,NDFI
      FI(K)=DFI(K)*PI/180.
      DO 110 J=1,NLOMDA
      LOMDA(J)=DLOMDA(J)*PI/180.
      Y(J)=-R*((1+H/R)*DCOS(LOMDA(J))-DSQRT(1-(1+H/R)*(1+H/R)*
     $DSIN(LOMDA(J))*DSIN(LOMDA(J))))*DSIN(LOMDA(J))
      PY(K,J)=-R*((1+H/R)*DCOS(LOMDA(J)+FI(K))-DSQRT(1-(1+H/R)*(1+H/R)*
     $DSIN(LOMDA(J)+FI(K))*DSIN(LOMDA(J)+FI(K))))*DSIN(LOMDA(J)+FI(K))
      DY(K,J)=PY(K,J)-Y(J)
      IF(Y(J).EQ.0.) GO TO 109
      PDY(K,J)=DABS(DY(K,J))*100./DABS(Y(J))
      GO TO 110
  109 PDY(K,J)=10.D100
  110 CONTINUE
  111 CONTINUE


      DO 130 K=1,NFI
      FI1(K)=DFI1(K)*PI/180.
      FI2(K)=DFI2(K)*PI/180.
      DO 120 J=1,NLOMDA
      LOMDA(J)=DLOMDA(J)*PI/180.
      BY1(K,J)=-R*((1+H/R)*DCOS(LOMDA(J)+FI1(K))-DSQRT(1-(1+H/R)*
     $(1+H/R)*DSIN(LOMDA(J)+FI1(K))*DSIN(LOMDA(J)+FI1(K))))*
     $DSIN(LOMDA(J)+FI1(K))
      BY2(K,J)=-R*((1+H/R)*DCOS(LOMDA(J)+FI2(K))-DSQRT(1-(1+H/R)*
     $(1+H/R)*DSIN(LOMDA(J)+FI2(K))*DSIN(LOMDA(J)+FI2(K))))*
     $DSIN(LOMDA(J)+FI2(K))
      DBY(K,J)=BY1(K,J)-BY2(K,J)
      B(K,J)=DBY(K,J)/(DFI1(K)-DFI2(K))
  120 CONTINUE
  130 CONTINUE
```

```
      DO 132 K=1,NOPSA
      DALFA(K)=(180.-DPSA(K))/2.
      PSA(K)=DPSA(K)*PI/180.
      ALFA(K)=DALFA(K)*PI/180.
      DO 131 J=1,NLAMDA
      LAMDA(J)=DLAMDA(J)*PI/180.
      RA(J)=R*((1+H/R)*DCOS(LAMDA(J))-CSQRT(1-(1+H/R)*(1+H/R)
     S*DSIN(LAMDA(J))*DSIN(LAMDA(J))))*DSIN(LAMDA(J))
      DOLTA(K,J)=(RA(J)*DSIN(PSA(K)))/DSIN(ALFA(K))
  131 CONTINUE
  132 CONTINUE


      DO 136 K=1,NPSI
      DPSI(K)=DPSI1(K)-DPSI2(K)
      DBETA(K)=(180.-DPSI(K))/2.
      PSI(K)=DPSI(K)*PI/180.
      BETA(K)=DBETA(K)*PI/180.
      DO 135 J=1,NLAMDA
      LAMDA(J)=DLAMDA(J)*PI/180.
      RA(J)=R*((1+H/R)*DCOS(LAMDA(J))-DSQRT(1-(1+H/R)*(1+H/R)*
     SDSIN(LAMDA(J))*DSIN(LAMDA(J))))*DSIN(LAMDA(J))
      DELTA(K,J)=(RA(J)*DSIN(PSI(K)))/DSIN(BETA(K))
      D(K,J)=DELTA(K,J)/DPSI(K)
  135 CONTINUE
  136 CONTINUE


      DO 206 K=1,NDTHE
      THETA(K)=DTHETA(K)*PI/180.
      DO 205 J=1,NLOMDA
      LOMDA(J)=DLOMDA(J)*PI/180.
      YO(J)=-R*((1+H/R)*DCOS(LOMDA(J))-DSQRT(1-(1+H/R)*(1+H/R)*DSIN
     S(LOMDA(J))*DSIN(LOMDA(J))))*DSIN(LOMDA(J))
      T1(K)=H*DTAN(THETA(K))
      T2(K,J)=-DABS(H/DCOS(THETA(K)))*DTAN(LOMDA(J))
      DEL(K,J)=DSQRT(T1(K)*T1(K)+T2(K,J)*T2(K,J))
      RHO(K,J)=DATAN(DEL(K,J)/H)
      SQURT(K,J)=R*((1+H/R)*DCOS(RHO(K,J))-DSQRT(1-(1+H/R)*(1+H/R)*DSIN
     S(RHO(K,J))*DSIN(RHO(K,J))))*DSIN(RHO(K,J))
      XI(K,J)=(SQURT(K,J)*T1(K))/DEL(K,J)
      YI(K,J)=(SQURT(K,J)*T2(K,J))/DEL(K,J)
      SHF(K,J)=DSQRT(XI(K,J)*XI(K,J)+(YI(K,J)-YO(J))*(YI(K,J)-YO(J)))
  205 CONTINUE
  206 CONTINUE


      DO 208 K=1,NTETA
      TETA1(K)=DTETA1(K)*PI/180.
      TETA2(K)=DTETA2(K)*PI/180.
      DO 207 J=1,NLOMDA
      LOMDA(J)=DLOMDA(J)*PI/180.
      TI1(K)=H*DTAN(TETA1(K))
      TI2(K)=H*DTAN(TETA2(K))
      TII1(K,J)=-DABS(H/DCOS(TETA1(K)))*DTAN(LOMDA(J))
      TII2(K,J)=-DABS(H/DCOS(TETA2(K)))*DTAN(LOMDA(J))
      DEL1(K,J)=DSQRT(TI1(K)*TI1(K)+TII1(K,J)*TII1(K,J))
```

ORIGINAL PAGE IS
OF POOR QUALITY

```
      DEL2(K,J)=DSQRT(TI2(K)*TI2(K)+TII2(K,J)*TII2(K,J))
      RHO1(K,J)=DATAN(DEL1(K,J)/H)
      RHO2(K,J)=DATAN(DEL2(K,J)/H)
      SQURT1(K,J)=R*((1+H/R)*DCOS(RHO1(K,J))-DSQRT(1-(1+H/R)*
     $(1+H/R)*DSIN(RHO1(K,J))*DSIN(RHO1(K,J))))*DSIN(RHO1(K,J))
      SQURT2(K,J)=R*((1+H/R)*DCOS(RHO2(K,J))-DSQRT(1-(1+H/R)*
     $(1+H/R)*DSIN(RHO2(K,J))*DSIN(RHO2(K,J))))*DSIN(RHO2(K,J))
      X11(K,J)=(SQURT1(K,J)*TI1(K))/DEL1(K,J)
      Y11(K,J)=(SQURT1(K,J)*TII1(K,J))/DEL1(K,J)
      X22(K,J)=(SQURT2(K,J)*TI2(K))/DEL2(K,J)
      Y22(K,J)=(SQURT2(K,J)*TII2(K,J))/DEL2(K,J)
      SHFT(K,J)=DSQRT((X11(K,J)-X22(K,J))*(X11(K,J)-X22(K,J))+
     $(Y11(K,J)-Y22(K,J))*(Y11(K,J)-Y22(K,J)))
      SEN(K,J)=SHFT(K,J)/(DTETA1(K)-DTETA2(K))
  207 CONTINUE
  208 CONTINUE


      DO 211 K=1,NCOM
      YAW(K)=DYAW(K)*PI/180.
      ROLL(K)=DROLL(K)*PI/180.
      PITCH(K)=DPITCH(K)*PI/180.
      DO 210 J=1,NLOMDA
      LOMDA(J)=DLOMDA(J)*PI/180.
      Y0(J)=-R*((1+H/R)*DCOS(LOMDA(J))-DSQRT(1-(1+H/R)*(1+H/R)*
     $DSIN(LOMDA(J))*DSIN(LOMDA(J))))*DSIN(LOMDA(J))
      T11(K)=H*DTAN(PITCH(K))
      T33(K,J)=-DABS(H/DCOS(PITCH(K)))*DTAN(LOMDA(J)+ROLL(K))
      DE1(K,J)=DSQRT(T11(K)*T11(K)+T33(K,J)*T33(K,J))
      RO1(K,J)=DATAN(DE1(K,J)/H)
      SQUT1(K,J)=R*((1+H/R)*DCOS(RO1(K,J))-DSQRT(1-(1+H/R)*(1+H/R)
     $*DSIN(RO1(K,J))*DSIN(RO1(K,J))))*DSIN(RO1(K,J))
      X2(K,J)=(SQUT1(K,J)*T11(K))/DE1(K,J)
      Y2(K,J)=(SQUT1(K,J)*T33(K,J))/DE1(K,J)
      X3(K,J)=X2(K,J)*DCOS(YAW(K))-Y2(K,J)*DSIN(YAW(K))
      Y3(K,J)=X2(K,J)*DSIN(YAW(K))+Y2(K,J)*DCOS(YAW(K))
      DIFF(K,J)=DSQRT((X3(K,J)-X0(J))*(X3(K,J)-X0(J))+(Y3(K,J)-Y0(J))*
     $(Y3(K,J)-Y0(J)))
  210 CONTINUE
  211 CONTINUE


      TAU=DTAU*PI/180.
      OMEGA=2.*PI/86400.
      DO 220 K=1,NDETA
      ETA(K)=DETA(K)*PI/180.
      V(K)=OMEGA*R*DCOS(ETA(K))
      SLUMDA(K)=DCOS(TAU)/DCOS(ETA(K))
      CLUMDA(K)=DSQRT(1-SLUMDA(K)*SLUMDA(K))
      VX(K)=V(K)*SLUMDA(K)
      VY(K)=V(K)*CLUMDA(K)
      DO 215 J=1,NDT
      DEX(K,J)=VX(K)*DT(J)
      DEY(K,J)=VY(K)*DT(J)
      ERR(K,J)=DSQRT(DEX(K,J)*DEX(K,J)+DEY(K,J)*DEY(K,J))
  215 CONTINUE
  220 CONTINUE
```

```
      VS=2.*PI*R/5545.484
      TAU=DTAU*PI/180.
      OMEGA=2.*PI/86400.
      DO 222 K=1,NDETA
      ETA(K)=DETA(K)*PI/180.
      V(K)=OMEGA*R*DCOS(ETA(K))
      SLUMDA(K)=DCOS(TAU)/DCOS(ETA(K))
      CLUMDA(K)=DSQRT(1-SLUMDA(K)*SLUMDA(K))
      VX(K)=V(K)*SLUMDA(K)
      VY(K)=V(K)*CLUMDA(K)
      VPX(K)=VX(K)-VS
      VP(K)=DSQRT(VPX(K)*VPX(K)+VY(K)*VY(K))
      ANGL(K)=DATAN(VPX(K)/VY(K))
      DANGL(K)=ANGL(K)*180./PI
      DO 221 J=1,NDT
      DELX(K,J)=VPX(K)*DT(J)
      DELY(K,J)=VY(K)*DT(J)
      ERRO(K,J)=DSQRT(DELX(K,J)*DELX(K,J)+DELY(K,J)*DELY(K,J))
  221 CONTINUE
  222 CONTINUE


      DO 237 [illegible]1,NDH
      WRITE(6,236) R,H,DH(K),(DLAMDA(I),I=1,NLAMDA),(XY(I),I=1,NLAMD
     $A),(PXY(K,I),I=1,NLAMDA),(DXY(K,I),I=1,NLAMDA),(PDXY(K,I),I=1,
     $NLAMDA)
  236 FORMAT(1H1,'******************** GEOMETRIC ERROR INDUCED BY',
     $' ALTITUDE ERROR ********************',//////////,
     $' EARTH RADIUS R =',F9.4,'KM',///,' NOMINAL ALTITUDE',
     $' H=',F4.0,'KM',///,' ALTITUDE ERROR DH =',F3.0,'KM',
     $//////////,' VIEW',5X,'ANGLE',/,' DLAMDA(DEGREES)',
     $12X,F2.0,9(9X,F2.0),///,' NOMINAL LOCATION (KM)',10D11.4,
     $///,' SHIFTED LOCATION (KM)',10D11.4,///,7X,'ERROR',6X,
     $'(KM)',10D11.4,///,4X,'ABS(ERROR)',3X,'(%)',2X,F5.3,
     $8X,F5.3,8(6X,F5.3))
  237 CONTINUE


      DO 239 J=1,NSDH
      WRITE(6,238) R,H,SDH(J),(DLAMDA(I),I=1,NLAMDA),(SXY(I),I=
     $1,NLAMDA),(PSXY(I,J),I=1,NLAMDA),(DSXY(I,J),I=1,NLAMDA),(S(I,J)
     $,I=1,NLAMDA)
  238 FORMAT(1H1,'******************** GEOMETRIC ERROR SENSITIVITY'
     $' WITH RESPECT TO ALTITUDE ERROR ********************',////////
     $//,' EARTH RADIUS R =',F9.4,'KM',///,' NOMINAL ALTITUDE H =',
     $F4.0,'KM',///,' ALTITUDE ERROR SDH =',F4.2,'KM',//////////,' VIEW'
     $,5X,'ANGLE',/,' DLAMDA(DEGREES)',12X,F2.0,9(9X,F2.0),///,
     $' NOMINAL LOCATION (KM)',10D11.4,///,' SHIFTED LOCATION (KM)',
     $10D11.4,///,7X,'ERROR',6X,'(KM)',10D11.4,//,6X,'ERROR',/,
     $'   SENSITIVITY (KM/KM)',10D11.4)
  239 CONTINUE


      WRITE(6,240) R,H,TDH1,TDH2,(DLAMDA(I),I=1,NLAMDA),(TXY1(I),I=
     $1,NLAMDA),(TXY2(I),I=1,NLAMDA),(DTXY(I),I=1,NLAMDA),(T(I),I=
```

ORIGINAL PAGE IS
OF POOR QUALITY

```
      $1,NLAMDA)
  240 FORMAT(1H1,'******************** GEOMETRIC ERROR SENSITIVITY'
     $' WITH RESPECT TO ALTITUDE ERROR *********************',
     $///////////,' EARTH RADIUS R =',F9.4,'KM',///,' NOMINAL'
     $' ALTITUDE H =',F4.0,'KM',///,' ALTITUDE ERROR 1 TDH1 =',
     $F4.2,'KM',///,' ALTITUDE ERROR 2 TDH2 =',F5.2,'KM',
     $/////////,' VIEW',5X,'ANGLE',/,' DLAMDA(DEGREES)',12X,
     $F2.0,9(9X,F2.0),///,' SHIFTED LOCATION',/,' DUE TO ERROR'
     $' 1    (KM)',10D11.4,///,' SHIFTED LOCATION',/,' DUE TO'
     $' ERROR 2    (KM)',10D11.4,////,'     DIFFERENCE     (KM)',
     $10D11.4,///,6X,'ERROR',/,'    SENSITIVITY (KM/KM)',10
     $D11.4)


       DO 246 K=1,NOFI
       WRITE(6,245) R,H,DFI(K),(DLOMDA(J),J=1,10),(Y(J),J=1,10),
     $(PY(K,J),J=1,10),(DY(K,J),J=1,10),(PDY(K,J),J=1,10),(DLOMDA(J),
     $J=11,NLOMDA),(Y(J),J=11,NLOMDA),(PY(K,J),J=11,NLOMDA),(DY(K,J),
     $J=11,NLOMDA),(PDY(K,J),J=11,NLOMDA)
  245 FORMAT(1H1,'********************* GEOMETRIC ERROR INDUCED BY',
     $' ROLL ERROR ********************',///////,
     $' EARTH RADIUS R =',F9.4,'KM',///,' NOMINAL ALTITUDE H =',
     $F4.0,'KM',///,' ROLL ERROR DFI =',F4.0,'DEGREE',//////,
     $' VIEW',5X,'ANGLE',/,' DLOMDA(DEGREES)',12X,F3.0,9(8X,F3.0),
     $///,' NOMINAL LOCATION (KM)',10D11.4,///,' SHIFTED',
     $' LOCATION (KM)',10D11.4,///,7X,'ERROR',6X,'(KM)',10D11.4,
     $///,4X,'ABS(ERROR)',5X,'(%)',F10.4,8F11.4,3X,F5.2,
     $//////,' VIEW',5X,'ANGLE',/,' DLOMDA(DEGREES)',13X,F2.0,
     $8(9X,F2.0),///,' NOMINAL LOCATION (KM)',9D11.4,///,' SHIFTED'
     $' LOCATION (KM)',9D11.4,///,7X,'ERROR',6X,'(KM)',9D11.4,
     $///,4X,'ABS(ERROR)',5X,'(%)',F10.4,8F11.4)
  246 CONTINUE


       DO 300 K=1,NFI
       WRITE(6,250) R,H,DFI1(K),DFI2(K),(DLOMDA(J),J=1,10),(BY1(K
     $,J),J=1,10),(BY2(K,J),J=1,10),(DBY(K,J),J=1,10),(B(K,J),J=
     $1,10),(DLOMDA(J),J=11,NLOMDA),(BY1(K,J),J=11,NLOMDA),(BY2
     $(K,J),J=11,NLOMDA),(DBY(K,J),J=11,NLOMDA),(B(K,J),J=11,NLOM
     $DA)
  250 FORMAT(1H1,'******************** GEOMETRIC ERROR SENSITIVI'
     $'TY WITH RESPECT TO ROLL ERROR ********************',/////
     $,' EARTH RADIUS R =',F9.4,'KM',///,' NOMINAL ALTITUDE H =',
     $F4.0,'KM',///,' ROLL ERROR 1 DFI1 =',F5.2,'DEGREE',///,
     $' ROLL ERROR 2 DFI2 =',F5.2,'DEGREE',/////,' VIEW',5X,
     $'ANGLE',/,' DLOMDA(DEGREES)',12X,F3.0,9(8X,F3.0),//,
     $' SHIFTED LOCATION',/,' DUE TO ERROR 1    (KM)',10D11.4
     $//,' SHIFTED LOCATION',/,' DUE TO ERROR 2    (KM)',
     $10D11.4,///,'     DIFFERENCE     (KM)',10D11.4,//,6X,
     $'ERROR',/,'    SENSITIVITY(KM/DEG)',10D11.4,/////,
     $' VIEW',5X,'ANGLE',/,' DLOMDA(DEGREES)',12X,F3.0,8(8X,
     $F3.0),//,' SHIFTED LOCATION',/,' DUE TO ERROR 1    (KM)',
     $9D11.4,//,' SHIFTED LOCATION',/,' DUE TO ERROR 2    (KM)',
     $9D11.4,///,'     DIFFERENCE     (KM)',9D11.4,//,6X,
     $'ERROR',/,'    SENSITIVITY(KM/DEG)',9D11.4)
  300 CONTINUE
```

```
      DO 321 K=1,NDPSA
      WRITE(6,320) R,H,DPSA(K),(DLAMDA(I),I=1,NLAMDA),
     $(DOLTA(K,J),J=1,NLAMDA)
  320 FORMAT(1H1,'********************** GEOMETRIC ERROR INDUCED'
     $' BY YAW ERROR **********************',/////////,' EARTH '
     $'RADIUS R =',F9.4,'KM',///,' NOMINAL ALTITUDE H =',F4.0,
     $'KM',///,' YAW ERROR DPSA =',F3.1,'DEGREE',/////////,
     $' VIEW',5X,'ANGLE',/,' DLAMDA(DEGREES)',12X,F2.0,9(9X,F2.0),
     $,////,7X,'ERROR',6X,'(KM)',10D11.4)
  321 CONTINUE


      DO 400 K=1,NPSI
      WRITE(6,350) R,H,DPSI1(K),DPSI2(K),(DLAMDA(I),I=1,NLAMDA),
     $(DELTA(K,J),J=1,NLAMDA),(D(K,J),J=1,NLAMDA)
  350 FORMAT(1H1,'********************** GEOMETRIC ERROR SENSITIVITY'
     $' WITH RESPECT TO YAW ERROR **********************',/////////,
     $' EARTH RADIUS R =',F9.4,'KM',///,' NOMINAL ALTIRUDE H =',
     $F4.0,'KM',///,' YAW ERROR 1 DPSI1 =',F5.2,'DEGREE',///,
     $' YAW ERROR 2 DPSI2 =',F5.2,'DEGREE',/////////,' VIEW',5X,
     $'ANGLE',/,' DLAMDA(DEGREES)',12X,F2.0,9(9X,F2.0),////,
     $'     TOTAL SHIFT    (KM)',10D11.4,///,6X,'ERROR',/,
     $'   SENSITIVITY(KM/DEG)',10D11.4)
  400 CONTINUE


      DO 451 K=1,NDTHE
      WRITE(6,450) R,H,DTHETA(K),(DLOMDA(J),J=1,10),(XO(J),J=1,10),
     $(YO(J),J=1,10),(XI(K,J),J=1,10),(YI(K,J),J=1,10),(SHF(K,J),J=1,10)
     $,(DLOMDA(J),J=11,NLOMDA),(XO(J),J=11,NLOMDA),(YO(J),J=11,
     $NLOMDA),(XI(K,J),J=11,NLOMDA),(YI(K,J),J=11,NLOMDA),(SHF(K,J),J=
     $11,NLOMDA)
  450 FORMAT(1H1,'********************** GEOMETRIC ERROR INDUCED BY'
     $' PITCH ERROR **********************',/////,' EARTH RADIUS R ='
     $,F9.4,'KM',///,' NOMINAL ALTITUDE H =',F4.0,'KM',///,' PITCH'
     $' ERROR DTHETA =',F5.1,'DEGREE',/////,' VIEW',5X,'ANGLE',/,
     $' DLOMDA(DEGREES)',12X,F3.0,9(8X,F3.0),///,' NOMINAL X COORD'
     $'. (KM)',7X,F2.0,9(9X,F2.0),///,' NOMINAL Y COORD. (KM)',
     $10D11.4,///,' SHIFTED X COORD. (KM)',10D11.4,///,' SHIFTED'
     $' Y COORD. (KM)',10D11.4,///,7X,'ERROR',6X,'(KM)',10D11.4,
     $/////,' VIEW',5X,'ANGLE',/,' DLOMDA(DEGREES)',12X,F3.0,
     $8(8X,F3.0),///,' NOMINAL X COORD. (KM)',7X,F2.0,8(9X,F2.0),
     $///,' NOMINAL Y COORD. (KM)',9D11.4,///,' SHIFTED X COORD.'
     $' (KM)',9D11.4,///,' SHIFTED Y COORD. (KM)',9D11.4,///,7X,
     $'ERROR',6X,'(KM)',9D11.4)
  451 CONTINUE


      DO 500 K=1,NTETA
      WRITE(6,480) R,H,DTETA1(K),DTETA2(K),(DLOMDA(J),J=1,10),
     $(X11(K,J),J=1,10),(Y11(K,J),J=1,10),(X22(K,J),J=1,10),
     $(Y22(K,J),J=1,10),(SHFT(K,J),J=1,10),(SEN(K,J),J=1,10),
     $(DLOMDA(J),J=11,NLOMDA),(X11(K,J),J=11,NLOMDA),
     $(Y11(K,J),J=11,NLOMDA),(X22(K,J),J=11,NLOMDA),
     $(Y22(K,J),J=11,NLOMDA),(SHFT(K,J),J=11,NLOMDA),
     $(SEN(K,J),J=11,NLOMDA)
```

ORIGINAL PAGE IS
OF POOR QUALITY

```
      480 FORMAT(1H1,'********************* GEOMETRIC ERROR SENSITIVI'
     $'TY WITH RESPECT TO PITCH ERROR ********************',////,
     $' EARTH RADIUS R =',F9.4,'KM',//,' NOMINAL ALTITUDE H =',
     $F4.0,'KM',//,' PITCH ERROR 1 DTETA1 =',F5.2,'DEGREE',//,
     $' PITCH ERROR 2 DTETA2 =',F5.2,'DEGREE',////,' VIEW',5X,
     $'ANGLE',/,' DLOMDA(DEGREES)',12X,F3.0,9(8X,F3.0),//,
     $' SHIFTED X COORD.',/,' DUE TO ERROR 1    (KM)',10D11.4,//,
     $' SHIFTED Y COORD.',/,' DUE TO ERROR 1    (KM)',10D11.4,//,
     $' SHIFTED X COORD.',/,' DUE TO ERROR 2    (KM)',10D11.4,//,
     $' SHIFTED Y COORD.',/,'.DUE TO ERROR 2    (KM)',10D11.4,///,
     $'     DIFFERENCE     (KM)',10D11.4,//,6X,'ERROR',/,'    SENSI'
     $'TIVITY(KM/DEG)',10D11.4,////,' VIEW',5X,'ANGLE',/,
     $' DLOMDA(DEGREES)',12X,F3.0,8(8X,F3.0),//,
     $' SHIFTED X COORD.',/,' DUE TO ERROR 1    (KM)',9D11.4,//,
     $' SHIFTED Y COORD.',/,' DUE TO ERROR 1    (KM)',9D11.4,//,
     $' SHIFTED X COORD.',/,' DUE TO ERROR 2    (KM)',9D11.4,//,
     $' SHIFTED Y COORD.',/,' DUE TO ERROR 2    (KM)',9D11.4,///,
     $'     DIFFERENCE     (KM)',9D11.4,//,6X,'ERROR',/,'    SENSI'
     $'TIVITY(KM/DEG)',9D11.4)
  500 CONTINUE


      DO 601 K=1,NCOM
      WRITE(6,600) R,H,DYAW(K),DPITCH(K),DROLL(K),(DLOMDA(J),J=1,10),
     $(X0(J),J=1,10),(Y0(J),J=1,10),(X3(K,J),J=1,10),(Y3(K,J),J=1,10),
     $(DIFF(K,J),J=1,10),(DLOMDA(J),J=11,NLOMDA),(X0(J),J=11,NLOMDA)
     $,(Y0(J),J=11,NLOMDA),(X3(K,J),J=11,NLOMDA),(Y3(K,J),J=11,NLOMDA)
     $,(DIFF(K,J),J=11,NLOMDA)
  600 FORMAT(1H1,'********************* GEOMETRIC ERROR INDUCED BY'
     $' YAW,PITCH AND ROLL ERRORS ********************',////,
     $' EARTH RADIUS R =',F9.4,'KM',///,' NOMINAL ALTITUDE H =',
     $F4.0,'KM',///,' YAW ERROR DYAW =',F4.1,'DEGREE',///,
     $' PITCH ERROR DPITCH =',F4.1,'DEGREE',///,' ROLL ERROR'
     $' DROLL =',F4.1,'DEGREE',////,' VIEW',5X,'ANGLE',/,' DLOMDA'
     $'(DEGREES)',12X,F3.0,9(8X,F3.0),///,' NOMINAL X COORD. (KM)'
     $,7X,F2.0,9(9X,F2.0),///,' NOMINAL Y COORD. (KM)',10D11.4,
     $///,' SHIFTED X COORD. (KM)',10D11.4,///,' SHIFTED Y COORD.'
     $' (KM)',10D11.4,///,7X,'ERROR',6X,'(KM)',10D11.4,////,
     $' VIEW',5X,'ANGLE',/,' DLOMDA(DEGREES)',12X,F3.0,8(8X,F3.0),
     $///,' NOMINAL X COORD. (KM)',7X,F2.0,8(9X,F2.0),///,
     $' NOMINAL Y COORD. (KM)',9D11.4,///,' SHIFTED X COORD. (KM)'
     $,9D11.4,///,' SHIFTED Y COORD. (KM)',9D11.4,///,7X,'ERROR',
     $6X,'(KM)',9D11.4)
  601 CONTINUE


      DO 705 K=1,NDETA
      WRITE(6,700) R,DTAU,DETA(K),V(K),(DT(J),J=1,NDT),(DEX(K,J),
     $J=1,NDT),(DEY(K,J),J=1,NDT),(ERR(K,J),J=1,NDT)
  700 FORMAT(1H1,'********************* GEOMETRIC ERROR INDUCED BY'
     $' EARTH ROTATION ********************',//////////,' EARTH'
     $' RADIUS =',F9.4,'KM',/////,' ORBIT INCLINATION =',F4.0,
     $'DEGREE',/////,' LATITUDE =',F4.0,'DEGREE',/////////,
     $' GROUND POINT SHIFT VELOCITY DUE TO EARTH ROTATION =',
     $D10.4,'KM/SEC',/////,
     $' TIME INTERVAL    (SEC)',3F15.2,///,'      SHIFT IN',/,
     $'    X DIRECTION     (KM)',3X,3D15.4,///,'      SHIFT IN',/,
```

```
      $'   Y DIRECTION    (KM)',3X,3D15.4,////,'    TOTAL SHIFT'
      $'   (KM)',3X,3D15.4)
  705 CONTINUE


      DO 707 K=1,NDETA
      WRITE(6,706) R,DTAU,DETA(K),V(K),VS,VP(K),DANGL(K),(DT(J),
     $J=1,NDT),(DELX(K,J),J=1,NDT),(DELY(K,J),J=1,NDT),(ERRO(K,J),
     $J=1,NDT)
  706 FORMAT(1H1,'********************** GROUND POINT SHIFT INDUCED'
     $' BY SHUTTLE MOTION AND EARTH ROTATION *********************'
     $,///////////,' EARTH RADIUS =',F9.4,'KM',////,' ORBIT'
     $' INCLINATION =',F4.0,'DEGREE',////,' LATITUDE =',F4.0,
     $'DEGREE',////,' GROUND POINT SHIFT VELOCITY DUE TO EARTH'
     $' ROTATION =',D10.4,'KM/SEC',////,' SHUTTLE GROUND SPEED =',
     $D10.4,'KM/SEC',////,' GROUND POINT SHIFT VELOCITY RELATIVE'
     $' TO NADIR POINT =',D10.4,
     $'KM/SEC',////,' ANGLE OF VELOCITY VECTOR WITH Y-AXIS =',
     $D10.4,'DEGREE',////,' TIME INTERVAL   (SEC)',3F15.2,///,
     $'      SHIFT IN',/,'   X DIRECTION    (KM)',3X,3D15.4,///,
     $'      SHIFT IN',/,'   Y DIRECTION    (KM)',3X,3D15.4,////,
     $'    TOTAL SHIFT   (KM)',3X,3D15.4)
  707 CONTINUE


      STOP
      END
```

```
41   CTP:.134   SUPS:10.789

.A SHUTEXP.IMAGE/ABS
283-JB  04/27/83  10:31:21

2  SUPS.736  CPU=.090  IO=.302  CC-ER=.433
```

ORIGINAL PAGE IS
OF POOR QUALITY

******************** GEOMETRIC ERROR INDUCED BY ALTITUDE ERROR ********************

ARTH RADIUS R =6356.7850KM

IOMINAL ALTITUDE H=800.KM

ILTITUDE ERROR DH = 1.KM

VIEW ANGLE DLAMDA(DEGREES)		0.	1.	2.	3.	4.	5.	6.	7.	8.	9.
NOMINAL LOCATION	(KM)	.0000	.6982+001	.1397+002	.2096+002	.2798+002	.3500+002	.4200+002	.4914+002	.5625+002	.6340+002
SHIFTED LOCATION	(KM)	.0000	.7000+001	.1400+002	.2102+002	.2804+002	.3509+002	.4210+002	.4926+002	.5639+002	.6356+002
ERROR	(KM)	.0000	.1746-001	.3492-001	.5242-001	.6995-001	.8753-001	.1052+000	.1229+000	.1407+000	.1586+000
ABS(ERROR)	(%)	.000	.250	.250	.250	.250	.250	.250	.250	.250	.250

******************** GEOMETRIC ERROR SENSITIVITY WITH RESPECT TO ALTITUDE ERROR ********************

EARTH RADIUS R =6356.7850KM

NOMINAL ALTITUDE H =800.KM

ALTITUDE ERROR 1 TDH1 = .01KM

ALTITUDE ERROR 2 TDH2 = -.01KM

VIEW ANGLE DLAMDA(DEGREES)		0.	1.	2.	3.	4.	5.	6.	7.	8.	9.
SHIFTED LOCATION DUE TO ERROR 1	(KM)	.0000	.6982+001	.1397+002	.2097+002	.2798+002	.3500+002	.4200+002	.4918+002	.5625+002	.6341+00
SHIFTED LOCATION DUE TO ERROR 2	(KM)	.0000	.6982+001	.1397+002	.2096+002	.2797+002	.3500+002	.4200+002	.4914+002	.5625+002	.6340+00
DIFFERENCE	(KM)	.0000	.3491-003	.6985-003	.1048-002	.1399-002	.1751-002	.2104-002	.2458-002	.2814-002	.3173-00
ERROR SENSITIVITY	(KM/KM)	.0000	.1746-001	.3492-001	.5242-001	.6995-001	.8753-001	.1052+000	.1229+000	.1407+000	.1586+00

ORIGINAL PAGE IS
OF POOR QUALITY

******************** GEOMETRIC ERROR INDUCED BY ROLL ERROR ********************

EARTH RADIUS R =6356.7850KM

NOMINAL ALTITUDE H =400.KM

ROLL ERROR DFI =1.DEGREE

VIEW ANGLE DLOMDA(DEGREES)	-9.	-8.	-7.	-6.	-5.	-4.	-3.	-2.	-1.	0.
NOMINAL LOCATION (KM)	.6340+002	.5625+002	.4914+002	.4206+002	.3500+002	.2798+002	.2096+002	.1397+002	.6982+001	.0000
SHIFTED LOCATION (KM)	.5625+002	.4914+002	.4206+002	.3500+002	.2798+002	.2096+002	.1397+002	.6982+001	.0000	-.6982+001
ERROR (KM)	-.7153+001	-.7114+001	-.7081+001	-.7057+001	-.7029+001	-.7010+001	-.6996+001	-.6987+001	-.6982+001	-.6982+001
ABS(ERROR) (%)	11.2809	12.6471	14.4103	16.7696	20.0802	25.0564	33.3704	50.0107	100.0000	*****

VIEW ANGLE DLOMDA(DEGREES)	1.	2.	3.	4.	5.	6.	7.	8.	9.
NOMINAL LOCATION (KM)	-.6982+001	-.1397+002	-.2096+002	-.2798+002	-.3500+002	-.4206+002	-.4914+002	-.5625+002	-.6340+002
SHIFTED LOCATION (KM)	-.1397+002	-.2096+002	-.2798+002	-.3500+002	-.4206+002	-.4914+002	-.5625+002	-.6340+002	-.7060+002
ERROR (KM)	-.6987+001	-.6996+001	-.7010+001	-.7029+001	-.7052+001	-.7081+001	-.7114+001	-.7153+001	-.7196+001
ABS(ERROR) (%)	100.0007	50.0035	33.4373	25.1255	20.1475	16.8565	14.4762	12.7153	11.3496

******************** GEOMETRIC ERROR SENSITIVITY WITH RESPECT TO ROLL ERROR ********************

EARTH RADIUS R =6356.7850KM

NOMINAL ALTITUDE H =400.KM

ROLL ERROR 1 DFI1 = .01DEGREE

ROLL ERROR 2 DFI2 = -.01DEGREE

VIEW ANGLE DLOMDA(DEGREES)	-9.	-8.	-7.	-6.	-5.	-4.	-3.	-2.	-1.	0.
SHIFTED LOCATION DUE TO ERROR 1 (KM)	.6333+002	.5618+002	.4907+002	.4199+002	.3493+002	.2790+002	.2089+002	.1390+002	.6912+001	-.6981-001
SHIFTED LOCATION DUE TO ERROR 2 (KM)	.6348+002	.5632+002	.4921+002	.4213+002	.3507+002	.2805+002	.2103+002	.1404+002	.7052+001	.6981-001
DIFFERENCE (KM)	-.1435+000	-.1427+000	-.1419+000	-.1413+000	-.1408+000	-.1404+000	-.1400+000	-.1398+000	-.1397+000	-.1396+000
ERROR SENSITIVITY(KM/DEG)	-.7173+001	-.7133+001	-.7097+001	-.7066+001	-.7040+001	-.7019+001	-.7002+001	-.6991+001	-.6984+001	-.6981+001

VIEW ANGLE DLOMDA(DEGREES)	1.	2.	3.	4.	5.	6.	7.	8.	9.
SHIFTED LOCATION DUE TO ERROR 1 (KM)	-.7052+001	-.1404+002	-.2103+002	-.2805+002	-.3507+002	-.4213+002	-.4921+002	-.5632+002	-.6348+002
SHIFTED LOCATION DUE TO ERROR 2 (KM)	-.6912+001	-.1390+002	-.2089+002	-.2790+002	-.3493+002	-.4199+002	-.4907+002	-.5618+002	-.6333+002
DIFFERENCE (KM)	-.1397+000	-.1398+000	-.1400+000	-.1404+000	-.1408+000	-.1413+000	-.1419+000	-.1427+000	-.1435+000
ERROR SENSITIVITY(KM/DEG)	-.6984+001	-.6991+001	-.7002+001	-.7019+001	-.7040+001	-.7066+001	-.7097+001	-.7133+001	-.7173+001

ORIGINAL PAGE IS
OF POOR QUALITY

******************** GEOMETRIC ERROR INDUCED BY PITCH ERROR ********************

EARTH RADIUS R =6356.7850KM

NOMINAL ALTITUDE H =400.KM

PITCH ERROR DTHETA =1.DEGREE

VIEW ANGLE DLOMDA(DEGREES)	-9.	-8.	-7.	-6.	-5.	-4.	-3.	-2.	-1.	0.
NOMINAL X COORD. (KM)	0.	0.	0.	0.	0.	0.	0.	0.	0.	0.
NOMINAL Y COORD. (KM)	.6340+002	.5625+002	.4914+002	.4200+002	.3500+002	.2790+002	.2096+002	.1397+002	.6982+001	.0000
SHIFTED X COORD. (KM)	.6988+001	.6980+001	.6985+001	.6984+001	.6984+001	.6983+001	.6983+001	.6982+001	.6982+001	.6982+001
SHIFTED Y COORD. (KM)	.6341+002	.5626+002	.4915+002	.4200+002	.3501+002	.2790+002	.2097+002	.1397+002	.6983+001	.0000
ERROR (KM)	.6988+001	.6980+001	.6985+001	.6985+001	.6984+001	.6983+001	.6983+001	.6982+001	.6982+001	.6982+001

VIEW ANGLE DLOMDA(DEGREES)	1.	2.	3.	4.	5.	6.	7.	8.	9.
NOMINAL X COORD. (KM)	0.	0.	0.	0.	0.	0.	0.	0.	0.
NOMINAL Y COORD. (KM)	-.6982+001	-.1397+002	-.2096+002	-.2790+002	-.3500+002	-.4200+002	-.4914+002	-.5625+002	-.6340+002
SHIFTED X COORD. (KM)	.6982+001	.6982+001	.6983+001	.6984+001	.6984+001	.6985+001	.6985+001	.6980+001	.6988+001
SHIFTED Y COORD. (KM)	-.6983+001	-.1397+002	-.2097+002	-.2790+002	-.3501+002	-.4200+002	-.4915+002	-.5626+002	-.6341+002
ERROR (KM)	.6982+001	.6982+001	.6983+001	.6984+001	.6984+001	.6985+001	.6985+001	.6980+001	.6988+001

******************** GEOMETRIC ERROR SENSITIVITY WITH RESPECT TO PITCH ERROR ********************

EARTH RADIUS R =6356.7850KM

NOMINAL ALTITUDE H =400.KM

PITCH ERROR 1 DTETA1 = .01DEGREE

PITCH ERROR 2 DTETA2 = -.01DEGREE

VIEW ANGLE DLOMDA(DEGREES)	-9.	-8.	-7.	-6.	-5.	-4.	-3.	-2.	-1.	0.
SHIFTED X COORD. DUE TO ERROR 1 (KM)	.6987-001	.6986-001	.6985-001	.6984-001	.6983-001	.6982-001	.6982-001	.6982-001	.6981-001	.6981-001
SHIFTED Y COORD. DUE TO ERROR 1 (KM)	.6340+002	.5625+002	.4914+002	.4200+002	.3500+002	.2790+002	.2096+002	.1397+002	.6982+001	.0000
SHIFTED X COORD. DUE TO ERROR 2 (KM)	-.6987-001	-.6986-001	-.6985-001	-.6984-001	-.6983-001	-.6982-001	-.6982-001	-.6982-001	-.6981-001	-.6981-001
SHIFTED Y COORD. DUE TO ERROR 2 (KM)	.6340+002	.5625+002	.4914+002	.4200+002	.3500+002	.2790+002	.2096+002	.1397+002	.6982+001	.0000
DIFFERENCE (KM)	.1397+000	.1397+000	.1397+000	.1397+000	.1397+000	.1396+000	.1396+000	.1396+000	.1396+000	.1396+000
ERROR SENSITIVITY(KM/DEG)	.6987+001	.6986+001	.6985+001	.6984+001	.6983+001	.6982+001	.6982+001	.6982+001	.6981+001	.6981+001

VIEW ANGLE DLOMDA(DEGREES)	1.	2.	3.	4.	5.	6.	7.	8.	9.
SHIFTED X COORD. DUE TO ERROR 1 (KM)	.6981-001	.6982-001	.6982-001	.6982-001	.6983-001	.6984-001	.6985-001	.6986-001	.6987-001
SHIFTED Y COORD. DUE TO ERROR 1 (KM)	-.6982+001	-.1397+002	-.2096+002	-.2790+002	-.3500+002	-.4200+002	-.4914+002	-.5625+002	-.6340+002
SHIFTED X COORD. DUE TO ERROR 2 (KM)	-.6981-001	-.6982-001	-.6982-001	-.6982-001	-.6983-001	-.6984-001	-.6985-001	-.6986-001	-.6987-001
SHIFTED Y COORD. DUE TO ERROR 2 (KM)	-.6982+001	-.1397+002	-.2096+002	-.2790+002	-.3500+002	-.4200+002	-.4914+002	-.5625+002	-.6340+002
DIFFERENCE (KM)	.1396+000	.1396+000	.1396+000	.1396+000	.1397+000	.1397+000	.1397+000	.1397+000	.1397+000
ERROR SENSITIVITY(KM/DEG)	.6981+001	.6982+001	.6982+001	.6982+001	.6983+001	.6984+001	[illegible]	[illegible]	[illegible]

******************** GEOMETRIC ERROR INDUCED BY YAW ERROR ********************

EARTH RADIUS R =6350.7850KM

NOMINAL ALTITUDE H =400.KM

YAW ERROR DPSA =1.DEGREE

VIEW ANGLE DLAMDA(DEGREES)	0.	1.	2.	3.	4.	5.	6.	7.	8.	9.
ERROR (KM)	.0000	.1219+000	.2438+000	.3658+000	.4883+000	.6109+000	.7340+000	.8576+000	.9818+000	.1107+001

******************** GEOMETRIC ERROR SENSITIVITY WITH RESPECT TO YAW ERROR ********************

EARTH RADIUS R =6350.7850KM

NOMINAL ALTIRUDE H =400.KM

YAW ERROR 1 DPSI1 = .01DEGREE

YAW ERROR 2 DPSI2 = -.01DEGREE

VIEW ANGLE DLAMDA(DEGREES)	0.	1.	2.	3.	4.	5.	6.	7.	8.	9.
TOTAL SHIFT (KM)	.0000	.2437-002	.4876-002	.7318-002	.9765-002	.1222-001	.1468-001	.1715-001	.1964-001	.2213-00
ERROR SENSITIVITY(KM/DEG)	.0000	.1219+000	.2438+000	.3658+000	.4883+000	.6109+000	.7340+000	.8576+000	.9818+000	.1107+00

******************** GEOMETRIC ERROR INDUCED BY YAW,PITCH AND ROLL ERRORS ********************

EARTH RADIUS R =6356.785KM

NOMINAL ALTITUDE H =400.KM

YAW ERROR DYAW =1.DEGREE

PITCH ERROR DPITCH =1.DEGREE

ROLL ERROR DROLL =1.DEGREE

VIEW ANGLE DLOMDA(DEGREES)	-9.	-8.	-7.	-6.	-5.	-4.	-3.	-2.	-1.	0.
NOMINAL X COORD. (KM)	0.	0.	0.	0.	0.	0.	0.	0.	0.	0.
NOMINAL Y COORD. (KM)	-.6346+002	-.5625+002	-.4914+002	-.4206+002	-.3500+002	-.2798+002	-.2096+002	-.1397+002	-.6982+001	.0000
SHIFTED X COORD. (KM)	-.6005+001	-.6128+001	-.6250+001	-.6372+001	-.6494+001	-.6616+001	-.6738+001	-.6859+001	-.6981+001	-.7103+001
SHIFTED Y COORD. (KM)	-.5637+002	-.4920+002	-.4210+002	-.3511+002	-.2816+002	-.2109+002	-.1424+002	-.7105+001	-.1230+000	-.6859+001
ERROR (KM)	.6245+001	.6296+001	.6353+001	.6414+001	.6480+001	.6550+001	.6625+001	.6704+001	.6787+001	.6874+001

VIEW ANGLE DLOMDA(DEGREES)	1.	2.	3.	4.	5.	6.	7.	8.	9.
NOMINAL X COORD. (KM)	0.	0.	0.	0.	0.	0.	0.	0.	0.
NOMINAL Y COORD. (KM)	-.6982+001	-.1397+002	-.2096+002	-.2798+002	-.3500+002	-.4206+002	-.4914+002	-.5625+002	-.6346+002
SHIFTED X COORD. (KM)	.7225+001	.7347+001	.7470+001	.7593+001	.7717+001	.7841+001	.7966+001	.8092+001	.8219+001
SHIFTED Y COORD. (KM)	-.1385+002	-.2080+002	-.2785+002	-.3480+002	-.4193+002	-.4901+002	-.5613+002	-.6328+002	-.70[illegible]
ERROR (KM)	.9966+001	.1006+002	.1016+002	.1026+002	.1037+002	.1048+002	.1059+002	.1072+002	.1[illegible]

******************** GROUND POINT SHIFT INDUCED BY SHUTTLE MOTION AND EARTH ROTATION ********************

EARTH RADIUS =6356.785KM

ORBIT INCLINATION = 85.DEGREE

LATITUDE = 0.DEGREE

GROUND POINT SHIFT VELOCITY DUE TO EARTH ROTATION = .4623+000KM/SEC

SHUTTLE GROUND SPEED = .7202+001KM/SEC

GROUND POINT SHIFT VELOCITY RELATIVE TO NADIR POINT = .7177+001KM/SEC

ANGLE OF VELOCITY VECTOR WITH Y-AXIS =-.8032+002DEGREE

TIME INTERVAL (SEC)		1.00	.10	.01
SHIFT IN X DIRECTION	(KM)	-.7162+001	-.7162+000	-.7162-001
SHIFT IN Y DIRECTION	(KM)	.4605+000	.4605-001	.4605-002
TOTAL SHIFT	(KM)	.7177+001	.7177+000	.7177-001

******************** GROUND POINT SHIFT INDUCED BY SHUTTLE MOTION AND EARTH ROTATION ********************

EARTH RADIUS =6356.7850KM

ORBIT INCLINATION = 85.DEGREE

LATITUDE = 20.DEGREE

GROUND POINT SHIFT VELOCITY DUE TO EARTH ROTATION = .4344+000KM/SEC

SHUTTLE GROUND SPEED = .7202+001KM/SEC

GROUND POINT SHIFT VELOCITY RELATIVE TO NADIR POINT = .7175+001KM/SEC

ANGLE OF VELOCITY VECTOR WITH Y-AXIS =-.6056+002DEGREE

TIME INTERVAL	(SEC)	1.00	.10	.01
SHIFT IN X DIRECTION	(KM)	-.7102+001	-.7102+000	-.7102-001
SHIFT IN Y DIRECTION	(KM)	.4325+000	.4325-001	.4325-002
TOTAL SHIFT	(KM)	.7175+001	.7175+000	.7175-001

******************** GROUND POINT SHIFT INDUCED BY SHUTTLE MOTION AND EARTH ROTATION ********************

EARTH RADIUS =6356.7850KM

ORBIT INCLINATION = 85.DEGREE

LATITUDE = 40.DEGREE

GROUND POINT SHIFT VELOCITY DUE TO EARTH ROTATION = .3541+000KM/SEC

SHUTTLE GROUND SPEED = .7202+001KM/SEC

GROUND POINT SHIFT VELOCITY RELATIVE TO NADIR POINT = .7171+001KM/SEC

ANGLE OF VELOCITY VECTOR WITH Y-AXIS =-.8719+002DEGREE

TIME INTERVAL	(SEC)	1.00	.10	.01
SHIFT IN X DIRECTION	(KM)	-.7102+001	-.7102+000	-.7102-001
SHIFT IN Y DIRECTION	(KM)	.3514+000	.3514-001	.3514-002
TOTAL SHIFT	(KM)	.7171+001	.7171+000	.7171-001

******************** GROUND POINT SHIFT INDUCED BY SHUTTLE MOTION AND EARTH ROTATION ********************

EARTH RADIUS =6356.785KM

ORBIT INCLINATION = 85.DEGREE

LATITUDE = 60.DEGREE

GROUND POINT SHIFT VELOCITY DUE TO EARTH ROTATION = .2311+000KM/SEC

SHUTTLE GROUND SPEED = .7202+001KM/SEC

GROUND POINT SHIFT VELOCITY RELATIVE TO NADIR POINT = .7165+001KM/SEC

ANGLE OF VELOCITY VECTOR WITH Y-AXIS =-.8014+002DEGREE

TIME INTERVAL	(SEC)	1.00	.10	.01
SHIFT IN X DIRECTION	(KM)	-.7162+001	-.7162+000	-.7162-001
SHIFT IN Y DIRECTION	(KM)	.2270+000	.2270-001	.2270-002
TOTAL SHIFT	(KM)	.7166+001	.7166+000	.7166-001

******************** GROUND POINT SHIFT INDUCED BY SHUTTLE MOTION AND EARTH ROTATION ********************

EARTH RADIUS =6356.785KM

ORBIT INCLINATION = 85.DEGREE

LATITUDE = 80.DEGREE

GROUND POINT SHIFT VELOCITY DUE TO EARTH ROTATION = .8027-001KM/SEC

SHUTTLE GROUND SPEED = .7202+001KM/SEC

GROUND POINT SHIFT VELOCITY RELATIVE TO NADIR POINT = .7162+001KM/SEC

ANGLE OF VELOCITY VECTOR WITH Y-AXIS =-.8944+002DEGREE

TIME INTERVAL	(SEC)	1.00	.10	.01
SHIFT IN X DIRECTION	(KM)	-.7162+001	-.7162+000	-.7162-001
SHIFT IN Y DIRECTION	(KM)	.8943-001	.8943-002	.8943-003
TOTAL SHIFT	(KM)	.7162+001	.7162+000	.7162-001

APPENDIX F

GROUND PATTERN AND IMAGING

DISTORTIONS GENERATION PROGRAM LISTINGS

```
0C00 I 006610 IM          0000 I 006021 IM1         0000 I 005706 IPT         0000 I 0
0600 I 005712 J           0000 I 006045 JDD         0000 I 005742 J6          0000 I 0
0000 I 006011 JM          0008 I 006022 JM1         0000 I 005723 JR          0000 I 0
0003 I 005714 L           0000 R 000000 LAMDA       0000 I 003030 LFLAG       0000 I 0
0000 R 000003 LRMDA       000C R 000002 LYMDA       0C00 I 001747 MFLAG       0000 I 0
0000 I 005673 NGX         0000 I 005674 NGY         0000 I 0C6050 NLIN        0000 I 0
0000 I 006065 NLIN3       0000 I 006070 NLIN4       0000 I 006073 NLIN5       0000 I 0
0C00 I 006047 NTIC        0008 I 006053 NTIC1       0000 I 006056 NTIC2       0000 I 0
0OC0 I 006072 NTIC5       0000 I 006061 NTIC6       0000 I 006075 NTIC7       0000 I 0
0000 R 006024  MEGA       0000 R 0C5646 PD          0000 R 005631 PI          0000 R 0
0000 R 005630 R           0000 R 005767 RA          0000 R 006037 RAA         0000 R 0
0000 R C05751 RHO1        0000 R 006000 ROLL        0000 R 005656 RS          0000 R 0
0C00 R 005752 SGURT1      0000 R 006023 TAU         0000 R 005743 TEHTA       0000 R 0
0000 R 006052 TIC1        0000 R 006055 TIC2        0000 R 006063 TIC3        0000 R 0
0000 R 006060 TIC6        0000 R 006074 TIC7        0000 R 005730 T1          C000 R 0
0000 R 005747 T21         0000 R C06026 V           0000 R 005636 VS          0000 R 0
0000 R 006034 VTY         0000 R 006031 VX          0000 R 006032 VY          0000 R 0
0C00 R 005740 V9          0000 R 006040 XBB         0000 R 005756 XB1         0000 R 0
0C00 R 005664 XCENT       0000 R 005757 XC1         0000 R 005220 XDD         0000 R 0
0000 R 003262 XF          0000 R 000612 XG          0000 R 004610 XG1         0000 R 0
0000 R 005754 XI1         0000 R 005770 XJ          0000 R 006005 XK          0000 R 0
0000 R 005675 XLEFT       0000 R 005667 XLEN        0000 R 006017 XL1         0000 R 0
0C00 R 005707 XNOM        0000 R 000202 XP          0000 R 002140 XP1         0000 R 0
0C00 R 003221 XP4         0000 R 003015 XP5         0000 R 005172 XP6         0000 R 0
0000 R 005661 XSTA        0000 R 006001 XSTAO       0C00 R 005774 XT          0000 R 0
0000 R 005720 XZ          0000 R 000421 Y           0000 R 005725 YA          0000 R 0
0000 R 005651 YAWD        0000 R 005652 YAWS        0000 R 005745 YA1         0000 R 0
000C R 005700 YBOT        0000 R 005755 YB1         0000 R 005703 YC          0000 R 0
0000 R 005760 YC1         0C00 R 005764 YD          0000 R 005411 YDD         0000 R 0
0C00 R 003453 YF          0C00 R 001003 YG          0000 R 005001 YG1         0000 R 0
0000 R 005753 YI1         0000 R 005771 YJ          0000 R 006002 YK          0000 R 0
0000 R 005670 YLEN        0000 R 006020 YL1         0000 R 001365 YN          0000 R 0
0C00 R 000215 YP          0000 R 002153 YP1         0000 R 002201 YP2         0000 R 0
0000 R 003247 YP5         0C00 R 005205 YP6         0000 R 005615 YP7         0000 R 0
0000 R 005644 YSTAP       0000 R 005645 YSTAP1      0000 R 005634 YSTAR       0000 R 0
0000 R 005701 YTOP        0C08 R 005713 YW          0000 R 000200 YY          0000 R 0
```

```
100      C      DECLAPE FARAPETERS
101             PARAMETER NLINES=11,NDT=400,NLAMDA=460,NLPMDA=310,
101            $NLYMDA=450,NLRMDA=480
103
103             REAL LAMDA,LFFDA,LYMDA,LRMDA
104             INTFSER FLAG,AFLAG
105
105      C      DIMENSION OF VARIABLES
105             DIMENSION XX(2),YY(2),XP(NLINES),YP(NLINES),X(NLINES,NLINES)
105            $,Y(NLINES,NLINES),XG(NLINES,NLINES),YG(NLINES,NLINES),
105            $XM(NLINES,NLINES),YM(NLINES,NLINES),NFLAG(NLINES,NLINES),
105            $MFLAG(NLINES,NLINES),XP1(NLINES),YP1(NLINES)
105            $,XP2(NLINES),YP2(NLINES),XH(NLINES,NLINES),YH(NLINES,NLINES)
105            $KFLAG(NLINES,NLINES),XP3(NLINES),YP3(NLINES),XP5(NLINES),
105            $LFLAG(NLINES,NLINES),XP4(NLINES),YP4(NLINES),YP5(NLINES),
105            $XF(NLINES,NLINES),YF(NLINES,NLINES),LFLAG1(NLINES,NLINES),
105            $XM1(NLINES,NLINES),YM1(NLINES,NLINES),NFLAG1(NLINES,NLINES),
```

ORIGINAL PAGE IS
OF POOR QUALITY

```
C0105          $XG1(NLINES,NLINES),YG1(NLINES,NLINES),XP6(NLINES),
00105          $YP6(NLINES),XDD(NLINES,NLINES),YDD(NLINES,NLINES),
00105          $AFLAG(NLINES,NLINES),XP7(NLINES),YP7(NLINES)
00106
C0106           DATA R,PI,F,D,YSTAR,DT,VS,H,DD,DS/6356.785,3.141592654,
00106          $1000000.,400.,-5.5,.004,7.1399,440.,.0039,.3/
00121           DATA EPS1,DET,YSTAP,YSTAP1,PD,PS,FLAG/.02,1.,
00121          $-5.,-434.7,.0055,.65,2/
00131           DATA YSTAY,YAWD,YAWS/-5.,.0037,.925/
CC135           DATA DROLL,YSTAO,RD,RS/0.,-5.0,.0042,1./
00142           DATA DTAU,DETA,XSTA,YSTA,VS4/85.,40.,0.,-5.,7.202/
CC150
C0150     C     INITIALIZE THE PLOTTER
00150           CALL BGNPLT
C0151
C0151     C     CENTER PLCT
00151           XCENT=6.0
C0152           YCENT=1.0
C0153           CALL ORIGIN(XCENT,YCENT)
00154
C0154     C     DEFINE THE FORM OF THE PLOT
C0154           PTYPE='LINLIN'
00155           XLEN=8.0
C0156           YLEN=8.0
00157           CALL PLFORM(PTYPE,XLEN,YLEN)
00160
00160     C     SCALE THE PLOT
00160           XX(1)=-8
C0161           XX(2)=8
C0162           YY(1)=-8
00163           YY(2)=8
C0164           NXX=2
00165           NYY=2
00166           NGX=-1
C0167           NGY=-1
C0170           CALL PLSCAL(XX,NXX,NGX,YY,NYY,NGY)
00171
CC171     C     TO START PLOTTING
C0171           CALL PLGRAF
00172
00172     C     DEFINE GRID LIMITS
C0172           XLEFT=-5
00173           XRIGHT=5
00174           XDEL=(XRIGHT-XLEFT)/(NLINES-1)
CC175           YBOT=-5
0C176           YTOP=5
C0177           YDEL=(YTOP-YBOT)/(NLINES-1)
00200
00200     C     CONSTRUCT DATA
00200           YC=YTOP
00201           DO 150 INOR=1,NLINES
00204           XC=XLEFT
00205           DO 100 IPT=1,NLINES
C0210           XNOM=R*SIN(XC/R)
00210     C     XD=(XC-XNOMS)*F
00210     C     XNOM=XC-XD
00211           YNOM=YC
```

```
0212            X(IHOR,IPT)=XNOM
0213            Y(IHOR,IPT)=YNOM
0214            XC=XC+XDEL
0215        100 CONTINUE
0217            YC=YC-YDEL
0220        150 CONTINUE
0222            IF(FLAG.EQ.1) GO TO 200
0224            IF(FLAG.EQ.2) GO TO 208
0226            IF(FLAG.EQ.3) GO TO 231
0230            IF(FLAG.EQ.4) GO TO 251
0232            GO TO 261
0233
0233        200 CONTINUE
0234            DO 202 I=1,NLINES
0237            DO 201 J=1,NLINES
0242            NFLAG(I,J)=0
0243        201 CONTINUE
0245        202 CONTINUE
0247            YW=YSTAR
0250            DO 206 L=1,NDT
0253            DLAMDA=DS
0254            DO 205 K=1,NLAMDA
0257            LAMDA=DLAMDA*PI/180.
0260            XW=-R*((1+H/R)*COS(LAMDA)-SQRT(1-(1+H/R)*(1+H/R)*
0260           $SIN(LAMDA)*SIN(LAMDA)))*SIN(LAMDA)
0261            DO 80 I=1,NLINES
0264            DO 70 J=1,NLINES
0267            XZ=XW-X(I,J)
0270            YZ=YW-Y(I,J)
0271            IR=I
0272            JR=J
0273            IF(ABS(XZ).LE.EPSI.AND.ABS(YZ).LE.EPSI) GO TO 204
0275         70 CONTINUE
0277         80 CONTINUE
0301            GO TO 99
0302        204 NFLAG(IR,JR)=1
0303            XF(IR,JR)=D*(-TAN(LAMDA))
0304            YF(IR,JR)=YSTAR+(L-1)*.0285
0305            WRITE(6,98) XW,YW,IR,JR,DLAMDA,XF(IR,JR),YF(IR,JR)
0316         98 FORMAT(/,2F10.5,2I4,3F10.5)
0317         99 DLAMDA=DLAMDA-DD
0320        205 CONTINUE
0322            YW=YSTAR+L*DT*VS
0323        206 CONTINUE
0325            GO TO 299
0326
0326        208 CONTINUE
0327            DO 2 I=1,NLINES
0332            DO 1 J=1,NLINES
0335            NFLAG(I,J)=0
0336          1 CONTINUE
0340          2 CONTINUE
0342            DTHETA=0.
0343            YA=YSTAR
0344            DO 217 L=1,NDT
0347            THETA=DTHETA*PI/180.
0350            DLAMDA=PS
```

ORIGINAL PAGE IS
OF POOR QUALITY

```
0351          DO 216 K=1,NLPMDA
0354          LPMDA=DLPMDA*PI/180.
0355          T1=D*TAN(THETA)
0356          T2=-ABS(D/COS(THETA))*TAN(LPMDA)
0357          DEL=SQRT(T1*T1+T2*T2)
0360          RHO=ATAN(DEL/D)
0361          SQURT=R*((1+D/R)*COS(RHO)-SQRT(1-(1+D/R)*(1+D/R)*SIN
0361         S(RHO)*SIN(RHO)))*SIN(RHO)
0362          YI=(SQURT*T1)/DEL
0363          XI=(SQURT*T2)/DEL
0364          YB=YI+YA
0365          XB=XI
0366          DO 22 I=1,NLINES
0371          DO 11 J=1,NLINES
0374          XC=XB-X(I,J)
0375          YC=YB-Y(I,J)
0376          IG=I
0377          JG=J
0400          IF(ABS(XC).LE.EPSI.AND.ABS(YC).LE.EPSI) GO TO 210
0402       11 CONTINUE
0404       22 CONTINUE
0406          GO TO 215
0407      210 NFLAG(IG,JG)=1
0410          XG(IG,JG)=D*(-TAN(LPMDA))
0411          YG(IG,JG)=YBOT+(L-1)*.0288
0412          WRITE(6,212) XB,YB,IG,JG,DLPMDA,XG(IG,JG),YG(IG,JG)
0423      212 FORMAT(/,2F10.5,2I4,3F10.5)
0424      215 DLPMDA=DLPMDA-PD
0425      216 CONTINUE
0427          YA=YSTAP+L*.0288
0430          DTHETA=L/2500.
0431      217 CONTINUE
0433          GO TO 299

0434
0434          DO 220 I=1,NLINES
0437          DO 219 J=1,NLINES
0442          NFLAG1(I,J)=0
0443      219 CONTINUE
0445      220 CONTINUE
0447          TENTA=DTHETA*PI/180.
0450          ET=DET*PI/180.
0451          YA1=YSTAP1
0452          DO 227 L=1,NDT
0455          DLPMDA=PS
0456          DO 226 K=1,NLPMDA
0461          LPMDA=DLPMDA*PI/180.
0462          T11=D*TAN(THETA+ET)
0463          T21=-ABS(D/COS(THETA+ET))*TAN(LPMDA)
0464          DEL1=SQRT(T11*T11+T21*T21)
0465          RHO1=ATAN(DEL1/D)
0466          SQURT1=R*((1+D/R)*COS(RHO1)-SQRT(1-(1+D/R)*(1+D/R)*
0466         $SIN(RHO1)*SIN(RHO1)))*SIN(RHO1)
0467          YI1=(SQURT1*T11)/DEL1
0470          XI1=(SQURT1*T21)/DEL1
0471          YB1=YI1+YA1
0472          XB1=XI1
```

```
0473          DO 222 I=1,NLINES
0476          DO 221 J=1,NLINES
0501          XC1=XB1-X(I,J)
0502          YC1=YB1-Y(I,J)
0503          IG1=I
0504          JG1=J
0505          IF(ABS(XC1).LE.EPSI.AND.ABS(YC1).LE.EPSI) GO TO 223
0507      221 CONTINUE
0511      222 CONTINUE
0513          GO TO 225
0514      223 KFLAG1(IG1,JG1)=1
0515          XG1(IG1,JG1)=D*(-TAN(LPMDA))
0516          YG1(IG1,JG1)=YSTAP1+(L-1)*.0288+Y11
0517          WRITE(6,224) XB1,YB1,IG1,JG1,DLPMDA,XG1(IG1,JG1),
0517         $YG1(IG1,JG1)
0530      224 FORMAT(/,2F10.5,2I4,3F10.5)
0531      225 DLPMDA=DLPMDA-PD
0532      226 CONTINUE
0534          YA1=YSTAP1+L*.0288
0535      227 CONTINUE
0537          GO TO 605
0540
0540      231 CONTINUE
0541          DO 4 I=1,NLINES
0544          DO 3 J=1,NLINES
0547          KFLAG(I,J)=0
0550        3 CONTINUE
0552        4 CONTINUE
0554          DYAW=0.
0555          YD=YSTAY
0556          DO 240 L=1,NDT
0561          YAW=DYAW*PI/180.
0562          DLYMDA=YAWS
0563          DO 238 K=1,NLYMDA
0566          LYMDA=DLYMDA*PI/180.
0567          RA=-R*((1+D/R)*COS(LYMDA)-SQRT(1-(1+D/R)*(1+D/R)*SIN(LYMDA)
0567         $*SIN(LYMDA)))*SIN(LYMDA)
0570          XJ=RA*COS(YAW)
0571          YJ=-RA*SIN(YAW)
0572          XE=XJ
0573          YE=YJ+YD
0574          DO 44 I=1,NLINES
0577          DO 33 J=1,NLINES
0602          XT=XE-X(I,J)
0603          YT=YE-Y(I,J)
0604          IH=I
0605          JH=J
0606          IF(ABS(XT).LE.EPSI.AND.ABS(YT).LE.EPSI) GO TO 233
0610       33 CONTINUE
0612       44 CONTINUE
0614          GO TO 235
0615      233 KFLAG(IH,JH)=1
0616          XH(IH,JH)=D*(-TAN(LYMDA))
0617          YH(IH,JH)=YROT+(L-1)*.0288
0620          WRITE(6,234) XE,YE,IH,JH,DLYMDA,XH(IH,JH),YH(IH,JH)
0631      234 FORMAT(/,2F10.5,2I4,3F10.5)
0632      235 DLYMDA=DLYMDA-YAWD
```

```
  238 CONTINUE
      YD=YSTAY+L*.0288
      DYAW=5.*SIN((L*PI)/174.)
  240 CONTINUE
      GO TO 299

  241 CONTINUE
      DO 6 I=1,NLINES
      DO 5 J=1,NLINES
      LFLAG(I,J)=0
    5 CONTINUE
    6 CONTINUE
      ROLL=DROLL*PI/180.
      XSTAO=R*((1+D/R)*COS(ROLL)-SQRT(1-(1+D/R)*(1+D/R)*SIN(ROLL)
     $*SIN(ROLL)))*SIN(ROLL)
      YK=YSTAO
      DO 250 L=1,NDT
      DLRMDA=RS
      DO 245 K=1,NLRMDA
      LRMDA=DLRMDA*PI/180.
      DIS=-R*((1+D/R)*COS(LRMDA+ROLL)-SQRT(1-(1+D/R)*(1+D/R)*SIN
     $(LRMDA+ROLL)*SIN(LRMDA+ROLL)))*SIN(LRMDA+ROLL)
      XK=DIS+XSTAO
      DO 66 I=1,NLINES
      DO 55 J=1,NLINES
      XL=XK-X(I,J)
      YL=YK-Y(I,J)
      IM=I
      JM=J
      IF(ABS(XL).LE.EPSI.AND.ABS(YL).LE.EPSI) GO TO 242
   55 CONTINUE
   66 CONTINUE
      GO TO 244
  242 LFLAG(IM,JM)=1
      XM(IM,JM)=D*(-TAN(LRMDA))
      YM(IM,JM)=YSTAO+(L-1)*.0288
      WRITE(6,243) XK,YK,IM,JM,DLRMDA,XM(IM,JM),YM(IM,JM)
  243 FORMAT(/,2F10.5,2I4,3F10.5)
  244 DLRMDA=DLRMDA-RD
  245 CONTINUE
      YK=YSTAO+L*.0288
  250 CONTINUE

  251 CONTINUE
      DO 8 I=1,NLINES
      DO 7 J=1,NLINES
      LFLAG1(I,J)=0
    7 CONTINUE
    8 CONTINUE
      ROLL=DROLL*PI/180.
      DER=0.
      XSTAO=R*((1+D/R)*COS(ROLL)-SQRT(1-(1+D/R)*(1+D/R)*SIN(ROLL)
     $*SIN(ROLL)))*SIN(ROLL)
      YK1=YSTAO
      DO 260 L=1,NDT
      ER=DER*PI/180.
```

```
0763          DLRMDA=RS
0764          DO 255 K=1,NLRMDA
0767          LRMDA=DLRMDA*PI/180.
0773          DIS1=-R*((1+D/R)*COS(LRMDA+ROLL+ER)-SQRT(1-(1+D/R)*(1+D/R)
0770         $*SIN(LRMDA+ROLL+ER)*SIN(LRMDA+ROLL+ER)))*SIN(LRMDA+ROLL+ER)
0771          XK1=DIS1+XSTAO
0772          DO 99 I=1,NLINES
0775          DO 77 J=1,NLINES
1000          XL1=XK1-X(I,J)
1001          YL1=YK1-Y(I,J)
1002          IM1=I
1003          JM1=J
1004          IF(ABS(XL1).LE.EPSI.AND.ABS(YL1).LE.EPSI) GO TO 252
1006       77 CONTINUE
1010       99 CONTINUE
1012          GO TO 254
1013      252 LFLAG1(IM1,JM1)=1
1014          XM1(IM1,JM1)=D*(-TAN(LRMDA))
1015          YM1(IM1,JM1)=YBOT+(L-1)*.0288
1016          WRITE(6,253) XK1,YK1,IM1,JM1,DLRMDA,XM1(IM1,JM1),
1016         $YM1(IM1,JM1)
1027      253 FORMAT(/,2F10.5,2I4,3F10.5)
1030      254 DLRMDA=DLRMDA-RD
1031      255 CONTINUE
1033          YK1=YSTAC+L*.0288
1034          DER=0.2*SIN((L*PI)/174.)
1035      260 CONTINUE
1037          GO TO 299
1040
1040      261 CONTINUE
1041          DO 263 I=1,NLINES
1044          DO 262 J=1,NLINES
1047          AFLAG(I,J)=0
1050      262 CONTINUE
1052      263 CONTINUE
1054          TAU=DTAU*PI/180.
1055          OMEGA=2.*PI/86400.
1056          ETA=DETA*PI/180.
1057          V=OMEGA*R*COS(ETA)
1060          SLUMDA=COS(TAU)/COS(ETA)
1061          CLUMDA=SQRT(1-SLUMDA*SLUMDA)
1062          VX=V*CLUMDA
1063          VY=V*SLUMDA
1064          VTX=-VX
1065          VTY=VS4-VY
1066          XAA=XSTA
1067          YAA=YSTA
1070          DO 270 L=1,NDT
1073          DLYMDA=YAWS
1074          DO 269 K=1,NLYMDA
1077          LYMDA=DLYMDA*PI/180.
1100          XAA=-R*((1+D/R)*COS(LYMDA)-SQRT(1-(1+D/R)*(1+D/R)*SIN
1100         $(LYMDA)*SIN(LYMDA)))*SIN(LYMDA)
1101          XBB=XAA+XAA
1102          YBB=YAA
1103          DO 265 I=1,NLINES
1106          DO 264 J=1,NLINES
```

ORIGINAL PAGE IS
OF POOR QUALITY

```
1111          XCC=XBB-X(I,J)
1112          YCC=YBB-Y(I,J)
1113          IDD=I
1114          JDD=J
1115          IF(ABS(XCC).LE.EPSI.AND.ABS(YCC).LE.EPSI) GO TO 266
1117      264 CONTINUE
1121      265 CONTINUE
1123          GO TO 268
1124      266 AFLAG(I,J)=1
1125          XDD(IDD,JDD)=D*(-TAN(LYMDA))
1126          YDD(IDD,JDD)=YSTA+(L-1)*.0288
1127          WRITE(6,267) XBB,YBB,IDD,JDD,DLYMDA,XDD(IDD,JDD),
1127         $YDD(IDD,JDD)
1140      267 FORMAT(/,2F10.5,2I4,3F10.5)
1141      268 DLYMDA=DLYMDA-DD
1142      269 CONTINUE
1144          XAA=XSTA+L*DT*VTX
1145          YAA=YSTA+L*DT*VTY
1146      270 CONTINUE
1150
1150    C     PLOT HORIZONTAL LINES
1150
1150      293 CONTINUE
1151          TIC=*+*
1152          NTIC=-1
1153          NLIN=NLINES
1154          DO 400 IHOR=1,NLINES
1157          DO 300 IPT=1,NLINES
1162          XP(IPT)=X(IHOR,IPT)
1163          YP(IPT)=Y(IHOR,IPT)
1164      300 CONTINUE
1166          CALL PLCURV(XP,YP,NLIN,NTIC,TIC)
1167      400 CONTINUE
1171
1171    C     PLOT VERTICAL LINES
1171          DO 500 IVERT=1,NLINES
1174          CALL PLCURV(X(1,IVERT),Y(1,IVERT),NLIN,NTIC,TIC)
1175      500 CONTINUE
1177          IF(FLAG.EQ.1) GO TO 655
1201          IF(FLAG.EQ.2) GO TO 805
1203          IF(FLAG.EQ.3) GO TO 901
1205          IF(FLAG.EQ.4) GO TO 909
1207          GO TO 921
1210
1210    C     PLOT HORIZONTAL LINES
1210
1210      655 CONTINUE
1211          TIC1=0
1212          NTIC1=0
1213          NLIN1=NLINES
1214          DO 750 IHOR=1,NLINES
1217          DO 700 IPT=1,NLINES
1222          XP1(IPT)=XF(IHOR,IPT)
1223          YP1(IPT)=YF(IHOR,IPT)
1224      700 CONTINUE
1226          CALL PLCURV(XP1,YP1,NLIN1,NTIC1,TIC1)
1227      750 CONTINUE
```

```
1231
1231       C      PLOT VERTICAL LINES
1231              DO 800 IVERT=1,NLINES
1234              CALL PLCURV(XF(1,IVERT),YF(1,IVERT),NLIN1,NTIC1,TIC1)
1235         800  CONTINUE
1237              GO TO 9999
1240
1240       C      PLOT HORIZONTAL LINES
1240         805  CONTINUE
1241              TIC2=0
1242              NTIC2=0
1243              NLIN2=NLINES
1244              DO 850 IHOR=1,NLINES
1247              DO 820 IPT=1,NLINES
1252              XP2(IPT)=XG(IHOR,IPT)
1253              YP2(IPT)=YG(IHOR,IPT)
1254         820  CONTINUE
1256              CALL PLCURV(XP2,YP2,NLIN2,NTIC2,TIC2)
1257         850  CONTINUE
1261
1261       C      PLOT VERTICAL LINES
1261              DO 851 IVERT=1,NLINES
1264              CALL PLCURV(YG(1,IVERT),YG(1,IVERT),NLIN2,NTIC2,TIC2)
1265         851  CONTINUE
1267              GO TO 9999

1270
1270       C      PLOT HORIZONTAL LINES
1270              TIC6=0
1271              NTIC6=0
1272              NLIN6=NLINES
1273              DO 854 IHOR=1,NLINES
1276              DO 853 IPT=1,NLINES
1301              XP6(IPT)=XG1(IHOR,IPT)
1302              YP6(IPT)=YG1(IHOR,IPT)
1303         853  CONTINUE
1305              CALL PLCURV(XP6,YP6,NLIN6,NTIC6,TIC6)
1306         854  CONTINUE
1310
1310       C      PLOT VERTICAL LINES
1310              DO 855 IVERT=1,NLINES
1313              CALL PLCURV(YG1(1,IVERT),YG1(1,IVERT),NLIN6,NTIC6,TIC6)
1314         855  CONTINUE
1316              GO TO 9999
1317
1317       C      PLOT HORIZONTAL LINES
1317         901  CONTINUE
1320              TIC3=0
1321              NTIC3=0
1322              NLIN3=NLINES
1323              DO 905 IHOR=1,NLINES
1326              DO 903 IPT=1,NLINES
1331              XP3(IPT)=XH(IHOR,IPT)
1332              YP3(IPT)=YH(IHOR,IPT)
1333         903  CONTINUE
1335              CALL PLCURV(XP3,YP3,NLIN3,NTIC3,TIC3)
1336         905  CONTINUE
```

```
01340
01340   C     PLOT VERTICAL LINES
01340         DO 907 IVERT=1,NLINES
01343         CALL PLCURV(XM(1,IVERT),YM(1,IVERT),NLIN3,NTIC3,TIC3)
0134.     907 CONTINUE
01346         GO TO 9999
01347
01347   C     PLOT HORIZONTAL LINES
01347     911 CONTINUE
01350         TIC4='+'
01351         NTIC4=-1
01352         NLIN4=NLINES
01353         DO 915 IHOR=1,NLINES
1356          DO 913 IPT=1,NLINES
1361          XP4(IPT)=YM(IHOR,IPT)
1362          YP4(IPT)=YM(IHOR,IPT)
1363      913 CONTINUE
1365          CALL PLCURV(XP4,YP4,NLIN4,NTIC4,TIC4)
1366      915 CONTINUE
1370
1370    C     PLOT VERTICAL LINES
1372          DO 917 IVERT=1,NLINES
1373          CALL PLCURV(XM(1,IVERT),YM(1,IVERT),NLIN4,NTIC4,TIC4)
1374      917 CONTINUE
1376
1376    C     PLOT HORIZONTAL LINES
1376      909 CONTINUE
1377          TIC5=0
1400          NTIC5=0
1401          NLIN5=NLINES
1402          DO 919 IHOR=1,NLINES
1405          DO 918 IPT=1,NLINES
1410          XP5(IPT)=YM1(IHOR,IPT)
1411          YP5(IPT)=YM1(IHOR,IPT)
1412      918 CONTINUE
1414          CALL PLCURV(XP5,YP5,NLIN5,NTIC5,TIC5)
1415      919 CONTINUE
1417
1417    C     PLOT VERTICAL LINES
1417          DO 920 IVERT=1,NLINES
1422          CALL PLCURV(XM1(1,IVERT),YM1(1,IVERT),NLIN5,NTIC5,TIC5)
1423      920 CONTINUE
1425          GO TO 9999
1426
1426    C     PLOT HORIZONTAL LINES
1426      921 CONTINUE
1427          TIC7=0
1430          NTIC7=0
1431          NLIN7=NLINES
1432          DO 923 IHOR=1,NLINES
1435          DO 922 IPT=1,NLINES
1440          XP7(IPT)=YDD(IHOR,IPT)
1441          YP7(IPT)=YDD(IHOR,IPT)
1442      922 CONTINUE
1444          CALL PLCURV(XP7,YP7,NLIN7,NTIC7,TIC7)
1445      923 CONTINUE
```

```
1447
1447   C      PLOT VERTICAL LINES
1447          DO 924 IVERT=1,NLINES
1452          CALL PLCURV(XDD(1,IVERT),YDD(1,IVERT),NLIN7,NTIC7,TIC7)
1453      924 CONTINUE
1455
1455   C      TO FINISH PLOTTING
1455     9999 CALL ENDPLT
1456
1456          STOP
1457          END

ND FLR:
PU:1.399   CTP:.115   SUPS:9.131

DELETE,A SHUTEYP.IMAGE-1/ABS
URPUR 2=3-JB  05/19/83  11:56:41

TP=.333  SUP=.737  CPU=.000  IO=.302  CC-ER=.433
```

End of Document